ZIRCONIUM- CONTAINING CRYSTALLINE, MICROPOROUS MOLECULAR SIEVES: SYNTHESIS, CHARACTERIZATION AND CATALYTIC PROPERTIES

A THESIS
SUBMITTED TO THE
UNIVERSITY OF PUNE
FOR THE DEGREE OF
DOCTOR OF PHILOSOPHY
(IN CHEMISTRY)

BY

Ms. BHAVANA P. RAKSHE

CATALYSIS AND INORGANIC CHEMISTRY DIVISION
NATIONAL CHEMICAL LABORATORY
PUNE – 411 008 (INDIA)

April - 1999

…..To my beloved

parents & grandparents

Acknowledgments

5th April, 1999

(BHAVANA P. RAKSHE)

CERTIFICATE

This is to certify that the work incorporated in the thesis " **Zirconium- containing crystalline, microporous molecular sieves: Synthesis, Characterization and Catalytic properties**" submitted by **Ms. Bhavana Rakshe**, for the Degree of **Doctor Of Philosophy**, was carried out by the candidate under my supervision in National Chemical Laboratory, Pune, India. Such material as has been obtained from other sources is duly acknowledged in the thesis.

(A. V. RAMASWAMY)
Research Guide

(VEDA RAMASWAMY)
Co-Guide

CONTENTS

CHAPTER 1

General Introduction

This chapter presents a brief introduction of the zeolite chemistry and the isomorphous substitution of silicon with other tetravalent metal ions in the zeolite lattice, particularly of MFI, MEL and BEA structures. It highlights the applications of different physicochemical techniques used in the said research work. It also covers a brief literature on the status of zirconium-containing solids in the field of catalysis. Finally, the objectives of the thesis work are defined.

1.1 INTRODUCTION

Zeolites are versatile materials, having applications in ion exchange, gas separation, and in petrochemicals. The zeolites are widely used as *heterogeneous catalysts* in many acid-catalyzed reactions as a result of their microporous structure and uniform pore size distribution. Zeolites catalyze several reactions such as cracking, alkylation and isomerization and synthesis of hydrocarbons thereby extending their applications to synthetic fuels, fine chemicals and pharmaceuticals. The widespread use of these catalysts is due to the enhanced selectivity for the desired products, easy work up and recovery from the reaction mixture, regeneration once it is deactivated and a lower tendency to form by-products. They are eco-friendly materials.

1.2 ZEOLITES/ MOLECULAR SIEVES

Cronsted[1], a Swedish mineralogist discovered that the mineral Stilbite liberated steam on heating which made him to invent the term *Zeolite* from the two Greek words, *Zeo* (to boil) and *lithos* (stone) in 1756.

Zeolites are crystalline, hydrated aluminosilicates with interconnected voids and channels of discrete size. Structurally, these are *framework* aluminosilicates, which are based on an infinitely extending three-dimensional network of AlO_4 and SiO_4 tetrahedra linked to each other by sharing of oxygens. A representative empirical formula[2] for a zeolite is expressed as follows:

$$M_{2/n}O: x\ Al_2O_3: y\ SiO_2: z\ H_2O$$
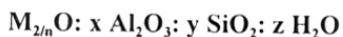
where n is the valence of M cation, M represents the exchangeable cations, generally alkali metal, although other metals, nonmetals and organic cations may also be used to balance the framework charge. The sum of (x + y) is the total number of tetrahedra in the unit cell of framework structure. The value of y is equal to or greater than 2 because Al^{3+} does not occupy adjacent tetrahedral sites according to Loewenstein[3] rule which forbids Al-O-Al linkages.

The definition of the term zeolite is restricted to aluminosilicates; but in practice, microporous, substituted aluminophosphates, silicalites (silica polymorphs) are termed as

1

molecular sieves. A molecular sieve framework is based on an extensive 3-dimensional network of oxygen ions containing generally tetrahedral sites. These cations need not be isoelectronic with Si^{4+} or Al^{3+} but must have the ability to occupy framework sites[4].

1.3 STRUCTURE OF ZEOLITES

In general, zeolites have structures based on TO_4 tetrahedra, where T is a Si or Al atom. The tetrahedra share all corners, thereby generating a 3-dimensional network. The resulting networks have interconnecting channels and voids. The structures are commonly discussed in terms of the basic tetrahedral units known as secondary building units $(SBU)^{5,6}$, comprising single or double-ring structures as represented in Figure 1.1(A)[7]. These SBUs, in turn are interlinked to generate a structure of the zeolite.

1.4 CLASSIFICATION OF ZEOLITES

Zeolites can be classified based on their morphology[8-11], crystal structure[8,9], chemical composition[12], pore topology[13] and their natural occurance[8]. According to Flanigen, the zeolites are classified on the basis of their silica to alumina molar ratios into three groups[12] as follows:

Classification	SiO_2/Al_2O_3	Example
Low silica zeolites	2 - 4	Zeolite A, X, etc.
Intermediate silica zeolites	4 - 10	Zeolite Y, L, Mordenite, etc.
High silica zeolites	10 - several thousands	ZSM-5, ZSM-11 (and their Silica polymorphs), ZSM-12 Zeolite β, etc.

Barrer[14] had classified zeolites into five groups, which was later modified by Sand. In this classification, all zeolites were classified by the size of pore opening, constituted by the number of oxygens, as follows:
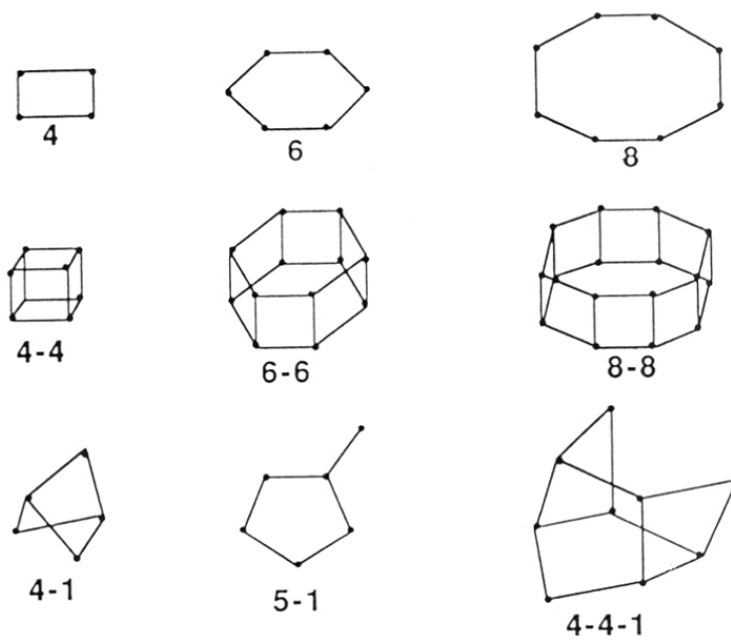
Figure 1.1 (A): Secondary building units (SBU) in zeolites.
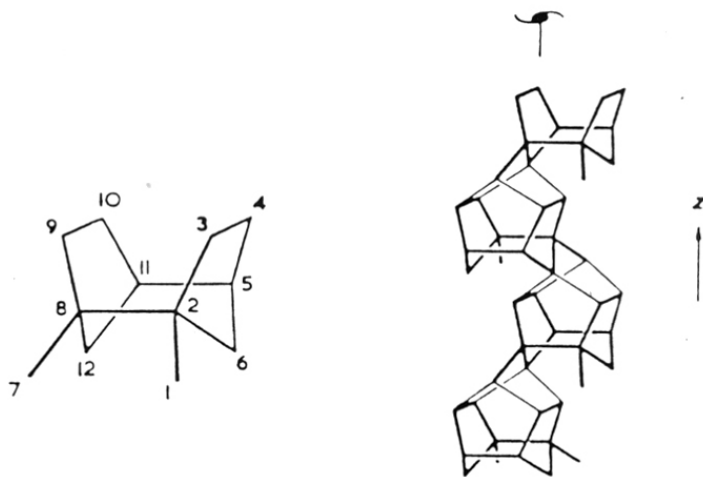
Figure 1.1(B): SBU in pentasil zeolites   **Figure 1.1(C):** Linkages of SBUs to form chain.

Classification	Pore diameter	Example
Small pore (8-membered ring)	3 – 4 Å	Erionite, Linde A, NU-1, etc.
Medium pore (10-membered ring)	5- 6 Å	ZSM-5, ZSM-11, Ferrierite, etc.
Large pore (12-membered ring)	> 7 Å	Faujasite, Beta (β), NCL-1, AlPO-8 (AET), CIT-5, etc.

Prior to the discovery of VPI-5, an 18-membered oxygen ring crystalline aluminophosphate in 1988, 12- membered ring systems such as faujasite, mordenite, AlPO-5, zeolite L, β, etc. had the largest pore diameter. Beginning with the declaration of VPI-5[15-17], an extensive research in the field of large pore molecular sieves has been undertaken. Recently, a few materials containing more than 12 T atoms, have been reported, for example, **CIT-5** (California Institute of Technology, No. Five)- a 14- membered ring structure with 1-dimensional pores[18] and Cloverite (**CLO**), a gallophosphate with a 20- and 8-membered oxygen ring dual pore structure[19]. These zeolite-type materials containing pore openings greater than 12 –member rings are called as *Ultra large pore molecular sieves*[20].

The *shape of the pore openings* varies from one zeolite to another; for example, it is circular and sinusoidal in ZSM-5, circular in ZSM-11, elliptical in $AlPO_4$-11 and teardrop shaped in ZSM-23. Zeolites also can be classified on the basis of *pore dimensions*, for example, 1-dimensional pores in ZSM-12 and ZSM-48, 2-dimensional in ZSM-5 and ZSM-11 and 3-dimensional in X, Y and β.

1.5 NOMENCLATURE OF ZEOLITES

Most of the applications of zeolites and molecular sieves are governed by their framework structures. The topology of a given framework structure that describes the connectivity of the T-atoms is termed as a structure type. For all unique and confirmed topologies, a three letter code, called as *structure type code* is assigned by the Structure Commission of International Zeolite Association, following the rules set up by an IUPAC Commission on Zeolite Nomenclature[21]. These structure codes are generally derived from the names of the type of materials, for example **AFN** for the type material $AlPO_4$-14. The

fourth edition of the Atlas of zeolite structure types lists 98 structure type codes for the unique topologies[22]. Since this last edition of the Atlas, 23 new structure codes[23] are added to the list. The latest codes are as follows:

Structure Code	Type Material	Structure Code	Type Material
ACO	ACP-1	**DFT**	DAF-2
SBS	UCSB-6GaCo	**ESV**	ERS-7
TSC	Tschörtnerite	**STT**	SSZ-23
AFN	ALPO-14	**STF**	SSZ-35
AWO	ALPO-21	**SFF**	SSZ-44

1.6 HYDROTHERMAL SYNTHESIS

There are about 50 *natural zeolites*. Successful application of several of these natural zeolites in the area of ion exchange has stimulated interest in preparing their synthetic analogs. At present, more than 300 synthetic zeolites are known[20]. Most natural zeolites are thermodynamically metastable products formed from siliceous hydrogels (mostly volcanic glass). Saline ground water attacks the surface of the glass, leaches out soluble oxides and salts which ultimately leaches to the formation of zeolite crystals on the glass surface. Only moderate heat is required to initiate the nucleation of the crystals. Recently, Galli *et al.*[24] have reported a new natural zeolite, Mutinaite that has a framework topology similar to ZSM-5 zeolite.

The *synthetic zeolites* are prepared under controlled conditions including the composition, pH of the gel, temperature, pressure and crystallization time. The hydrothermal crystallization is normally carried out from aqueous alkaline gels containing sources of silica, alumina and cations in the temperature range of ~ 360 - 473 K, under autogenous pressure[25]. The use of the organic cations as templates, for example the tetraalkylammonium cation NR_4^+ is of prime interest in sophisticated routes of zeolite synthesis in order to direct the zeolite synthesis towards specific, novel products[26]. In the as synthesized form, the channels or voids of the zeolite frameworks are usually filled with inorganic or organic guest/template molecules, which can be decomposed by heating, a

process termed as *calcination* or ion-exchange with other cations or molecules. The chemical sources and their role in zeolite synthesis are given in Table 1.1. The nature of the product is controlled by kinetic factors and small changes in the experimental conditions during the synthesis[4].

To accelerate the synthesis and to promote the formation of the desired phase, *seeds* are often added to the synthesis gels[4]. These may be in the form of completely crystallized zeolites from previous synthesis batches or nuclei. It is also evident that addition of various *promoter* ions such as perchlorate, phosphate, nitrate, sulphate and carbonate in the synthesis gel enhance the rate of formation of the oligomeric silicate ions responsible for nucleation and growth of the zeolite crystals[27].

Table 1.1: Chemical Sources and their Functions in zeolite synthesis[28]

Sources		Function(s)
SiO_2	⇨	Primary building unit(s) of the framework
AlO_2^-	⇨	Origin of the framework charge
OH^-	⇨	Mineralizer, guest molecule
Alkali cation	⇨	Counterion of framework charge
Template	⇨	Counterion of framework charge, guest molecule, structure directing agent
water	⇨	Solvent, guest molecule

Out of several synthetic zeolites reported, the pentasil zeolites, as their structures are constructed from five-membered rings, are of prime importance in the field of catalysis. ZSM-5 can be synthesized by organic molecules such as tetrapropylammonium bromide (TPABr) or tetrapropylammonium hydroxide (TPAOH) as a *template* in the synthesis gel. In as synthesized form, these templates fill the intracrystalline void space either as organic cations or as occluded molecules[29]. The concentration of it can be in the range of 5-15 wt.% of the final zeolite. Amines[26], alcohols[30] and ethers[31] have also been used as structure directing agents in zeolite synthesis. Within a narrower compositional space, ZSM-5 can also be synthesized in the absence of an organic directing agent[32-35].

ZSM-5, ZSM-11 and NU-87 have 2-dimensional intersecting channels. The SBU on which the *pentasil* structures are based, are shown in Figure 1.1 (B) and (C). In ZSM-5, the neighbouring layers are connected so that they are related by an inversion (I) operator; in a closely related structure- ZSM-11, a reflection operator (σ) relates the neighbouring layers. The channel structure differs in these two zeolites: ZSM-5 (pore size 5.4 × 5.6 Å) consists of both straight and sinusoidal channels, whereas in ZSM-11 (pore size 5.1 × 5.5 Å), both the interconnecting channels are straight. Both HZSM-5 and HZSM-11 are highly stable acidic catalysts. Unlike other zeolites, they have pores of uniform dimensions and do not have large supercages. A high silica content, geometrical constraint imposed by the 10-membered ring structures and the absence of bottleneck pore systems, are believed to be the remarkable factors for their unusual low coke formation as acidic catalysts. These factors make it sterically difficult to form large polynuclear hydrocarbons, responsible for coking and irreversible deactivation[36-38]. In the synthesis of these zeolites, an intergrowth of the two structural types is quite possible[39].

The synthesis of zeolites is mostly performed in alkaline medium to form the soluble species on dissolution of silica and alumina sources using mineralizing\templating agent in the gel. A different route to prepare particularly, pentasil zeolites was reported by Guth *et al.*[40] in the presence of fluoride ions. Most commonly hydrogen fluoride (HF) and ammonium fluoride (NH_4F) sources are used in the synthesis as a mineralizer. The advantages of zeolite synthesis in presence of fluoride ions are as follows:

- A large variation in crystal size with the concentration of fluoride ions
- Incorporation of metal ions which are sparingly soluble (Co^{2+}) and/or unstable in alkaline medium (Cr^{2+}).

The synthesis of metallosilcates with MFI structure in the presence of HF/methylamine mineralizer also provides a broader range of zeolite crystals in a neutral medium[41]. The presence of neutral amine base also helps to maintain the alkaline environment necessary for zeolite crystallization.

Silica polymorphs of ZSM-5 and ZSM-11 are known as *Silicalite-1*[42] and *Silicalite-2*[43], respectively. Moreover several other pentasil zeolites have been synthesized in recent years, for example, NU-87, a high silica ($SiO_2/Al_2O_3 = 20$) zeolite by Casci *et al.*[44,45].

Most recently, the synthesis of a number of large pore zeolites such as CIT-5[18],

SSZ-42[46], SSZ-45[47] and SSZ-47[48] are reported in the literature and proposed for use in refining reactions as catalysts.

Kresge et al.[49] have reported the synthesis of MCM-41, a new family of ordered mesoporous molecular sieves having an hexagonal array of uniform cylindrical channels with a pore size distribution in the range of 20-100 Å.

1.7 MODIFICATION OF ZEOLITES

The diverse applications of zeolites in the field of catalysis have been increasing quite rapidly due to the emergence of new as well as modified materials. Much attention has been focused on oxidation chemistry with isomorphously substituted molecular sieves which also have a wide range of acidic and basic properties.

1.7.1 Isomorphous substitution by hydrothermal method

In the last few years, many researchers have demonstrated that isomorphously substituted zeolites can be prepared either by direct synthesis or by post-treatment methods. It has been claimed that the elements such as germanium[50], boron[51], iron[52], chromium[53], titanium[54-56] and vanadium[57-60] can substitute aluminium or silicon in the zeolite/ molecular sieve framework. In recent years, isomorphous substitution of silicon by Sn[61-63], Mo[64,65] and Zr[66] in the medium pore as well as large pore silicate/ aluminosilicate framework of zeolites is also reported. These metallosilicates, especially titanosilicate catalysts have opened up a new area in the selective oxidation[67] of a variety of organic reactants under mild conditions using aqueous H_2O_2 or tert-butyl hydroperoxide (TBHP). However, quantitative identification of framework substitution was found to be quite difficult in these metallosilicate molecular sieves.

Due to the variations in ionic radii and T-O bond distances, the unit cell parameters and consequently, the unit cell volume (UCV) changes gradually with the degree of metal substitution in the zeolite framework. Substitution of other T-atoms into the framework may have an impact on diffusion characteristics of the zeolites either as: (a) a change of the pore size due to the shortening or lengthening of the M-O-Si bond length and ultimately of M-O-Si bond angle or (b) a change in the affinity of the diffusing molecule for the substituted T-atom. A variation in ionic radii and T-O bond distances of different isomorphously substituted cations, is shown in Table 1.2.

Table 1.2: Ionic radii[68] and T-O bond distances of isomorphous substituted cations

Cation	Ionic radii, Å	T-O bond distance, Å
Si^{4+}	0.26	1.61
V^{5+}	0.36	1.71
Al^{3+}	0.39	1.74
Ti^{4+}	0.42	1.77
Sn^{4+}	0.55	1.90
Zr^{4+}	0.59	1.94

1.7.2 Post-synthesis methods

Szostak has summarized the effects of various postsynthesis modification methods such as ion exchange, mineral acid treatment, steaming, EDTA treatment, $SiCl_4$ treatment, $(NH_4)_2SiF_6$ treatment, organic adsorption, chemical vapour deposition of organometallics on acid activity and on zeolite shape selectivity[69]. The most common methods that are used for post-synthesis modification of zeolites are as follows:

Cation Exchange: Zeolites are synthesized in presence of alkali metal atoms such as sodium and potassium and/or in the presence of organic templates. To produce the protonic or hydrogen form of a zeolite, the preferred technique is to carry out ammonium exchange in aqueous solutions. For acid catalyzed reactions, the zeolite is calcined in an inert gas atmosphere or in air to convert the ammonium form of zeolite into the hydrogen form.

Solid-state reactions: Solid-state ion-exchange reaction has proved to be a powerful technique for post-synthesis modification of microporous zeolites with alkaline, alkaline earth, rare earth, transition and noble metal cations[70]. The main prerequisite for these reactions is to prepare an intimate mixture of two components, i.e. microporous solid and the compound, which contains the in-going cation.

Metal Impregnation: This post-modification method consists of contacting the molecular sieve material with a solution containing the components to be deposited on the zeolite surface. The even distribution of adsorbed active species is quite difficult to attain and sometimes pore blockage may occur in impregnated zeolites. However, impregnation by

soaking or with an excess of solution[71] allows the distribution of the active species to be controlled with a high dispersion. The activity of isomorphously substituted zeolite catalysts can be compared to that of impregnated catalyst of same structure in the reaction.

Chemical vapour deposition: In this technique, the deposition of volatile organic molecules such as $Si(OCH_3)_4$, $Si(OC_2H_5)_4$, etc., takes place in the vapour phase onto smooth surface of zeolites to passivate the external acid sites. The ability to control the constriction of the pore mouth precisely can contribute to enhanced shape selectivity by changing the relative diffusivity of molecules[72].

1.8 STRUCTURAL INVESTIGATIONS

The modified zeolite samples synthesized by hydrothermal method have been characterized by various techniques as given in the following section to investigate the location of new active sites in the framework. The information obtained on structural investigations of most important Ti/V- containing metallosilicate analogues of zeolites, is summarized in Table 1.3.

1.8.1 Powder X-ray diffraction

For zeolite samples with good crystallinity and polycrystalline nature, a long-range order exists and hence, powder X-ray diffraction technique plays a major role in the structural investigations of the zeolite crystals. Although it has become a standard mandatory technique for solids in the identification of crystalline phases, yet it is extensively used for the determination of unit cell parameters, analysis of structural imperfections, crystallite size determination and recently, in the refinement of the structures[73]. The ability to recover high-quality structural information from powder data was first established by the technique of Rietveld or profile refinement in the early 1970s[74]. The difficulty in synthesizing single crystals has necessitated the use of high resolution powder diffraction data with the help of synchrotron radiation. In these scans, the resulting Bragg peaks are narrow, intense and well resolved. The corrected interplanar distances with respect to silicon (internal standard) can be refined to calculate unit cell parameters using least square fittings. As explained in the preceding section 1.7 of this chapter, an isomorphous substitution of metal atom in place of Si^{4+} results in a change of unit cell volume (UCV). The extent of this change depends on the size (ionic radii) of the incorporated metal (T) atom and the corresponding T-O bond distance (Table 2). Notari[75]

Table 1.3: Structural investigations of titanium and vanadium silicate analogs of zeolites

Techniques	Information obtained
Chemical analysis	Ti, V and Al content.
Powder X-ray diffraction	Crystallinity/phase purity, unit cell expansion due to Ti/V incorporation.
Scanning electron microscopy/ EDAX	Morphology, average size of particles; presence of amorphous matter; Ti/V distribution.
Adsorption methods (gravimetric and/or volumetric)	Amorphous matter within pores and crystallinity, micropore volume
Thermal analysis	Structural stability, distribution and amount of template.
FTIR framework hydroxyl bands	Band around 960 cm^{-1} due to Si-O-Ti/ Si-O-V Broad band at 3400-3500 (Ti) or 3200-3600 (V) cm^{-1}
Acidity Ti-silicates V-silicates	 Weak Lewis acidity; no Brönsted acidity Medium Lewis acidity and weak Brönsted acidity
NMR Ti-silicates V-silicates	 Broad ^{29}Si signal. ^{51}V peak at -573 ppm.
Ion exchange capacity Ti-silicates V-silicates	 No ion exchange capacity. Exchangeable protons (Na/V = 0.5 - 0.7).
UV-Visible spectra Ti-silicates V-silicates	 210 nm due to Ti^{4+} in T_d, 238 nm due to Ti^{4+} in O_h (influenced by H_2O adsorption). CT band below 400 nm and absence of 550 nm band indicates V^{4+} in T_d coordinations.
ESR	No peaks in the case of Ti^{4+}/ V^{5+}; V^{4+} = -8 line spectrum (g = 1.932; g = 1.981; A = 185 G; A = 72 G).
ESCA	Surface composition, absence of extra O_{1s} peak due to Ti/V oxides
EXAFS/XANES Ti-silicates	 Si-O-Ti bond distance, Ti in defect, not regular T sites.

has derived an equation based on the changes in the UCV on isomorphous substitution of Si^4 with bigger Ti^{4+} ions, with respect to pure silicalite, as given below. Similarly, the isomorphous substitution of other tetravalent metal atoms such as V[76], Sn[61] and Mo[65] etc. in the silicalite as well as aluminosilicate frameworks is extensively studied by many researchers.

The equation is:

$$V_x = V_{Si} - V_{Si} (1-d^3_M/ d^3_{Si})\, x$$

where V_{Si} is the UCV of pure silicalite, d^3_M and d^3_{Si} are the tetrahedral T-O bond distances for the substituted tetravalent metal and silicon atoms, mostly reported in the crystal chemistry of these elements and $x = M/(Si+M)$ the atomic ratios in the product. This 'x' value correlated with the UCV of metallosilicates with the different degree of substitution. The experimental values are in good agreement with the values calculated using this equation.

1.8.2 Scanning electron microscopy

In scanning electron microscopy, topographical images are formed from backscattered primary or low energy secondary electrons. It provides information about the identification of phases and structural information such as surface morphology and particle size, on zeolite crystals[77].

1.8.3 Thermal analysis (TG/DTA)

Thermal analysis provides information on the dehydration of the as-synthesized materials and decomposition temperatures of organic additive/template molecules entrapped or occluded into the channels of a zeolite structure. This technique has been widely used to study the structural stability of as-synthesized forms of high silica zeolites such as ZSM-5 and beta, at elevated temperatures[78]. In thermogravimetric (TG) analysis, the weight loss corresponding to the decomposition of template cations with rise in temperature can be attributed to the amorphous and crystalline phases present in the samples. As the crystallinity increases, the template decomposition temperature also increases.

1.8.4 Nuclear magnetic resonance spectroscopy

NMR technique offers new insights into the structure, in particular short range

order of a zeolite material. ^{29}Si liquid NMR provides detailed information on the nature of silicate species that exists in the synthesis gel[79]. It is rather possible to study the changes that occur in the relative concentrations of various species during the precrystalline stages of a hydrothermal synthesis. In addition to these studies, NMR technique has been applied to the identification of framework structures in the zeolites.

The magic angle technique (MAS-NMR) allows to obtain high resolution data for solids due to high speed spinning of the sample at an angle of 54°.44' that effectively removes most of the line broadening. As the chemical shift depends upon the local environment of the nucleus, different shifts are observed depending on whether a particular silicon atom has 0,1,2,3 or 4 silicon atoms in the four surrounding tetrahedral sites, which also can be explained in the terms of 'Q' units, the structural units in the silicate anions[80]. In the zeolite systems, the Q-unit is always Q^4, where each silicate is surrounded by four silicate or aluminate units, thus there are five possibilities as follows:

$$Q^4 \text{ (nAl, (4-n)Si) where n = 0 - 4}$$
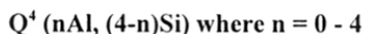
Such information assists the development of structural models for the short-range order of silicon and aluminium atoms over the tetrahedral sites. ^{29}Si MAS-NMR reveals the details of Si, Al ordering in the framework, while ^{27}Al NMR probes the chemical status of aluminium. ^{1}H NMR allows the structure of the Brönsted active sites to be determined. Although a large amount of valuable ^{29}Si NMR data have been collected for aluminosilicates, relatively little information is available in the literature for metallosilicates. Recently, Balmer[81] *et al.* have examined the relationship among the ^{29}Si NMR chemical shift, the number of titanium polyhedra coordinating each silicon tetrahedron and the oxygen formal charge for titanosilicates with known crystal structures.

1.8.5 Diffuse reflectance UV-visible spectroscopy

This technique measures the scattered light reflected from a surface of samples in the UV-visible range (200-600 nm). For most of the isomorphously substituted zeolite samples, the transitions in the UV region (200-400 nm) are of prime interest. This spectroscopic technique is used to determine the coordination state of transition metal ions substituted in the zeolite matrix, involving ligand-to-metal charge transfer transitions at ~ 200- 220 nm.

1.8.6 Fourier transform Infra-red (FTIR) spectroscopy

In a FTIR instrument, the polychromatic source is modulated into an interferogram that contains the entire frequency region of the source and hence all frequencies are measured simultaneously.

Infrared spectroscopy technique has provided useful information about structural details of zeolites. It has been used to confirm crystal purity[82], isomorphous substitution[83] and acid characteristics[84]. Some structural features are observed in most of the zeolites. The infrared spectrum can be classified into two groups of vibrations (as described in Table1.4, given below): (1) internal vibrations of the framework TO_4, which are insensitive to structural variation; and (2) vibrations related to the external linkages of the TO_4 units in the structure, which are sensitive to structural variation. Mid-infrared spectroscopy has

Table 1.4: Zeolite infrared assignments

Internal tetrahedra	Wavenumber, cm^{-1}
Asymmetric stretching	1250 - 950
Symmetric stretching	720 - 650
T-O bending	420 - 500
External linkages:	Wavenumber, cm^{-1}
Double ring	650 - 500
Pore opening	300 - 420
Symmetric stretching	750 - 820
Asymmetric stretching	1050 - 1150 (sh)

spectroscopy has been applied to further identify framework incorporation of other elements. The shifts in band positions of the symmetric and asymmetric vibration modes have been observed with successful incorporation of gallium, iron, boron and titanium into the silicate\aluminosilicate structures.

1.8.7 Extended X-ray absorption fine structure

An increasingly important role in zeolite structure studies is being played by the X-

ray absorption spectroscopic method, for example, the extended X-ray Absorption Fine Structure (EXAFS). It examines the oscillations of X-ray absorption coefficient in intensity, which occur at the high-energy side of X-ray absorption edges caused by the excitation of electrons from core levels into continuum states. The oscillations arise from back scattering of the photoelectron created by the excitation of surrounding atoms, which interferes with the outgoing photoelectron wave. The method is particularly applied to investigate the local environment of extra-framework as well as framework cations[85] and also to monitor the changes in the local environment of a particular metal atom during the catalytic reaction[86].

1.8.8 Computational and theoretical methods

The theoretical methods applied in the zeolite chemistry to reproduce zeolite structures and subsequently to investigate the stabilities and structural properties of new hypothetical zeolites and/or isomorphously substituted zeolites, with the minimum experimental input. Such calculations can be used to assist the refinement of the structures in experimental studies. These numerical optimization procedures allow to estimate the configuration of minimum lattice energy or free energy in the zeolite structures. Both semiempirical[87] and *ab initio*[88] methods have been employed to investigate the reaction pathways of sorbed molecules in the zeolite pores.

1.8.9 Adsorption methods

Pore Volume is a property that has been utilized extensively in characterizing a molecular sieve material due to its ability to adsorb selected molecules. It is always determined using several probe molecules such as n-hexane, water, nitrogen, etc. These probe molecules of various sizes also have been used to gain information on the size of the pore openings, using gravimetric adsorption methods. For example, n-hexane is readily adsorbed in the 8-, 10- and 12-ring zeolites while the larger cylcohexane is not taken up by the small and medium pore zeolites.

The Brunauer-Emmett-Teller (BET) volumetric gas adsorption (nitrogen, argon, etc.) is a standard method for the determination of the surface area and pore size distribution of finely divided porous samples[89]. It is customary to apply BET equation in the linear form,

$$P \div [n \times (p_o - p)] = 1 \div (V_m \times C) + (C-1)p \div (V_m \times C \, p_o)$$

where 'n' is the no. of moles adsorbed per gm of adsorbent at the relative pressure p/p_0. 'C' is the BET constant and 'V_m' is the monolayer capacity of surface. The relation between the amount adsorbed and the equilibrium pressure of the gas at constant temperature is defined by the *adsorption isotherm*. Type I adsorption isotherm is a characteristic of the microporous zeolites, having relatively small external surfaces. The *t-plot* analysis, a plot of the amount adsorbed versus the thickness of the adsorbed gas on the walls of the pores, is mostly applied to differentiate between the adsorption mechanism in micropores and that occur in mesopores and macropores.

1.8.10 Electron spin resonance spectroscopy

Electron spin resonance (ESR) spectroscopy is the resonance absorption of the electromagnetic (microwave) radiation by magnetically split states of unpaired electrons. In the case of some paramagnetic molecules, the formation of a charge-transfer complex can be determined by this technique. It is possible when the electron of donor molecule interacts with the nuclear spin of the electron-acceptor site. Thus, this technique provides a valuable information on the redox sites and the intermediate species formed in the catalytic reaction. With help of this information, it is easier to focus on the status of framework and nonframework species formed in the transition metal incorporated molecular sieves.

1.9 ACTIVE SITES FOR CATALYSIS

1.9.1 Acidity and Basicity

The reactivity and selectivity of zeolites as catalysts are always determined by their active sites in terms of Brönsted as well as *Lewis* acidic and basic sites. The acidic or basic character of a zeolite is related to the framework electronegativity. The basic strength of the framework oxygen increases at low framework electronegativity and the acid strength varies in opposite direction[90].

The *Brönsted acid sites* are able to perform a proton-transfer from the solid to a suitable adsorbed molecule and the *Lewis acid sites* are able to accept an electron pair from a suitable adsorbed molecule. Bridging hydroxyl groups are the most important Brönsted acid sites in zeolite catalysis. These sites are generated when a tetrahedral site of a pure silica framework, a silicon atom is replaced by an aluminium atom and a proton is added to maintain charge neutrality. The acidic hydroxyl groups protonate unsaturated organic

molecules or basic groups. Thus, proton transfer is the initial elementary reaction of acidic catalysis by Brönsted sites. These protonated species, however, strongly depend on other acid-base properties such as Lewis acidity and basicity of the framework oxygen ions.

The Lewis acidity arises from Al or other cation species, alkaline, alkaline earth or other cations. In a similar way the basic sites may be considered of Brönsted or Lewis type. A *Brönsted base* shows a tendency to accept a proton and a *Lewis base* to donate an electron pair. The former consists of basic OH groups and the later, framework oxygen atoms. The basicity of zeolites depends upon the electronegativity of the framework atoms, the bond angles and bond lengths, the structure ionicity, the crystallographic occupancy of the oxygen, the location of Al. It is well known that Brönsted acids and bases are conjugated and those weak acids have strong conjugate bases and reciprocally strong acids have weak conjugated bases[91]. A similar interpretation has been reported in the case of titanium silicates by Bittar *et al.*[92]. The origin of Lewis acidity in the samples is due to a strong polarization of $Si-O^{\delta-}... Ti^{\delta+}$ bridges, which may be the preferable sites for the adsorption of polar molecules. The tetrahedral Ti in the silicalite lattice bears a δ^+ charge so that the O...Ti bond may be viewed as a *Lewis acid-base pair*. A similar approach may be invoked to other metalllosilicate catalysts having weak acid sites.

Each oxygen type falls into different categories according to its local environment (Si-O-Si and Si-O-T, where T = Al, or other metal atom). It could be explained on the basis of the relation between the softness of an atom and its environment. Aluminium is harder than silicon and softens the neighbouring oxygens. This can probably help in understanding of the electron donor capacity (basicity) of oxygens in zeolites, since softness is closely related to charge capacitance. Aluminium atoms due to their hardness enhance the electron donor capacity of the oxygens and therefore, increase basicity with increasing Al content[93]. These variations in the nature of charged species, are found to affect the activity and selectivity of the catalyst[94].

A large number of studies have been reported in the literature[95-97] for the determination of nature, number, strength and location of active sites in zeolite samples, which are listed below:

- *IR spectroscopy*: qualitative and quantitative measurements of surface hydroxy groups and adsorption of the bases such as pyridine, ammonia and carbon monoxide.
- Temperature programmed desorption (TPD) of chemisorbed bases

- Microcalorimetric measurements during adsorption of suitable probe molecules
- Solid state NMR of OH groups and sorbed bases
- ESR spectroscopy
- Amine titration and adsorption of indicators to determine the total amount of acid sites and also the acid site distribution.
- Acid catalyzed reactions such as cracking of alkenes and isomerization of m-xylene, to probe the catalytic acid nature of the zeolite material.

1.10 CHARACTERISTICS OF ZEOLITES

The *structural* characteristics[98] of any zeolite can be categorized as follows:
- Framework topology
- Thermodynamic stability
- The feasibility of synthesis.

In addition, assessment of other physical and chemical properties of the zeolites, such as its ability to function as a catalyst in terms of its diffusivity or as a molecular sieve may also be required. Zeolite intracrystalline *diffusivity* is influenced by a large number of *physicochemical* factors[99] as follows:
- Size, shape and polarity of diffusing molecules
- Zeolite channel geometry, connectivity and dimensions
- Chemical composition of framework
- Cation type , size, distribution, charge and concentration
- Lattice defects (e.g. stacking faults)
- Detritus (debris) within the diffusion pathways
- Carbonaceous deposits within or near the zeolite pores
- Zeolite crystallite size and morphology.

Several of these factors, including zeolite geometry, crystallite size and morphology are essentially fixed during the synthesis of the zeolite. The framework chemical composition can be modified by postsynthesis, chemical or hydrothermal treatments. Cation type and concentration are normally changed during the formulation of the final product in the form of a catalyst or a sorbent. Lattice defects and alumina or silica debris can be introduced at any stage. During the usage of the catalyst, the carbonaceous deposits are considered.

The importance of zeolites to industrial catalysis can be attributed to their unique

properties:

◆ High internal surface areas.

◆ Uniform pores with one or more discrete size.

◆ Ion exchange ability produces highly dispersed catalytically active sites, such as acidic sites when the exchangeable cations are replaced by protons. A good thermal stability to withstand the drastic experimental conditions.

◆ An ability to sorb and concentrate hydrocarbons.

Since the pores of these zeolites are similar in size to many organic molecules of practical interest, it became possible to design novel catalysts on a molecular level by controlling diffusion of reactant and product molecules through them, called as *shape selective catalysts*. These catalysts such as small pore zeolites were applied to perform the selective conversion of straight chain molecules. Their industrial application has been extended by ZSM-5 and other medium pore zeolites. These medium pore zeolites can selectively convert both linear and selected branched molecules and single ring aromatics, naphthenes and nonhydrocarbons with critical molecular dimensions < 6 Å. They also open up an entirely new regime for molecular transport or diffusion in the microporous solids, known as the regime of configurational diffusion or micropore diffusion.

1.11 SHAPE SELECTIVITY IN ZEOLITES

Selectivity is achieved by choosing the zeolites that can distinguish between molecules of different size and shape. Even though the shape selectivity effect is always known to have reactant and product shape selectivity which are based on the principle of molecular exclusion or molecular sieving, some other selectivities also exist in the microporous solids such as configurational diffusion controlled selectivity, reverse molecular selectivity, confinement or surface curvature effects and molecular traffic control effect[100].

Reactant Selectivity: It occurs when the feedstock contains two types of molecules, one of which is too large to pass through the zeolite channel system. It has been demonstrated by the Selectoforming process in which octane rating of the reformate is raised by selective cracking of n-alkanes[101].

Product Selectivity: It occurs when the reactant molecules entering the pores of the zeolite are converted to products, only some of which can diffuse out from the zeolite cavities,

depending upon the size of product molecules. It was demonstrated by the absence of branched chain products in the cracking of n-alkanes[102].

Transition state selectivity or spatioselectivity: It occurs when both the reactant and product molecules are small enough to diffuse through the intracrystalline channels, but the reaction intermediates are larger than either the reactants or the product, and are spatially constrained by size or orientation. This effect is illustrated by the absence of symmetrical trialkylbenzenes (1,3,5- isomer) in the disproportionation product of dialkylbenzenes over H-mordenite, a large pore zeolite[103].

1.12 APPLICATIONS OF ZEOLITES

Catalysis: Zeolites, as shape selective acid catalysts, catalyze several types of catalytic reactions. Most important are cracking, isomerization and hydrocarbon synthesis. There are increasing applications of zeolites in the field of synthesis of organic fine chemicals[104].

Ion exchange: Hydrated cations within zeolite pores are loosely bound extraframework species. Therefore, they can be readily exchanged with other cations in aqueous media[8]. The traditional application is in water softening and hence applicable in the detergents to remove phosphates. Zeolites are also widely used due to their ion-exchange properties in nulcear waste treatment to remove radioactive Cs^+ and Sr^+ ions; in chicken- and pig-feed additives.

Gas separation: Different molecules always have different equilibrium constants for sorption and different diffusion coefficients within the pores, which enables zeolites to be used as molecular sieves in gas separation processes, e.g. for separating branched from straight chain hydrocarbons[105].

Other applications: Due to the possibility of *in situ* precipitation and polymerization within the zeolite pores and cages, it is quite easier to encapsulate semiconducting materials[106], electronically conducting polymers with unusual physical properties[107] and the inorganic molecules such as copper phthalocyanines. The reactions of these encapsulated materials are modified by the constraints imposed by the zeolite cage[108]. Such *in situ* synthesis offers the possibility of extending the range of applications in the field of zeolite chemistry. The search for new regiospecific and stereoselective molecular sieve-based catalytic systems is being explored in featuring transition metal complexes occluded in zeolites, the use of molecular sieves as host-lattices for radical and photochemical

reactions, novel shape-selective and dual-functional reaction systems and creative use of solvents and adsorption/ desorption techniques to control reaction path.

1.13 PHYSICAL PROPERTIES OF ZIRCONIUM[109]

- Atomic Number = 40
- Atomic Weight = 91.22
- Natural abundance = 11.23
- Most abundant mineral = Zircon
- Electronic Configuration = $[Kr]\ 4d^2 5s^2$
- Most important oxidation state = Zr(IV)
- Covalent radius of Zr : 1.45 Å; Ionic radii of Zr^{4+} : 0.59 Å
- Melting point: 1857°C; Density: 6.51 g cm^{-3};
- Pauling's electronegativity = 1.4
- NMR active nuclei = ^{91}Zr = 5/2

1.14 ZIRCONIUM IN CATALYSIS

Zirconium containing catalysts are being increasingly applied commercially for the following processes:

Environmental[110, 111]

Polymerization[123]

Isomerization[112, 113]

HDS/HDN[121, 122]

Reduction[114]

Zr

Oxidation[120]

Reforming[115, 116]

Dehydrogenation[119]

Dehydration[117]

Hydrogenation[118]
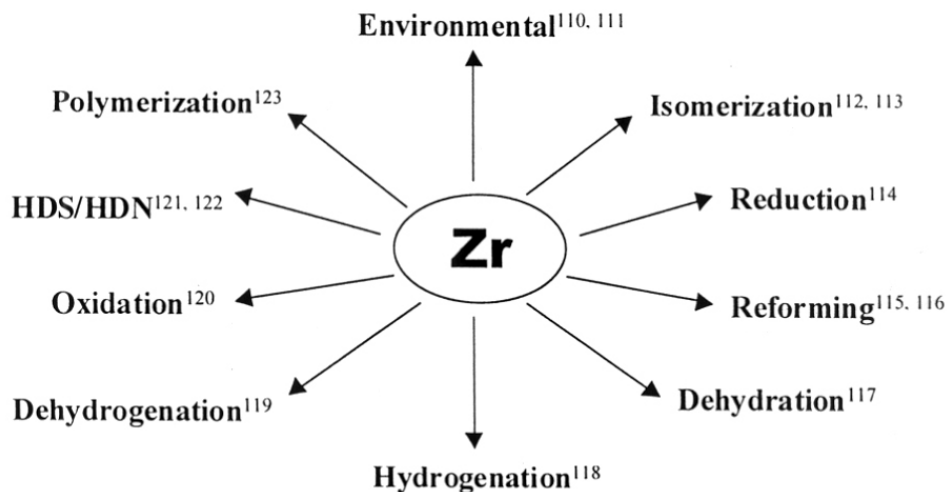
The demanding applications of zirconium, distinctively its oxide form, *i.e.* zirconia, in catalysis are due to its following characteristics:

◆ Zirconia is a versatile support for the catalysts due to its chemical inertness and ability to sustain a high surface area.

◆ It is amphoteric, being able to show both mildly acidic and basic properties.

◆ It can be converted into a superacid.

◆ It stabilizes the active components but does not interact so vigorously as to deactivate the catalyst.

1.14.1 Miscellaneous applications of zirconia

Zirconia plays a prominent role in the synthesis of both synthetic fuels and higher alcohols, as follows:

◆ *The Fischer-Tropsch process* (conversion of synthesis gas to liquid transport fuels): The role of zirconia component in $Co/ZrO_2/SiO_2$ catalyst is to increase the activity of the catalyst without changing the high level of selectivity to higher hydrocarbons[124].

◆ *Automotive Exhaust purification:* Addition of zirconia to the outer layer of *autocatalyst* markedly improves the removal of hydrocarbons and also gives increased conversion of carbon monoxide and nitric oxide[125].

◆ *Environmental protection:* Another application of zirconia in pollution control relates to the Claus process[126] for the removal of atmospheric sulphur dioxide, which is a major contributor of acid rain.

◆ *Sulphated zirconia:* Tanabe[127] has shown that sulfated zirconia, known as superacids are active in many acid catalyzed reactions such as Friedel-Crafts acylation. These catalysts have also been shown to be active in the isomerization of n-butane to isobutane at temperatures as low as 483 K[128].

Other applications:

◆ V_2O_3/ZrO_2 catalysts have been found to be effective for the removal of NO_x from flue gases[129].

◆ Zirconium is one of the few transition metals, which can be used to form stable oxide *pillars* between the silicate layers of smectite clays[130]. These materials have potential use in hydrocracking, for the selective formation of C_2-C_4 olefins from methanol or CO/H_2.

1.15 ZIRCONIUM- CONTAINING MOLECULAR SIEVES

The isomorphous substitution of Si^{4+} by other tetravalent metal ions such as Ti^{4+}, Sn^{4+}, etc. in the medium pore as well as large pore, microporous molecular sieves with as MFI, MEL and BEA structures has lead to the invention of novel metallo-silicate molecular sieves which show significant improvements in product selectivities in the oxidation as well as acid catalyzed reactions, respectively.

Since zirconium is a versatile element, it can be included in any classification of materials considered to have interesting and potential catalytic properties. A demand for the catalysts having improved stability, activity and selectivity has encouraged research into the possible use of zirconium as a functional element in heterogeneous catalysis.

1.15.1 A brief literature on zirconium- containing molecular sieves

There are many reports in the literature concerning the modification of zeolites/ molecular sieves with zirconium compounds using post-synthesis methods such as impregnation, grafting and ion exchange as well as hydrothermal methods.

Absil et al.[131] have claimed that an addition of Zr-containing complex for example, hydroxychlorides of Zr and Al to the zeolites such as ZSM-5, ZSM-23 and beta improves the dispersibility characteristics of supported noble metal components in the zeolites. Such catalysts showed a significant activity in hydrogenation, dehydrogenation, hydroprocessing and reforming. A similar study was carried out by Herbst et al.[132]. They claimed that the use of zirconium in the form of $Al_3Zr(OH)_9Cl_4$ as a stabilizing component improves the hydrothermal stability and physical strength of zeolite beta catalyst in the catalytic cracking reactions. Vosmerikov et al.[133] have shown that modification of H-form of high silica ZSM-5 zeolite with Zr strengthens the acid sites and increases the selectivity for aromatic hydrocarbons. The properties of the ZSM-5 zeolite with ZrO^{2+} ions in an *ion-exchange* reaction in aqueous solution were investigated by Romotowski et al.[134]. Activity of ZrO-HNaZSM-5 zeolite samples in the ammoxidation of m-xylene suggested that these zeolites have not only centers for acid-base catalysis but also some redox centers although a change in Zr valence would appear difficult to attain. Yang et al.[135] have shown that ZrO_2-NaZSM-5 catalysts with different ZrO_2 loadings enhances the activity and selectivity of Na-ZSM-5 for the dehydration of EtOH to ethylene as well as in the conversion of n-$PrNH_2$ to propylene and propionitrile.

Some reports are available on the hydrothermal synthesis of Zr-ZSM-5 zeolites. The effect of Na_2O/SiO_2 and SiO_2/ZrO_2 molar ratios on the synthesis of Zr[ZSM-5] zeolites and their catalytic properties in phenol hydroxylation has been investigated by Wang et al.[136]. Attempts have been made to synthesize Al-free Zr-containing MFI-type silicalites (Zr-Silicalite-1) in alkaline[137-142] as well as fluoride[143,144] medium by many researchers. However neither the status of zirconium atoms in the zeolite framework, nor their role in catalytic processes have been satisfactorily explained.

Very few reports are available on the synthesis of large pore Zr-containing zeolites. Zr-ZSM-12 type molecular sieves were hydrothermally synthesized for the first time using $MeEt_3NBr$ as a template[145]. Recently, a few publications are reported on the hydrothermal synthesis of Zr-aluminophosphates (Zr-APO$_5$)[146] and silica-aluminophosphates (Zr-SAPO-11)[147] molecular sieves. In n-butene isomerization reaction, Zr-SAPO-11 catalyst exhibited a higher isobutene selectivity as compared to SAPO-11 catalyst. Since both the samples showed same acid strength, the change in selectivity may be related to the reduced porosity of Zr-SAPO-11.

Tuel et al.[148,149] have reported the synthesis of a novel Zr-containing mesoporous silca using hexadecylamine as surfactant. This new material showed very interesting properties in the oxidation of large and bulky substrates with H_2O_2 and alkyl peroxides. Wong et al.[150] have also reported the synthesis of zirconium oxide mesoporous molecular sieves (Zr-TMS1) using dodecylphosphate surfactant which formed a mesostructure similar to MCM-41.

Recently, the application of Zr-containing molecular sieves is further extended in the field of catalysis by grafting the Zr-containing chiral alkene polymerization catalyst, rac-ethenebis(indenyl) zirconium dichloride onto the surface of mesoporous MCM-41 structure and utilized to prepare highly isotactic polypropene with a unique spherulite morphology[151].

1.16 OBJECTIVES OF THE WORK

As it is quite crucial to locate the framework zirconium within the zeolite channels, the substitution of silicon by zirconium in the zeolite framework structures by hydrothermal synthesis is not really substantiated so far by experimental evidences. Therefore, our aim is to incorporate Zr(IV) in the microporous silicalite as well as

24

aluminosilicates, which may lead to an improvement in their catalytic properties and to investigate the presence of zirconium in the framework structures by various analytical techniques.

The major objectives of the work are as follows:

1. To synthesize Zr- containing medium pore molecular sieves such as Silicalite-1 (MFI topology), Silicalite-2 (MEL topology) and large pore Al-beta (BEA topology).

2. To investigate the presence of Zr^{4+} ions in the framework using various characterization techniques.

3. To study the effect of zirconium in Silicalite-1, Silicalite-2 and Al-beta on the acid properties and hence on the catalytic activity in the hydroxylation of phenol, decomposition of propan-2-ol, dehydrogenation of ethanol and acid catalyzed reactions such as m-xylene isomerization, respectively.

The thesis consists of 5 chapters, namely a general introduction to the subject in this *Chapter 1*. *Chapter 2* describes the work on crystalline, microporous Zr-silicate molecular sieves with MFI structure (their hydrothermal synthesis, characterization and catalytic properties). A similar study was made for Zr-silicate with MEL topology and presented in *Chapter 3*. The work on the synthesis, characterization and catalytic properties of a large pore Zr-containing Al-beta with BEA topology is described in *Chapter 4*.

Finally, the results obtained in all for three types of Zr-containing molecular sieves are summarized in *Chapter 5*.

1.17 REFERENCES

1.   A. F. Cronsted, Adak. Handl. Stockholm 17 (1756) 120.

2.   D. W. Breck, J. Chem. Edn. 41 (1969) 41.

3.   W. Lowenstein, Am. Minerals 39 (1954) 92.

4.   R. Szostak, *Molecular Sieves: Principles of Synthesis and Identification* (Van Nostrand Reinhold, New York, 1989) p. 3.

5.   F. Liebau, *Structural Chemistry of Silicates: Structure, Bonding and Classification,* (Springer-Verlag Series, Berlin, 1985).

6.   C. R. A. Catlow, *Modelling of Structure and Reactivity in Zeolites* (Academic Press Limited, London, 1992).

7.   W. M. Meier and D. H. Olson, *Atlas of Zeolite Structures* (Butterworth, London, 1987).

8.   D. W. Breck, *Zeolite Molecular Sieve Structure, Chemistry and Use* (Wiley and Sons, London, 1974), reprinted by R. E. Krieger (Malabar, FL, 1984).

9.   R. M. Barrer, *Hydrothermal Chemistry of Zeolites* (London, Academic Press, 1982).

10.   W. L. Bragg, *The Atomic Structure of Minerals* (Cornell University press, Ithaca, New York, 1937).

11.   W. M. Meier, *Molecular Sieves*, Vol. 10 (Soc. of Chem. Ind., London, 1968).

12.   E. M Flanigen, *Proceedings of 5th Inter. Conf. on Zeolites*, 1980) p. 760.

13.   L. B. Sand, Econ. Geol. (1967) 191.

14.   R. M. Barrer, *Zeolites and Clay Minerals as Sorbents and Molecular Sieves* (Academic Press, New York, London, 1978) Chap. 2.

15.   M. E. Davis, C.H. Saldarriaga, C. Montes, J. M. Garces and C. Crowder, Zeolites 8 (1988) 362.

16.   M. E. Davis, C.H. Saldarriaga, C. Montes, J. M. Garces and C. Crowder, Nature 331 (1988) 698.

17.   M. E. Davis, C.H. Saldarriaga, C. Montes, and J. M Garces, Am. Chem. Soc. Symp. Ser. 398 (1989) 291.

18.   P. Wagner, M. Yoshikawa, K. Tsuji and M. E. Davis, Chem. Commun. (Cambridge), 22 (1997) 2179.

19.   M. Estermann, L. McCusker, Ch. Baerlocher, A. Merrouche and H. Kessler, Nature 352 (1991) 320.

20.   M. E. Davis, Acc. Chem. Res. 26 (1993) 111.

21.   R. M. Barrer, Pure and Appl. Chem. 51 (1979) 1091.

22. W. M. Meier, D. H. Olson and Ch. Baerlocher, *Atlas of Zeolite Structure Types*, Fourth Revised Edition (Elsevier, London, 1996).

23. http://www.iza.sc.ethz.ch/IZA.SC/updates (last updates on 10th December, 1998).

24. E. Galli, G. Vezzalini, S. Quartieri, A. Alberti and M. Fraanzini, Zeolites 19 (1997) 318.

25. R. M. Barrer, J. Chem. Soc., Chem. Commun. (1948) 2158.

26. B. M. Lok, T. R. Cannan and C. A. Messina, Zeolites 3 (1983) 282.

27. R. Kumar, A. Bhaumik, R. Ahedi and S. Ganapathy, Nature 381 (1996) 298.

28. J. C. Jansen, S. T. Wilson, Stud. Surf. Sci. Catal. 58 (1991) 77.

29. Argauer and Landolt, US Patent 3702886 (1972).

30. W. Hölderich, W. D. Mross and M. Schwarzmann, EP 77946 (1993) BASF AG.

31. W. Hölderich, L. Marosi, W. D. Mross and M. Schwarzmann, EP 51741 (1982) BASF AG.

32. C. J. Plank, E. J. Rosinski, M. K. Rubin, US Patent 4,175, 114 (1979).

33. F. Wang, W. Cheng, S. J. Chang, J. Catal. (Chinese) 2 (1981) 282.

34. J. M. Bezak, and R. Mostowicz, Stud. Surf. Sci. Catal. 24 (1985) 47.

35. A. Nastro, C. Colella, and R. Aiello, Stud. Surf. Sci. Catal. 24 (1985) 39.

36. L. D. Rollmann and D. E. Walsh, J. Catal. 56 (1979) 139.

37. D. E. Walsh and L. D. Rollmann, J. Catal. 56 (1979) 195.

38. E. G. Derouane, Stud. Surf. Sci. Catal. 20 (1985) 221.

39. J. M. Thomas and C. R. Milward, J. Chem. Soc., Chem. Commun. (1982) 1380.

40. J. L. Guth, H. Kessler and R. Wey, *Proc. 7th Int. Conf. On Zeolite* (Tokyo, 1986) p. 121.

41. M. Costantini, J. L. Guth, A. Lopez and J. M. Popa, EP 466,545 (1990); US Patent 5,399,336 (1995).

42. E. M. Flanigen, J. M. Bennet, R. W. Grose, R. L. Patton, J. P. Cohen, R. M. Kirchner and J. V. Smith, Nature 271 (1978) 512.

43. D. M. Bibby, N. B. Milestone and L. P. Aldridge, Nature 280 (1979) 664.

44. M. D. Shannon, J. L. Casci, P. A. Cox and S. J. Andrews, Nature 353 (1991) 417.

45. J. L. Casci and A. Stewart, EP 0,377,291 (1990).

46. C. Chen, L. W. Finger, R. C. Medrud, C. L. Kibby, A. P. Crozier, Y. I. Chan and B. L. Thomas, Chem. Eur. J. 4 (1998) 1312.

47. I. S. Zones and L. Yuen (Chevron Inc., USA), Appl. WO 9829338 A1 (1998).

48. I. S. Zones and G. S. Lee (Chevron Inc., USA), Appl. WO 9829336 A1 (1998).

49.	C. T. Kresge, M. E. Leonowicz, W. J. Roth, J. C. Vartuli and J. S. Breck, Nature 359 (1992) 710.

50.	J. R. Goldsmith, Min. Mag. 29, 952 (1952).

51.	M. R. Klotz, US Patent 4,268,420 (1981).

52.	L. M. Kustov, V. B. Kazansky and P. Ratnasamy, Zeolites 7 (1987) 79.

53.	A. V. Kucherov, A. A. Slinkin, G. K. Beyer and G. Borbely, Zeolites 14 (1995) 130.

54.	M. Taramasso, G. Perego and B. Notari, US Patent 4,410,501 (1983).

55.	J. S. Reddy, R. Kumar and P. Ratnasamy, Appl. Catal. 58 (2) (1990) L1.

56.	M. A. Camblor, A. Corma and J. Pérez-Pariente, Zeolites 13 (1993) 82.

57.	M. S. Rigutto and H. van Bekkum, Appl. Catal. 68 (1,2) (1991) L1.

58.	P. R. Hari Prasad Rao, A.V. Ramaswamy and P. Ratnasamy, J. Catal. 137 (1992) 225.

59.	A. Sayari, I. L. Moudrakovski, C. I. Ratcliffe, J. A. Ripmeester and K. F. Preston, Syn. of Porous Mat. 69 (1997) 417.

60.	K. R. Reddy, A.V. Ramaswamy and P. Ratnasamy, J. Catal. 143 (1993) 275.

61.	N.K. Mal, V. Ramaswamy, S. Ganapathy and A.V. Ramaswamy, J. Chem. Soc., Chem. Commun. (1994) 1933.

62.	N.K. Mal, V. Ramaswamy, S. Ganapathy and A.V. Ramaswamy, Appl. Catal. A: General 125 (1995) 233.

63.	N. K. Mal and A. V., Ramaswamy, Chem. Commun. (1997) 425.

64.	J. Kornatowski and M. Rozwadowski, Pol. Patent PL 161696 B1 (1993).

65.	P. S. Raghavan, V. Ramaswamy, T. T. Upadhya, A. Sudalai, A.V. Ramaswamy and S. Sivasanker, J. Mol. Catal. A: Chem. 122 (1997) 75.

66.	S. Chakib, Ph. D. thesis, Univ. of Lyon (1989).

67.	P. B. Vento, Microporous Mater. 2 (1994) 151.

68.	R. D. Shannon, Acta. Cryst. A 32 (1976) 751.

69.	R. Szostak, Stud. Surf. Sci. Catal. 58 (1991) 53.

70.	H. G. Karge, Stud. Surf. Sci. Catal. 105 (1997) 1901.

71.	J. P. Brunelle, *Preparation of Catalysts, II*. B. Delmon, P. Grange, P. A. Jacobs, G. Ponecelet (Elsevier, Amsterdam, 1979) p. 211.

72.	I. Wang, C. L. Ay, B. J. Lee and M. H. Chen, *Proc. Of 9th Inter. Congr. Catal.* (Eds. Chem. Inst., Canada, 1988) p. 324.

73.	R. L. Synder; Ed. R. A. Young, *The Rietveld Method*; IUCr Monographs on Crystallography 5; Inter. Union of Crystallography, (Oxford University, 1993) p. 111.

74.	H. M. Rietveld, J. Appli. Cryst. 2 (1969) 65.

75.	B. Notari, Catal. Today 18 (1993) 163.

76.   T. Inui, Appl. Catal. 18 (1985) 311.

77.   J. I. Goldstein, D. E. Newbury, P. Echlin, D. C. Joy, C. Fiori and E. Lifshin, *Scanning Electron Microscopy and X-ray Microanalysis* (New York, 1983).

78.   F. Crea, A. Nastro, J. B. Nagy and R. Aiello, Zeolites 8 (1988) 262.

79.   G. Engelhardt and D. Michel, *High Resolution NMR of Silicates and Zeolites* (Wiley, New York, 1987).

80.   G. Engelhardt, D. Zeigan, H. Jancke, D. Hoebbel and W. Weiker, Z. Anorg. Chem. 418 (1975) 17.

81.   M. L. Balmer, B. C. Bunker, L. Q. Wang, C. H. F. Peden and Y. Su, J. Phys. Chem. B 101 (1997) 9170.

82.   P. A. Jacobs, H. K. Beyer and J. Valyon, Zeolites 1 (1981) 161.

83.   H. Kosslick, V. A. Tuan, R. Fricke, Ch. Penker, W. Pilz and W. J. Storek, Phys. Chem. 97 (1993) 5678.

84.   H. Karge, Stud. Surf. Sci. Catal. 65 (1991) 133.

85.   D. Trong On, L. Bonneviot, A. Bittar, A. Sayari and S. Kaliaguine, Catal. Lett. 16 (1992) 85.

86.   E. Dooryhee, C.R.A. Catlow, J. W. Couves, P. J. Maddox, J. M. Thomas, G. N. Greaves, A. T. Steel and R. P. Townsend, J. Phys. Chem. 95 (1991) 4514.

87.   J. Sauer, P. Hbza and R. Zaharadnik, J. Phys. Chem. 84 (1980) 3318.

88.   R. Schliebs, D. Heidrich, A. Barth and J. Hoffmann, React. Kinet. Catal. Lett. 10 (1979) 83.

89.   J. M. Thomas and J. W. Thomas, *Principles and Practice of Heterogeneous Catalysis* (VCH: Weinheim, Germany) 1996.

90.   D. Barthomeuf, J. Phys. Chem. 88 (1984) 42.

91.   W. B. Jenson, *The Lewis Acid-base concepts. An Overview* (Wiley, 1980) p. 51.

92.   A. Bittar, A. Adnot, A. Sayari and S. Kaliaguine, Reserach on Chemical Intermediates 18 (1992) 49.

93.   D. Barthomeuf, Stud. Surf. Sci. Catal. 65 (1991) 157.

94.   C. Mirodatos and D. Barthomeuf, J. Catal. 93 (1983) 246.

95.   W. E. Farneth and R. J. Gorte, Chem. Rev. 95 (1995) 615.

96.   D. Barthomeuf, Mat. Chem. Phys. 17 (1989) 49.

97.   A. Goursot, F. Fajula, F. Figueras, C. Daul and J. Waber, Helv. Chim. Acta. 73 (1990) 112.

98. G. D. Price, I. G. Wood and D. E. Akporiaye, *Modelling of Structure and Reactivity in Zeolites* (Academic Press Ltd., London, 1992) p. 19.

99. S. Bhatia, L. Beltramini and D. D. Do, Catal. Rev.-Sci. Eng. 31 (1989-90) 431.

100. N. Y. Chen, T. F. Degnan, and C. Moris Smith, *Molecular Transport and Reaction in Zeolites* (VCH Publishers, 1994) Chap. 3.

101. P. B. Weisz, J. Catal. 6 (1968) 278.

102. R. H. Heck and N. Y. Chen, Appl. Catal. 86 (1992) 83.

103. S. M. Csicery, J. Catal. 23 (1971) 124.

104. C. B. Dartt and M. E. Davis, Catal. Today 19 (1994) 151.

105. C. G. Coe, G. E. Parris, R. Srinivasan and S. R. Auvil, Stud. Surf. Sci. Catal. 28, (1986) 1033.

106. N. Herron, Y. Wang, M. M. Eddy, G. D. Stuky, D. E. Cox, K. Möller and T. Bein, J. Am. Chem. Soc. 111 (1989) 530.

107. P. Enzel and T. Bein, J. Phys. Chem. 93 (1989) 6270.

108. J. Weitcamp, *Catalysis and adsorption by Zeolites*, Eds. G. Öhlmann, H. Pfeifer and R. Fricke (Elsevier, Amsterdam, 1991) p. 21.

109. J. D. Lee, *Concise Inorganic Chemistry*, Fourth Ed. (Chapman and Hall Ltd., London, 1991) p. 684.

110. Matsushita Electric Industrial Co., Jap. Patent 58,219,941 (1983).

111. Matsushita Electric Industrial Co., Jap. Patent 58,191,704 (1983).

112. H. Owen, P. B. Venuto and E. T. Habib, US Patent 4,046,827 (1975).

113. M. Hino and K. Arata, J. Chem. Soc., Chem. Commun. (1980) 851.

114. Mitsubishi Chemical Industries Co., Jap. Patent 8,127,286 (1981).

115. R. L. Mieville, US Patent 4,297,205 (1981).

116. L. A. Bruce, G. J. Hope and J. F. Matthews, Appl. Catal. 8 (1983) 349.

117. D. C. Hargis and L. J. Kehoe, US Patent 4,072,732 (1976).

118. J. Kondo, K. Domen, K. Maruya and T. Onishi, J. Chem. Soc., Faraday Trans. 86 (1990) 3665.

119. J. C. Wu, C. S. Chung, C. L. Ay and I. Wang, J. Catal. 87 (1984) 98.

120. N. K. Nag, J. Fransen and P. Mars, J. Catal. 68 (1981) 77.

121. R. J. Mikowsky and A. J. Silvestri, US Patent 4,128,505 (1975).

122. B. S. Parekh and S. W. Weller, J. Catal. 55 (1978) 58.

123. A. Anderson, W. Kaminsky *et al.*, Angew. Chem. Int. Engl. 15 (1976) 630.

124. Shell, EP 0,110,449 (1983).

125. H. K. Stepien, W. B. Williamson and H. S. Ghandi, Amer. Soc. Auto. Eng. 800 (1980) 843.

126. Rhone-Poulenc Chimie, EP 244, 301 (1986).

127. K. Tanabe, Mol. Chem. and Physics 16 (1986) 67.

128. G. Larsen, E. Lotero, M. Nabity, L. M. Petkovic and D. S. Shobe, J. Catal. 164 (1996) 246.

129. Y. Murakami, M. Inomata, K Mori, T. Ui, K. Suzuki, A. Miyamoto and T. Hattori, *Prep. of Catal. III* (Elsevier Amsterdam, 1983).

130. D. E. W. Vaughan, ACS Sympos. Ser. 368 (1988) 308.

131. R. P. L. Absil and Y. Y. Huang, US Patent 87-131596 (1987).

132. A. J. Herbst and Y. Y. Huang, US Patent 4837396 A (1989).

133. V. Vosmerikov and V. I. Erofeev., Zh. Prikl. Khim. 63 (1990) 2329.

134. T. Romotowski, J. Komorek, J. Stoch and V. M. Mastikhin, Polish J. Chem. (1995) 69.

135. M. Yang and B. Xu, Cuihua Xuebao (Chinese), 17 (1996) 59.

136. G. R. Wang, X. Q. Wang, X. S. Wang, S. X. Yu, Stud. Surf. Sci. Catal. 83 (1994) 67.

137. D.A. Young, US Patent 3,329,480 and 3,329,481 (1967).

138. B. Herbert, L. Heinz, L. Ernst Ingo and W. Friedrich, EP 77, 523 A2 (1983).

139. W. Pang, L. Yu and Y. Wu, Chemical Journal of Chinese Universities 7 (1986) 63.

140. M.K. Dongare, P. Singh, P. Moghe and P. Ratnasamy, Zeolites 11 (1991) 690.

141. R. Fricke, H. Kosslick, V.A Tuan, I. Grohmann, W. Pilz, W. Storek, and G. Walther, Stud. Surf. Sci. Catal. 83 (1994) 57.

142. G. J. Kim, K. H. Kim, W. S. Ko, D. S. Cho, J. H. Kim, Kiongop Hwahak (Japan) 5 (1994) 714.

143. M. Costantini, J.L. Guth, A. Lopez, and J.M. Popa, EP 466,545 (1990); US Patent 5399336 (1995).

144. W. Pang, L. Yu and Y. Wu, Gaodeng Xuexiao Huaxue Xuebao, 10 (1989) 951.

145. Y. Long and W. Pang, Shiyou Jiagong (Chinese) 10 (1994) 56.

146. J. Kornatowski, M. Rozwadoski, W. Lutz, M. Sychev, G. Pieper, G. Finger and W. H. Baur, Stud. Surf. Sci. Catal. 98 (1995) 13.

147. P. Mariaudeau, V. A. Tuan, L. N. Hung, F. Lefebvre and H. P. Nguyen, J. Chem. Soc., Faraday Trans. 93 (1997) 4201.

148. A. Tuel, S. Gontier and R. Teissier, Chem. Commun. (1996) 651.

149. S. Gontier and A. Tuel, Appl. Catal., A 143 (1996) 125.

150. S. M. Wong, M. D. Antonelli and J. Y. Ying, Nanostruct. Mater. 9 (1997) 165.

151. J. Tudor and D. O'Hare, Chem. Commun. (Cambridge) 6 (1997) 603.

CHAPTER 2

Crystalline, microporous Zr-silicate molecular sieves with MFI structure (Zr-Silicalite-1)
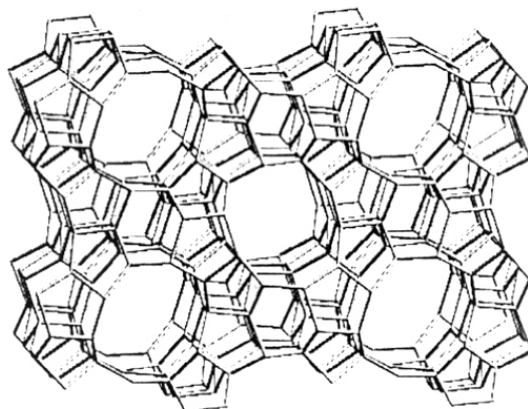
This chapter deals mainly with the synthesis, characterization and catalytic properties of crystalline, microporous Zr-silicate molecular sieves with MFI structure (Zr-Silicalite-1). These zirconium silicates synthesized in an alkaline medium are compared with those synthesized in neutral medium. The physico-chemical and catalytic properties of these samples are discussed.

2.1 INTRODUCTION

The isomorphous substitution of Si^{4+} by other tetravalent metal ions such as Ti^{4+}, Sn^{4+}, etc. in the MFI structure has led to the discovery of selective oxidation catalysis[1-3]. Few attempts were made to synthesize Zr-containing molecular sieves, particularly with MFI structure. Hydrothermal synthesis of Zr- and other Group IVB metal- containing crystalline high silica zeolites with MFI structure was claimed by Young[4]. Subsequently, some publications on the hydrothermal synthesis of Zr-ZSM-5 zeolites in presence[5,6] as well as in the absence[7,8] of Al atoms were reported. The effect of Na_2O/SiO_2 and SiO_2/ZrO_2 molar ratios on the synthesis of Zr[ZSM-5] zeolites and their catalytic properties in phenol hydroxylation has been studied by Wang *et al.*[9]. The hydrothermal synthesis of Al-free Sn- or Zr-containing MFI-type silicalites in the presence of HF/CH_3NH_2 mineralizer and their application in the hydroxylation of phenol and phenol ethers has been claimed by Costantini *et al.*[10]. However, the material showed a lower selectivity for the desired product, viz., hydroquinone, in the hydroxylation of phenol in comparison to the o-product, catechol. No reports were found in the literature about the location and environment of Zr^{4+} ions in the framework.

It is essential to confirm and quantify the incorporation of zirconium in the lattice. For this, one has to compare the physico-chemical as well as catalytic properties of the isomorphously substituted samples with those samples having extraframework zirconium, i.e., Zr-impregnated samples. This is the case with all isomorphously substituted transition metals in the framework. So far, substitution of silicon by zirconium in the framework of ZSM-5 (MFI) by hydrothermal synthesis has not been substantiated by experimental evidence.

Recently, we have reported the synthesis of crystalline Al-free zirconium silicates with MFI structure, using $ZrCl_4$ as a precursor in alkaline as well as in HF/CH_3NH_2 medium[11]. These materials were investigated using powder X-ray diffraction, FTIR, diffuse reflectance UV-visible and ^{29}Si MAS NMR spectroscopic techniques to elucidate the incorporation of zirconium in the MFI framework. Their catalytic activity was tested in the hydroxylation of phenol, using hydrogen peroxide as oxidant and compared them with Zr-impregnated Silicalite-1 sample.

2.2 EXPERIMENTAL METHODS

2.2.1 Hydrothermal synthesis

Zirconium containing, Al-free medium pore molecular sieves (Si/Zr molar ratios = 300 - 50) with MFI structure have been synthesized both in alkaline and in HF/CH$_3$NH$_2$ media. For comparison, a *Silicalite-1* and a *Zr-impregnated silicalite* sample (Si/Zr = 158) were also prepared. An *amorphous Zr-silica* sample (Si/Zr = 158) was also prepared from the precursor gel solution which was not subjected to autoclaving and crystallization.

2.2.1.1 Alkaline medium

The hydrothermal synthesis of zirconium-silicates with MFI structure (Zr-Sil-1) was carried out using the following molar composition of the gel: 1.0 SiO$_2$: x ZrO$_2$: 0.5 TPAOH: 30 H$_2$O, where x = 0.0033 - 0.02 and TPAOH = tetrapropylammonium hydroxide. In a typical synthesis, 0.08 g of zirconium tetrachloride, ZrCl$_4$ (Merck, 99%) in 5 g of distilled water was added to 21.25 g of tetraethyl orthosilicate, Si(OC$_2$H$_5$)$_4$ (Aldrich, 98%) under slow stirring. After 15-20 min. of stirring, 50.84 g of tetrapropylammonium hydroxide, (Aldrich, 20% aqueous) was added dropwise. The stirring was continued for 1 h. The remaining volume (8.0 g) of water was added and the resulting mixture was stirred for further 30 min. to get a homogenous clear gel (pH = 12.25) and was transferred to a stainless steel autoclave. The crystallization was conducted at 433 K for 48 h, under static condition. After the crystallization, the solid product was filtered, washed with deionized water, dried at 383 K and calcined in air at 823 K for 16 h. The product yield was 85 wt.%. Four such samples having different Si/Zr ratios, viz. 300, 200, 100 and 50 were prepared and the samples are designated as A to D, respectively. All Zr-Sil-1 samples were treated with 1 M ammonium acetate solution to remove alkali metal impurities, if any and then further calcined at 773 K in air for 8 h.

2.2.1.2 Neutral medium

The hydrothermal synthesis of Zr-Sil-1 samples was carried out in HF/CH$_3$NH$_2$ medium using the following molar composition of the gel: 1.0 SiO$_2$: x ZrO$_2$: 0.5 TPABr: 3.0 F: 10.0 CH$_3$NH$_2$: 70 H$_2$O, where x = 0.005 - 0.02, TPABr = tetrapropylammonium bromide. In a typical synthesis, 0.23 g of ZrCl$_4$ in 5 g of distilled water was added to a solution containing 6.0 g of fumed silica (Sigma, 99%) and 30 g of water. After stirring for 30 min., 13.2 g of TPABr (Aldrich, 98%) in 20 g of water and 11 g of HF (AR grade,

40% aqueous) in 10 g of water were added. The stirring was continued for 1 h and then, 50 g of methylamine (CH_3NH_2) (40% aqueous) was added dropwise to the reaction mixture. Finally, 10 g of water was added and mixture was stirred for 30 min (pH of the gel = ~~11.0~~ 7.5). Before subjecting this gel to crystallization, 1 - 2 wt.% Silicalite-1 seeds were added to reduce the crystallization time. The milky gel was transferred to a Teflon-lined steel autoclave. The crystallization was carried out at 473 K for 5 h. After the crystallization, the solid product was filtered, washed thoroughly to get chloride free filtrate, dried at 383 K and calcined in air at 823 K for 16 h. The product yield was 75 wt.%. Three such samples having different Si/Zr ratios, viz. 200, 100 and 50 were prepared and the samples were designated as E to G, respectively. The physico-chemical properties of Zr-Sil-1 samples A - G are listed in Table 2.1.

2.2.2 Post-synthesis method: *Zr- impregnated Silicalite-1*

In a typical synthesis of *Zr-free Silicalite-1(Sil-1)*, 50.84 g of TPAOH (Aldrich, 20% aqueous) was added dropwise to 21.25 g of TEOS (Aldrich, 98%) under slow stirring. The stirring was continued for 1 h. Finally, 13.0 g of water was added and the resulting mixture was stirred for further 30 min. to get a homogenous clear gel (pH = 12.25) and was transferred to a stainless steel autoclave. The crystallization was conducted at 433 K for 48 h, under static condition. After the crystallization, the solid product was filtered, washed with deionized water, dried at 383 K and calcined in air at 823 K for 16 h.

For the preparation of *Zr-impregnated Silicalite-1 (Zr-impreg. Sil-1)*, 2 g of this Sil-1 sample was mixed with 0.17 g of $ZrCl_4$ in ~ 5 g of deionized water and made into a fine slurry with stirring for 30 min. The resultant mixture was dried at 383 K. Finally the dried powder was mixed in a mortar to obtain a homogeneous mixture. Then it was calcined in air at 773 K for 8 h to get 3.3 wt.% Zr loading on Silicalite-1.

2.2.3 ^{29}Si liquid NMR spectroscopy of the synthesis gels

Two different methods were used during the gel preparation of Zr-Sil-1 molecular sieves in an alkaline medium and distinguished on the basis of ^{29}Si liquid NMR studies. These methods are summarized in the schematic diagram, Figure 2.1. The course of hydrolysis of TEOS and $ZrCl_4$ by TPAOH was studied systematically. ^{29}Si liquid NMR (59.6 MHz) measurements of the gels were carried out in a Bruker MSL 300 FT-NMR signals arising from the background of the glass tube, the measurements were carried out
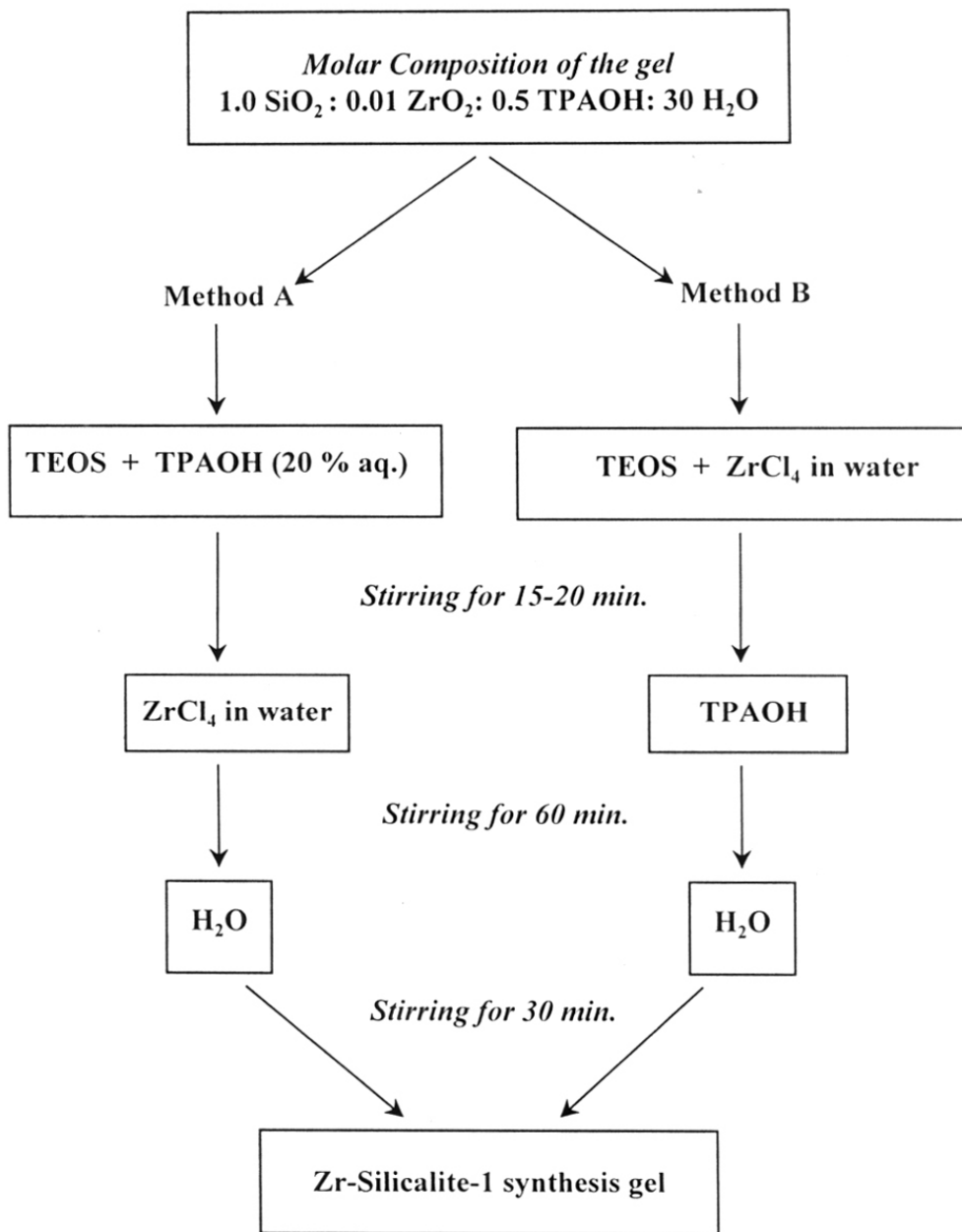
Figure 2.1: Two different methods during the gel preparation of Zr-Sil-1 molecular sieves

using a sealed plastic tube (outer diameter = 10 mm) in non-spinning mode (static) with a horizontal solenoidal coil probe, which is commonly employed for the wide line NMR studies. The chemical shifts were recorded with reference to tetramethyl silane (TMS).

2.2.4 Characterization

The calcined samples were characterized by powder X-ray diffraction, scanning electron microscopy, diffuse reflectance UV-visible spectroscopy, FTIR and NMR spectroscopic methods. The elemental analysis was performed using ICP emission spectroscopy and X-ray fluorescence spectroscopic (XRF) methods. The micropore areas and micropore volumes were determined from the N_2 adsorption isotherms at liquid nitrogen temperature. The possible location of Zr(IV) active sites in the zirconium silicates was investigated on the basis of electronic structure calculations.

2.2.4.1 *Powder X-ray diffraction*

Powder XRD patterns of the calcined Zr-Sil-1 samples were obtained on a Rigaku diffractometer (model D-MAX III VC), using Ni filtered CuKα radiation (λ = 1.5406 Å) and graphite crystal monochromator. The patterns were recorded in the 2θ range of 5° - 50° at a scan rate of $1°min^{-1}$. The samples were subjected to a continuous rotation during the scanning. Silicon was used as an internal standard. All 2θ values were corrected with respect to 2θ value of Si standard at 28.45°. The phase purity of all the samples was checked by comparing the X-ray data available in the literature for silica polymorph with MFI topology[12]. The degree of crystallinity of the calcined samples was determined with reference to a highly crystalline Zr-free Silicalite-1 sample (prepared under similar conditions) as follows:

$$\% \, Crystallinity = \frac{\text{Peak area between } 2\theta = 22.5° - 25° \text{ of the sample}}{\text{Peak area between } 2\theta = 22.5° - 25° \text{of the standard sample}} \times 100$$

The unit cell parameters were calculated from the corrected *d* values and refined by using least squares fitting (HOCT and PDP-11 softwares). In order to determine the extent of isomorphous substitution in the Zr-Sil-2 samples, the calculated values of unit cell volume (UCV) were compared to those of theoretical values using the following equation:

$$V_x = V_{Si} - V_{Si} (1 - d^3_M / d^3_{Si}) x$$

where V_{Si} is the UCV of pure silicalite, d^3_M and d^3_{Si} are the tetrahedral T-O bond distances for the substituted tetravalent metal and silicon atoms and $x = M/(Si+M)$ the atomic ratios in the product (as explained in Chapter 1 of the thesis).

2.2.4.2 Scanning electron microscopy

The morphology and particle size were determined using a Leica Stereoscan 440 scanning electron microscope. The fine powder of the samples was loaded on a metallic sample holder, after dispersing it in ethyl alcohol. It was then coated with a thin layer of silver paste (conductivity paint) to prevent surface charging and to protect any thermal damage due to the electron beam.

2.2.4.3 Thermal analysis

In order to determine the decomposition temperature of occluded template within the channels of the zeolite and also to check the thermal stability of the sample at elevated temperatures, thermogravimetry (TG) and differential thermal analysis (DTA) were carried out using a Setaram TG/DTA – 92 instrument. A dried and as-synthesized sample of about 30 mg was placed in a platinum crucible and α-alumina was used as a reference. The measurements were performed with a heating rate of 10 K min^{-1} in the temperature range of 298 – 1273 K, under air flow.

2.2.4.4 Chemical analysis

In a typical analysis, around 100 mg of sample was heated in a Pt crucible until a constant weight to obtain the dry sample. This anhydrous sample was treated with hydrofluoric acid (HF, 40% aqueous) to remove silicon by evaporation in the form of H_2SiF_6 and SiF_4. After complete evaporation of silicon, the sample was ignited, equilibrated in a desiccator and weighed. The loss in the weight of the sample on ignition was determined to calculate the content of silica. The residue thus obtained was dissolved in 2-3 drops of concentrated sulphuric acid + 10 mL of HF and then transferred to a Teflon container equipped with a tight lid. This solution mixture was heated at 383 K for 6 h. After cooling down the container, the solution was diluted to 100 mL in a plastic volumetric flask and then analyzed with *inductively coupled plasma* (ICP) spectrometer (Model TJA Atomscan-25).

The Si/Zr molar ratios of the calcined samples were also determined by *X-ray*

fluorescence spectrometer (XRF), Rigaku, model 3070, using CuKβ radiation. The samples were analyzed using (99.9%) silica and zirconia samples of similar molar concentrations as external standards.

The surface chemical composition of Zr-Sil-1 samples was studied by *X-ray Photoelectron spectroscopy* (XPS) using a V.G. Scientific ESCA-3, MK II X-ray photoelectron spectrometer. The X-ray radiation used was MgKα (hν = 1253.6 eV). The binding energy values were corrected for charge effects with reference to the C (1s) core level at 285.0 eV.

2.2.4.5 Diffuse reflectance UV-visible spectroscopy

Diffuse reflectance (DR) UV-visible spectra of fine powder samples (about 0.5-0.7 g) were recorded on a Shimadzu spectrophotometer (model UV-VIS 2101 PC). $BaSO_4$ was used as an external standard to correct the baseline in the spectra. All the samples were recorded in the range of 200-800 nm, though only charge transfer transitions in the UV region (200-400 nm) are of interest. No absorptions were found in the visible region.

2.2.4.6 Adsorption methods

The surface area measurements were determined using N_2 as adsorbate on a 100CX Omnisorp system (Coulter) at liquid nitrogen temperature (77 K). The samples were outgassed at 673 K for 3 h prior to the adsorption experiments upto a $p/p_0 = 0.6$, where p is the adsorption pressure and p_0 is the saturation vapour pressure at 77 K. The micropore volume and mesopore area were calculated using *t-plot* method.

The uptake of molecules viz., water, n-hexane and cyclohexane adsorbed over the calcined samples was measured gravimetrically ($p/p_0 = 0.5$) at 293 K on a Cahn (2000G) electrobalance. Samples of 50 mg in the form of pellet were outgassed at 673 K for 5 h prior to the adsorption of probe molecules.

2.2.4.7 ^{29}Si MAS NMR spectroscopy

The solid state ^{29}Si MAS NMR spectra of the samples were obtained at room temperature on a Bruker MSL-300 MHz spectrometer at a resonance frequency of 59.6 MHz. The chemical shifts (in ppm) were recorded with respect to tetramethylsilane (TMS) in an external magnetic field of 7.0 Tesla.

2.2.4.8 Fourier transform infra-red spectroscopy

The framework IR spectra were recorded in the region of $400 - 1300$ cm^{-1} using a 60 SXB Nicolet FTIR spectrophotometer. The samples were prepared by KBr pellet (1:300 mg) technique. For the study of surface acid sites, *in situ* IR spectra were recorded in the hydroxyl region ($4000 - 3000$ cm^{-1}), using self supported wafers which were outgassed in *vacuo* (P = 1.33×10^{-4} Pa) at 673 K and cooled to 323 K. Then these wafers were equilibrated with 0.7 KPa of pyridine for 1h. All spectra were run at a resolution of 4 cm^{-1}, after evacuation of the wafers at various temperatures (373 - 573 K).

2.2.4.9 Electronic structure calculations

The extent of interaction of orbitals in pyridine and zirconium silicate was measured by the magnitude of the one-electron energy level splitting predicted by Extended Hückel Molecular Orbital Calculations. The adsorption characteristics of pyridine over the Brönsted and Lewis acid sites were studied by calculating the interaction energy values of orbitals. The ease of Zr atom substitution at the 12 crystallographically distinct sites in the MFI structure was calculated with respect to substitution energy values.

2.2.5 Catalytic properties

2.2.5.1 Oxidation reactions: Hydroxylation of phenol

The hydroxylation of phenol was carried out using H_2O_2 (Aldrich, 30 % aqueous) as oxidant. In a standard run, 5 g of phenol, 10 g of water and 0.5 g of catalyst were taken in a 50 mL glass round bottomed flask and heated to 353 K in an oil bath. To this, 2.13 g H_2O_2 (phenol /H_2O_2 mole ratio = 3) was added dropwise and the reaction continued for 10 h at the same temperature. The products were analyzed by GC (HP-5880A) equipped with methyl-silicon gum capillary column and a flame ionization detector.

H_2O_2 selectivity was calculated by assuming that the formation of phenol and parabenzoquinone are consecutive reactions and hence considering that 1 mole of parabenzoquinone consumes 2 moles of H_2O_2.

2.3. RESULTS AND DISCUSSION

2.3.1 ^{29}SI liquid NMR spectroscopy of the synthesis gels

Various techniques have been used for the determination of the nature and concentration of the silicate species in aqueous solution[13,14]. Barrer has postulated that

zeolite nuclei are formed from the precursors present as soluble aluminosilicate species in the synthesis gel solutions[15]. The soluble di-, tri-, and tetrameric silicate species (Q^0 - Q^4) in solution are in equilibrium with each other and distribution of such silicate species depends upon the pH, the nature of template, the nature of silica, the metal precursor and the crystallization temperature[14]. Booxhorn *et al.*[16] observed a redistribution of the silicate species in a tetrapropylammonium-silicate solution after the addition of methanol, ethanol or dimethyl sulphoxide. Recently, Kumar *et al.*[17] have studied the nature of soluble silicate species during the crystallization in the presence of promoter ions by ^{29}Si liquid-state NMR studies. However, no report is available on the nature of silicate precursors, formed during the gel preparation of the zirconium silicate molecular sieves. In our investigation, ^{29}Si liquid-state NMR experiments of the gels were carried out in order to study the changes that occur during the precrystalline stage. Since these zirconium silicates can be prepared from clear gel solutions, an attempt has been made to investigate the entities responsible for the formation of possible Si-O-Zr linkages in Zr-Sil-1 samples.

Two different methods, method A and B were used during the gel preparation of Zr-Sil-1 molecular sieves in alkaline medium. These methods were distinguished on the basis of ^{29}Si liquid NMR studies (Figure 2.1). In *method A*, Zr precursor, $ZrCl_4$ in water was added to tetraethyl orthosilicate (TEOS) prior to its hydrolysis by tetrapropylammonium hydroxide (TPAOH) whereas in *method B*, $ZrCl_4$ in water was added after complete hydrolysis of TEOS by TPAOH.

A spectrum of TEOS showed a sharp signal at - 82.5 ppm, which is characteristic of silicate species (Figure 2.2 a). In *method A*, $ZrCl_4$ was added to TEOS, stirred for 20 min. and then TPAOH was added. On addition of $ZrCl_4$ to TEOS, no significant changes were observed. Thus TEOS acts only as a solvent for $ZrCl_4$ and intermittent stirring of the gel gives a clear solution. To this solution, addition of TPAOH initiates hydrolysis of $Si(OC_2H_5)_4$ (TEOS) to form the monomeric $Si(OH)_4$ species, Q^0 at – 72.2 ppm (Figure 2.2 b). On further stirring for 30 min., these species immediately react to combine with other monomeric species to form Q^1- Q^3 species (Figure 2.2 c). Figure 2.2 d indicates that Q^0 species almost disappears and Q^3 (- 99.7 ppm) species predominates over Q^1 (- 81.9 ppm), Q^2 (- 90.3 ppm) and Q^4 (- 110.6 ppm). In addition, ^{29}Si NMR clearly shows that the relative concentration of Q^3 species increases with time. A trend of the concentrations of these species is: Q^3> Q^2 >Q^4> Q^1.
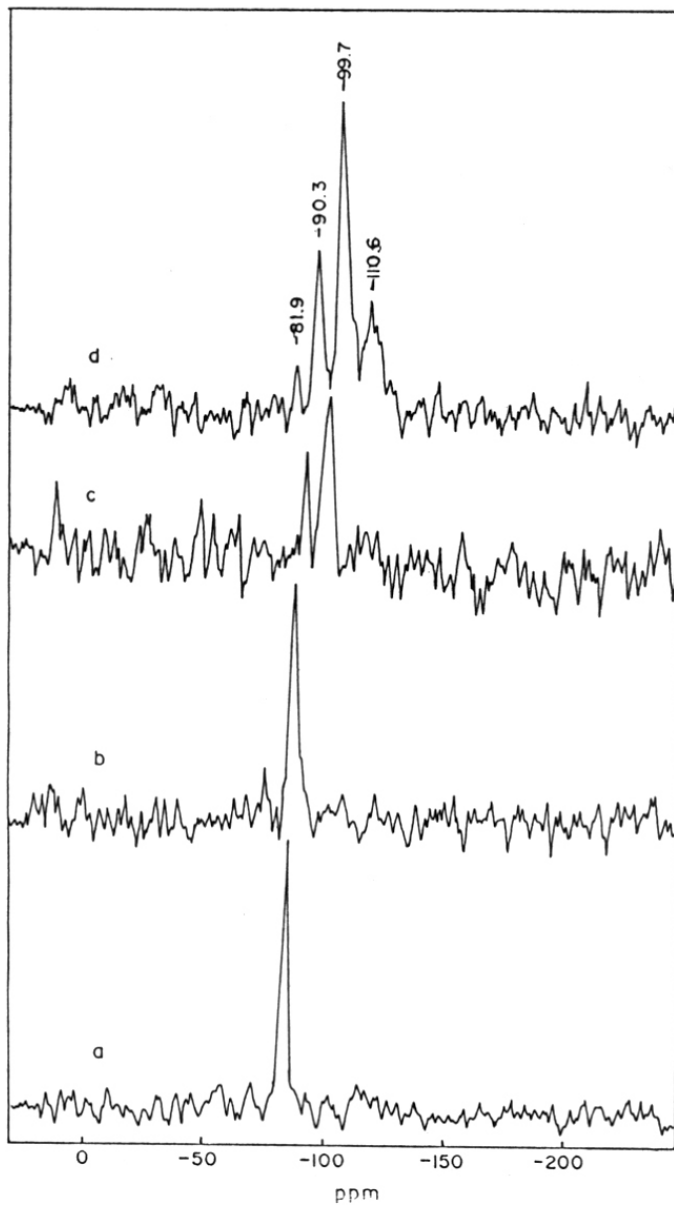
Figure 2.2: *Method A:* ^{29}Si liquid NMR spectra of TEOS **(curve a)**; [1.0 TEOS: 0.01 ZrCl$_4$] stirred for 20 min. and then spectra recorded immediately **(curve b)**; after addition of TPAOH to the gel (b) and stirred for 30 min. **(curve c)**; on further stirring for 60 min. **(curve d)**, respectively.

The reaction is almost complete within 30 min. Further stirring of the gel for 60 min. did not show any significant change in the nature of silicate species.

In *method B*, addition of TPAOH to TEOS under stirring for 10 min., induced hydrolysis of Si(OEt)$_4$ immediately (Figure 2.3 a). Further stirring for 30 min. resulted in the rapid transformation of Q^0 (- 70.5 ppm) species to Q^1 (-82.2 ppm), Q^2 (- 89.6 ppm) and Q^3 (- 98.7 ppm) species. The concentrations of Q^3 and Q^2 species were nearly the same. The stirring of reaction mixture was further continued for 30 min. and then ZrCl$_4$ was added to the gel. After the addition of ZrCl$_4$, only a small fraction of Q^4 species (- 108 ppm) was observed, as shown in Figure 2.3 b. However, Q^0 species were still left in the gel and needed some more time to hydrolyze further. Thus the hydrolysis of precursor species was not complete. The trend is as follows:

$Q^3 > Q^2 \approx Q^1 > Q^0 > Q^4$

Further stirring for 60 min. did not lead to any significant changes in the relative concentrations of silicate species present in the gel. Figure 2.3 c shows that the Q^4 species are not well resolved and are present in the form of a broad envelope of resonance centered at − 108 ppm. The trend in the concentrations of the silicate species is as follows:

$Q^3 > Q^2 > Q^1 > Q^4$
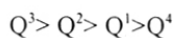
The chemical shift values of NMR signals of the silicate species detected are given in Table 2.1.

Thus, *method A* in which ZrCl$_4$ was added to TEOS prior to its hydrolysis by TPAOH was found to be better than method B in which ZrCl$_4$ was added to the gel after complete hydrolysis of TEOS by TPAOH. These samples obtained through method A were crystallized at 433 K, in 1-2 days with yields of 85%. It could be due to the formation of oligomeric, mainly tetrameric (Q^4) species in the synthesis gel which are responsible for nucleation process and growth of crystals. These oligomers are formed probably through –Si-O-Zr-O-Si- linkages. The samples synthesized by method B, were crystallized at the same temperature, after 3 days with low yields (70%). Therefore, samples synthesized by method A were selected for further characterization and catalytic studies.
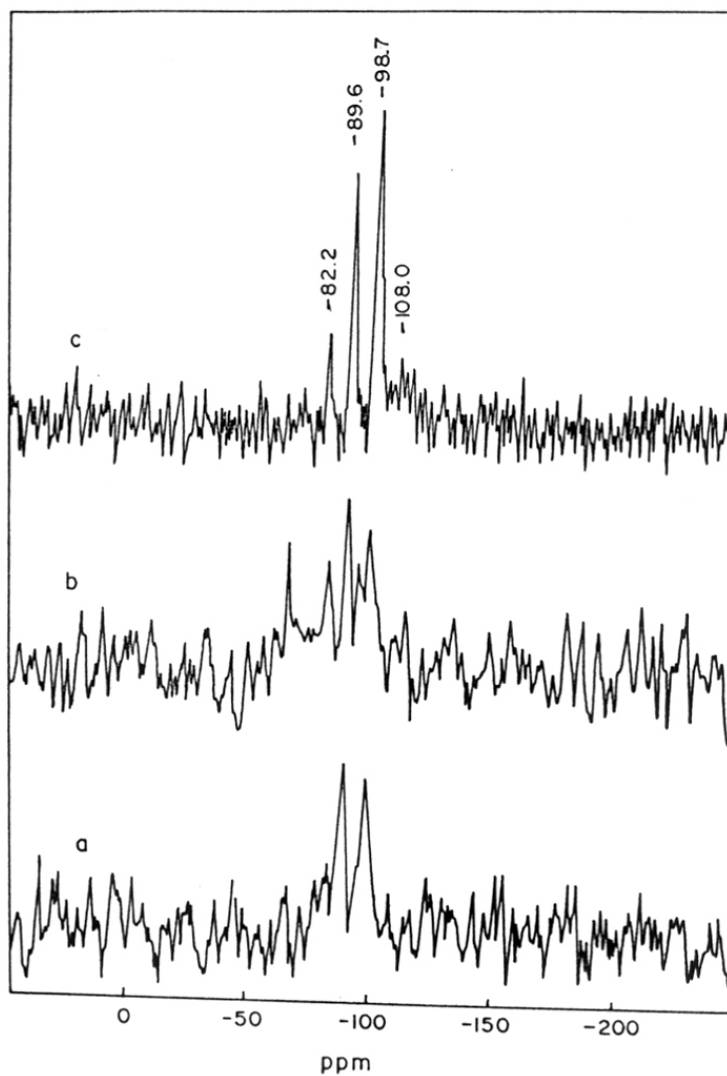
Figure 2.3: *Method B:* ^{29}Si liquid NMR spectra of TEOS **(curve a)**; [1.0 TEOS: 0.055 TPAOH] stirred for 30 min. and then 0.01 M ZrCl$_4$ in water was added and the spectra recorded immediately **(curve b)**; after stirring the gel (b) for another 1 h **(curve c)**, respectively.

Table 2.1: The silicate species in the synthesis gels detected by ^{29}Si liquid NMR.

Silicate Species	^{29}Si Signal (ppm)		Identification
	Method A	Method B	
1. Si(OEt)$_4$	- 82.5	- 82.5	TEOS
2. Si(OH)$_4$	- 72.2	- 70.5	Q^0 (monomer)
3. (OH)$_3$-Si-O-M(OH)$_3$	- 81.9	- 82.2	Q^1
4. (OH)$_2$Si-[OM(OH)$_3$]$_2$	- 90.3	- 89.6	Q^2
5. (OH)Si-[OM(OH)$_3$]$_3$	- 99.7	- 98.7	Q^3
6. Si[OM(OH)$_3$]$_4$	- 110.6	- 108.0	Q^4

M = Si or Zr.

Method A: Si(OEt)$_4$ + ZrCl$_4$ + TPAOH.

Method B: Si(OEt)$_4$ + TPAOH + ZrCl$_4$.

2.3.2 Characterization

2.3.2.1 Powder X-ray diffraction

Figure 2.4 (A) shows XRD profiles of the calcined Sil-1 (curve a) and Zr-Sil-1 samples A to D (curves b to e, respectively). All Zr-Sil-1 samples exhibit a high crystallinity, without any impurity phase. The XRD profiles of Zr-Sil-1 are found to be similar to that of Sil-1 and sample F (curve f), except that they do not undergo symmetry change (orthorhombic to monoclinic), on calcination in air at 773 K. The interplanar d spacings of Silicalite-1 shift to higher values due to the incorporation of the larger zirconium ions (Shannon ionic radii: Si^{4+} = 0.26 Å and Zr^{4+} = 0.59 Å)[18]. There is an increase in the unit cell volume (UCV) from 5321 to 5342 $Å^3$ with decrease in Si/Zr molar ratio (Table 2.2). It is reasonable to consider that this expansion in UCV corresponds to isomorphous substitution of zirconium in the silicalite framework. Figure 2.4(B) compares the experimental UCV with that calculated assuming replacement of Si^{4+} by Zr^{4+} in tetrahedral positions. A very good agreement between the two, within the experimental errors (shown by error bars) up to a metal concentration (x) of 0.0063 (Si/Zr = 158) is observed. But in the case of Zr-Sil-1 sample (D), the UCV is equal to that of Sil-1 sample which may be due to the presence of extraframework zirconium, at higher concentration of zirconium (Figure 2.4 B). It suggests that only a small amount of zirconium (0.6 atom/unit cell) can be incorporated with a uniform distribution within the MFI framework due to its larger size.

2.3.2.2 Scanning electron microscopy

Scanning electron micrograph (SEM) confirms the absence of any amorphous material around Zr-Sil-1 crystals (Figure 2.5 a). The particle size of Sil-1 sample is about 3 - 5 μm while Zr-Sil-1 samples A to D are much smaller (0.2 - 0.5 μm) and are cuboid crystals of uniform morphology. However, the samples E to G, synthesized in HF/CH$_3$NH$_2$ medium form much larger particles (10 - 15 μm) and their morphology is similar to that of a typical ZSM-5 structure. The typical SEM photographs of the representative samples are shown in Figure 2.6.

2.3.2.3 Thermal analysis

All as-synthesized Zr-Sil-1 samples were monitored in the range of 373 -1173 K by TG/DTA analysis (Figure 2.6 A and B). *Thermogravimetric (TG) analysis* showed a sharp
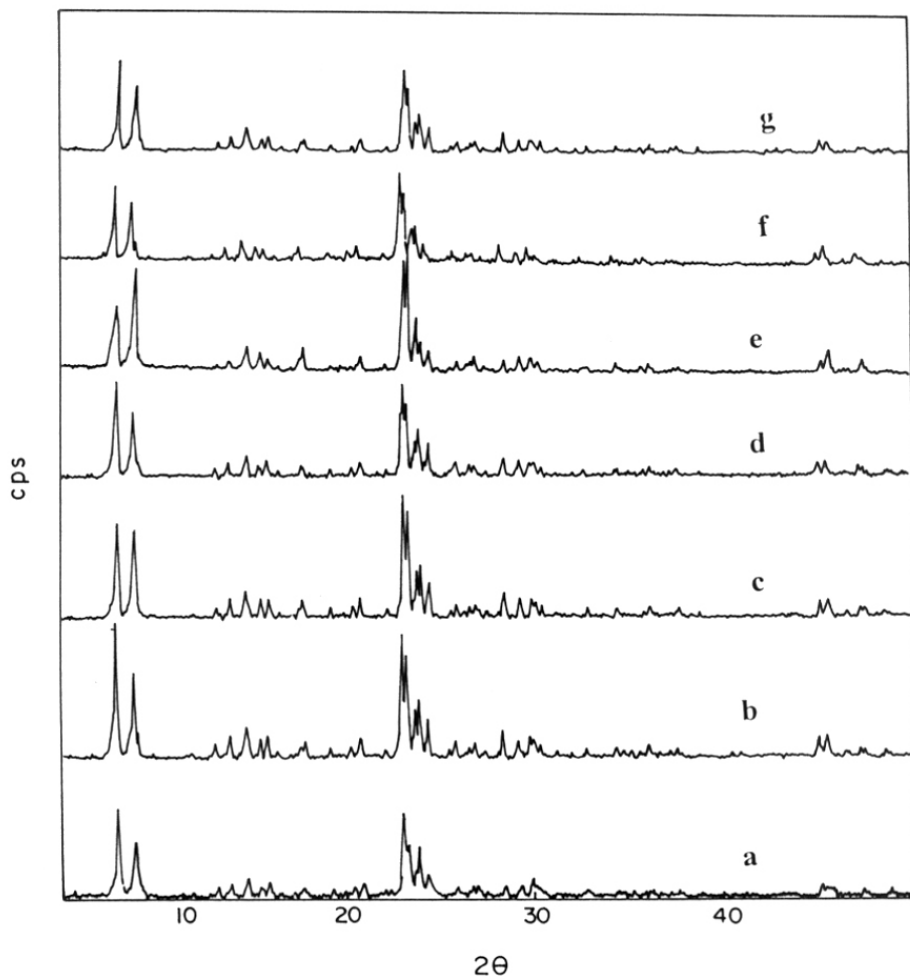
Figure 2.4 (A): X-ray diffraction profiles of calcined Sil-1 sample **(curve a)**, Zr-Sil-1 samples A to D prepared by hydrothermal synthesis in alkaline medium **(curves b to e)** and samples E and F, synthesized in HF/CH$_3$NH$_2$ medium **(curves f and g)**, respectively.
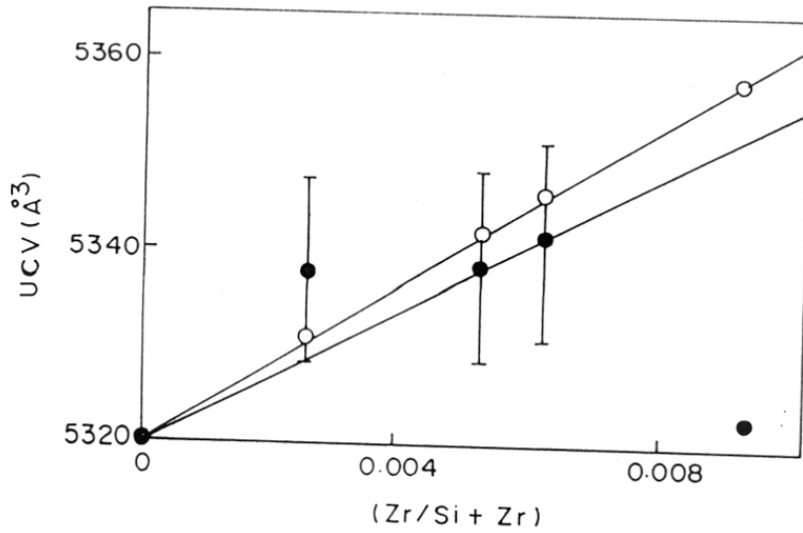
Figure 2.4 (B): The variation of unit cell volume with Zr/(Si+Zr) molar ratios in Zr-Sil-1 samples prepared in alkaline medium (V_{uc}, Å^3), theoretical (o) and experimental (•).

Table 2.2: Unit cell parameters of Zr-Silicalite-1 samples

Sample	Si/Zr (molar ratio) gel	Si/Zr (molar ratio) product	Zr/uc[a]	Unit cell parameters (Å) a	Unit cell parameters (Å) b	Unit cell parameters (Å) c	UCV (Å³)
Silicalite-1	-		-	20.0300	19.8660	13.3730	5321
A[b]	300	355	0.27	20.0600	19.8740	13.3904	5338
B[b]	200	188	0.51	20.0608	19.8742	13.3905	5339
C[b]	100	158	0.61	20.0620	19.9020	13.3800	5342
D[b]	50	105	0.91	20.0201	19.8860	13.3700	5323
E[c]	200	228	0.42	20.0602	19.8860	13.3810	5338
F[c]	100	160	0.60	20.0890	19.8640	13.3823	5340
G[c]	50	116	0.83	20.0673	19.8942	13.3790	5341

[a]Total amount (molar output) of Zr in the product per unit cell.

[b]Samples A to D were synthesized in alkaline medium.

[c]Samples E to G were synthesized in HF/CH_3NH_2 medium.
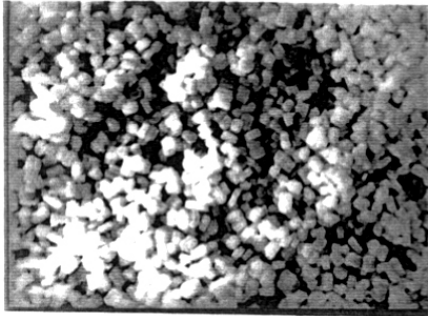
a
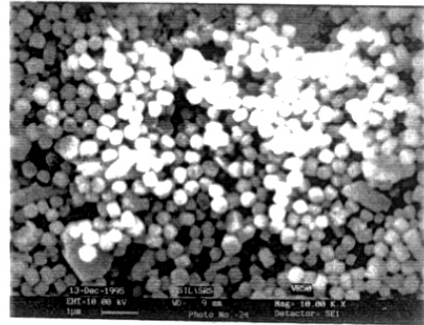
b
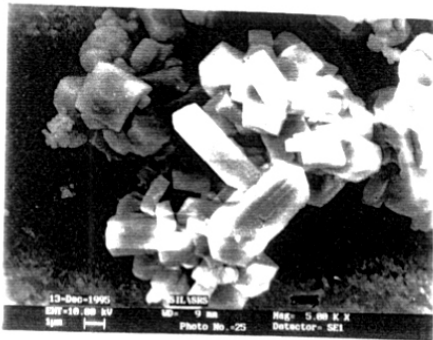
c
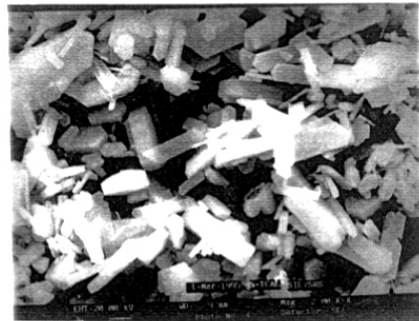
d

Figure 2.5: Scanning electron micrographs of Zr-Sil-1 sample A (a), sample D (b), sample F (c) and Sil-1 (d).

weight loss in the range of 593 – 986 K, which is due to the decomposition of the occluded template within the channels of the zeolite structure. The total weight loss due to removal of the occluded template is about 11.0 – 11.5 wt.% for all samples.

Differential thermal analysis (DTA) for the samples synthesized in alkaline medium and in HF/CH$_3$NH$_2$ medium (samples C and F) showed that the decomposition of template occurs in two distinct steps. The first exothermic peak (weak) observed at 663 K is probably due to the inner strained bulky TPA$^+$ ion, which neutralizes the defect Si-O$^-$ group in the silicalite framework. The second exothermic peak (strong) at 712 – 729 K may be attributed to the removal of more symmetrical TPA$^+$ ions from the channels of the molecular sieve[19]. These peaks are shifted to higher temperatures than that for pure Silicalite-1 (691 K). This increase in the temperature of template decomposition may be attributed to the lattice distortion, as a result of the presence of Zr^{4+} ions in the framework[8] and also due to the stronger interaction of template with Zr^{4+} ions in the framework.

2.3.2.4 X-ray photoelectron spectroscopy

The experimental X-ray photoelectron spectra of Zr-Sil-1(C) sample was resolved using a gaussian fit. As seen in Figure 2.7, Zr-Sil-1 exhibited two peaks for Zr (3d$_{5/2}$) electron with the binding energies (BE) of 174.8 and 184.0 eV (intensity ratio = 1:4), respectively and two peaks for Zr (3d$_{3/2}$) electron with binding energies of 178.4 and 186.0 eV (intensity ratio = 1:3), respectively. It confirms the presence of zirconium in 4+ oxidation state as the main species, in addition to a different coordination which may have Zr = O linkages. The shift in Zr 3d (184 -186 eV) as well as O 1s (535 eV) signals of Zr-Sil-1 towards higher binding energy values than those observed for monoclinic ZrO$_2$ (Zr 3d = 183 eV and O 1s = 534 eV) indicates the presence of well dispersed zirconium atoms in the crystalline material. This suggestion is supported by XPS studies of Zr$_{76}$Fe$_{24}$ Metglass[20] wherein a similar shift in the binding energies, due to metallic Zr and ZrO$_2$ species was observed.

2.3.2.5 Diffuse reflectance UV-visible spectroscopy

Diffuse reflectance UV-visible spectrum of sample C (Si/Zr = 158) (Figure 2.8,
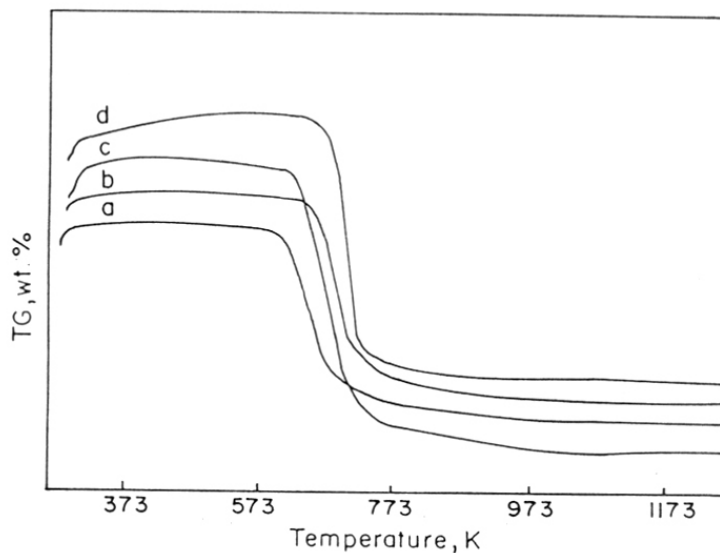
Figure 2.6(A): Thermograms (TG) of Sil-1 **(curve a)**, Zr-Sil-1 samples A, C and F **(b to d)**, respectively.
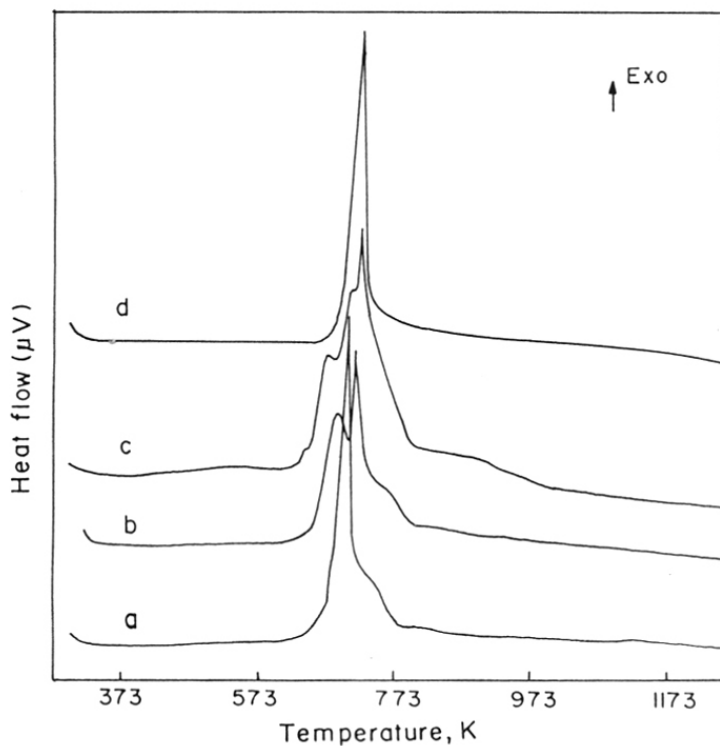
Figure 2.6(B): Differential thermal analysis (DTA) curves of Sil-1 **(curve a)**, Zr-Sil-1 samples A, C and F **(curves b to d)**, respectively.
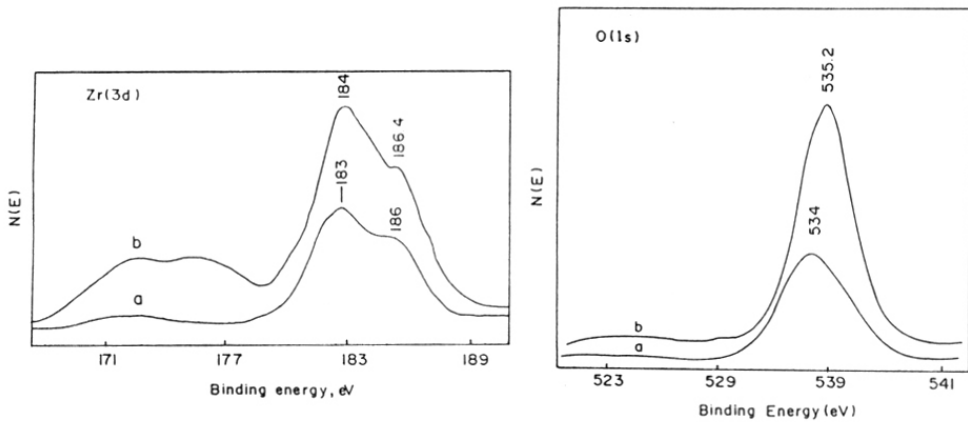
Figure 2.7(A): X-ray photoelectron spectra: Zr 3d and O1s spectra of ZrO_2 and Zr-Sil-1 sample C **(curves a and b)**, respectively.
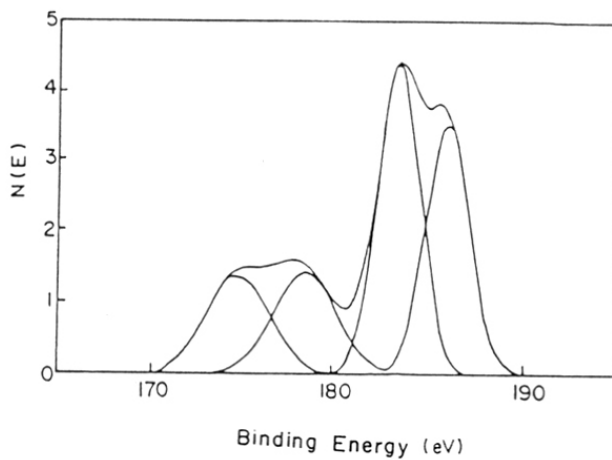
Figure 2.7(B): X-ray photoelectron spectra resolved using a gaussian fit: of Zr-Sil-1 sample C.
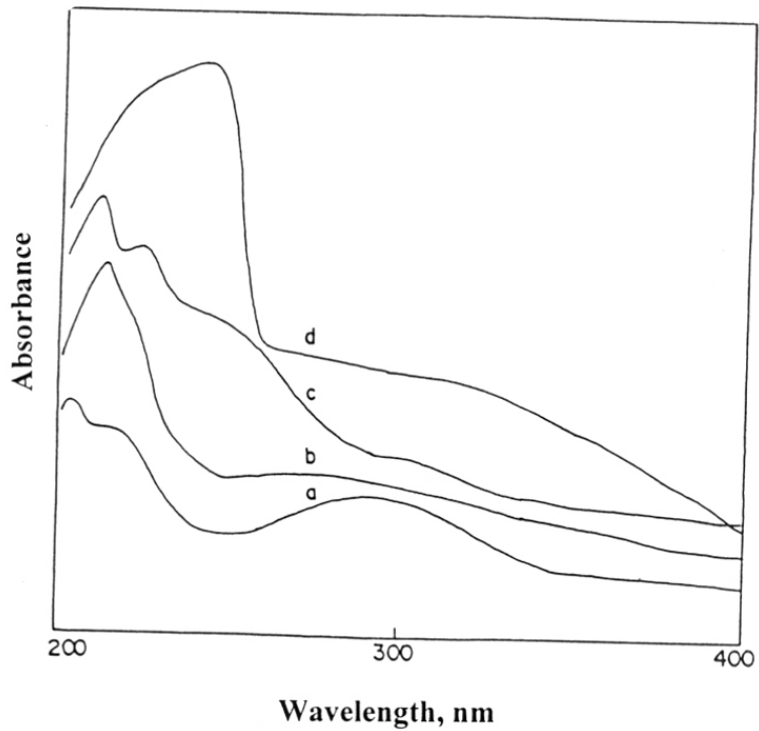
Figure 2.8: DR UV-visible spectra of Zr-impreg. Sil-**1 (curve a)**, Zr-Sil-1 sample C **(curve b)**, sample E **(curve c)** and pure ZrO_2 **(curve d)**.

curve b) shows the presence of a characteristic absorption at about 212 nm attributable to charge transfer transitions involving the Zr(IV) (tetrahedral configuration) sites[9]. Zr-Sil-1 sample F, prepared in HF/CH_3NH_2 medium in addition shows an absorption at 230 nm (curve c) which may be due to Zr(IV) in other coordinations. This absorption is absent in the spectrum of Zr-impreg. Sil-1 sample (curve a). These electronic transitions are clearly distinguishable from those in pure ZrO_2 (monoclinic symmetry) which shows absorption at about 240 and 310 nm (curve d). It confirms the atomic dispersion of Zr(IV) species in the form of Si-O-Zr linkages and not in the formation of Zr-O-Zr species.

2.3.2.6 Adsorption methods

The N_2 adsorption isotherms of Zr-Sil-1 samples are characteristic of microporous materials (Figure 2.9). The Sil-1 and sample F (Si/Zr = 158) in HF/CH_3NH_2 medium showed a sharp step in the adsorption isotherm while Zr-Sil-1 samples A to D in alkaline medium did not show such changes. The higher amount of N_2 adsorption in the zeolite channels is probably due to the presence of defect sites in the framework of the samples synthesized in alkaline medium[21]. The micropore areas for samples A-D are in the range of 386 - 436 m^2/g as against a value of 291 m^2/g obtained for Sil-1 while the samples synthesized in HF/CH_3NH_2 medium showed a decrease in the surface area, due to its bigger particle size (Table 2.3).

2.3.2.7 ^{29}Si MAS NMR spectroscopy

Only a few reports of solid state ^{91}Zr NMR spectroscopy are available in the literature, which depicts the various phases of zirconia by their distinctive nuclear quadrupolar patterns[22,23]. However, it is difficult to record ^{91}Zr NMR signals for the samples with a lower Zr content. Therefore, attempts have been made to study the effect of precursors in the $ZrO_2.4SiO_2$ material using solid-state ^{29}Si NMR spectroscopy[24].

Since Zr^{4+} is a quadrupolar nuclei, it was not possible to get information on the local coordination of Zr^{4+} by MAS NMR experiments. ^{29}Si MAS NMR analysis of samples A to G exhibited predominately an intense and broad signal at -113.7 ppm which was assigned to $Q^4[Si(OSi)_4]$ species. The broadening of this resonance line was observed with an increase in Zr content. This strong signal was flanked by a shoulder at -116 ppm, which was assigned to the distorted Si environment due to Si-O-Si or Si-O-Zr linkages (Figure 2.10). In the case of titanium silicates with MFI structure (TS-1), this peak at -116 ppm has
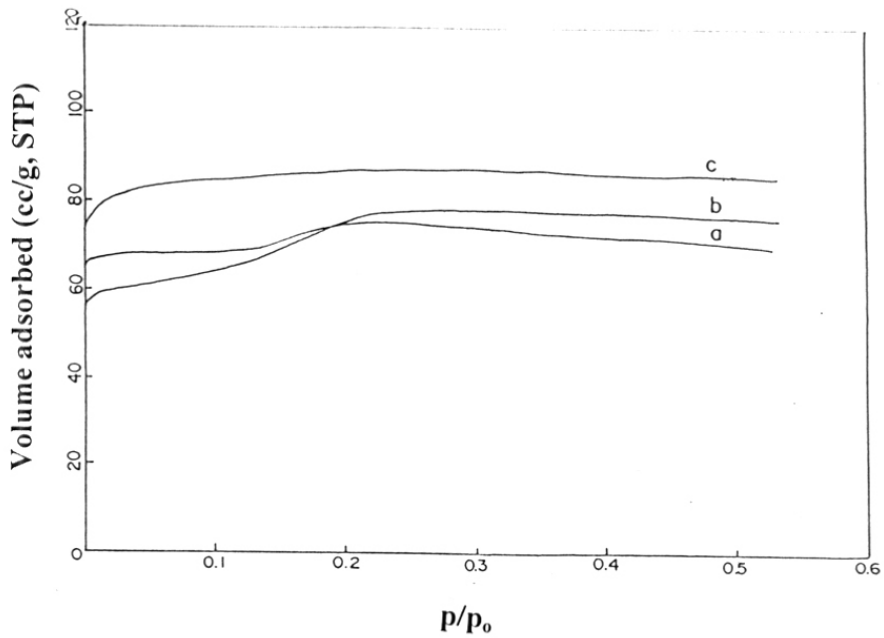
Figure 2.10: Nitrogen adsorption isotherms at 77K of Sil-1 **(curve a)**, Zr-Sil-1 sample F **(b)** and sample C **(c)**.
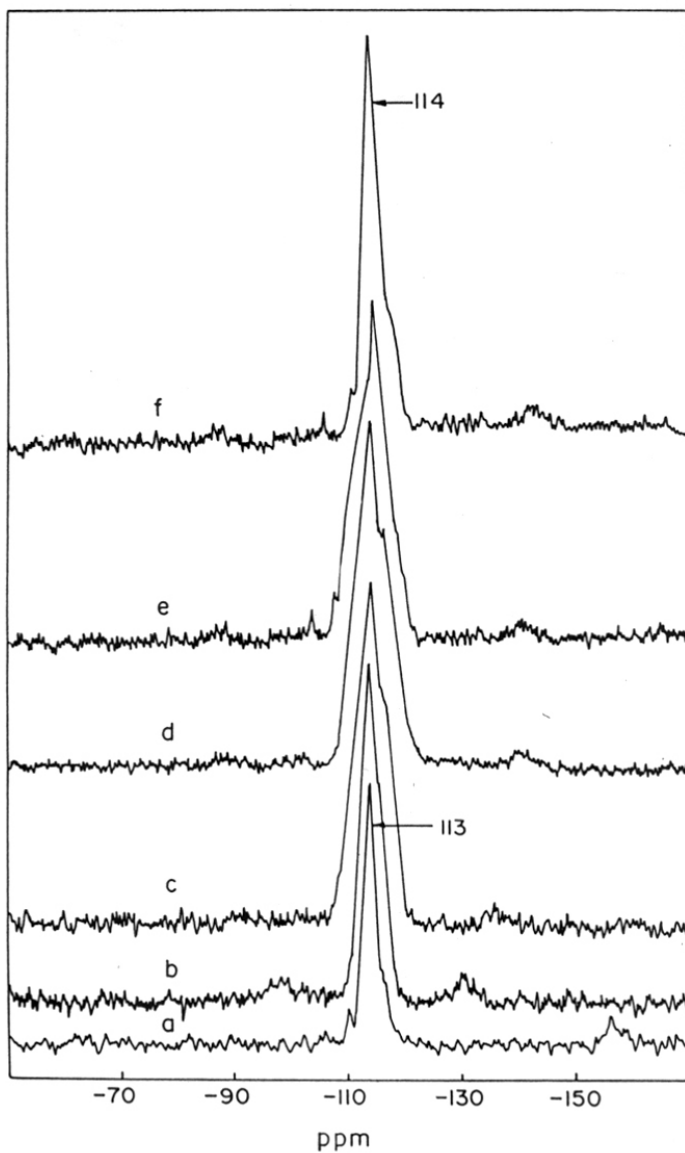
Figure 2.9: ^{29}Si MAS NMR spectra of Sil-1 **(curve a)**, Zr-Sil-1 samples A to D and F **(curves b to f)**, respectively.

Table 2.3: Physico-chemical properties of Zr-Sil-1 samples

| Sample | Zr/uc[a] | $v_{T\text{-}O\text{-}T}$ cm^{-1} | Sorption mass (wt.%)[b] | | | Surface area m^2.g^{-1} | Micropore volume mL.g^{-1} |
			water	cyclo-hexane	n-hexane		
Silicalite-1	-	1100	4.8	4.0	12.5	291	0.16
A[c]	0.27	1108	8.0	4.1	13.0	436	0.18
B[c]	0.51	1107	7.3	6.8	13.3	386	0.16
C[c]	0.61	1103	6.9	4.0	12.8	391	0.17
D[c]	0.91	1101	9.1	7.4	14.0	433	0.18
E[d]	0.42	1106	7.0	6.2	13.4	265	0.16
F[d]	0.60	1101	7.2	4.5	12.9	259	0.17
G[d]	0.83	1100	8.5	7.0	13.6	257	0.18

[a]Total amount (molar output) of Zr in the product per unit cell.

[b]Gravimetric adsorption at $p/p_o = 0.5$ and at 298 K.

[c]Samples synthesized in alkaline medium.

[d]Samples synthesized in HF/CH$_3$NH$_2$ medium.

been attributed to the distorted tetrahedral silicon environment, containing Si-O-Ti linkages[25]. These results indicated that Zr^{4+} ions are probably linked to the defect silanol groups in tetrahedral coordination.

The amounts of water, n-hexane and cyclohexane probe molecules adsorbed on the samples are comparable to that of Sil-1 (Table 2.3). The sorption capacities of Zr-Sil-1 indicate the absence of any pore blockage due to occluded or amorphous material in the microporous structure.

2.3.2.8 FTIR spectroscopy

(i) Isomorphous substitution

The framework FTIR spectra (Figure 2.11) shows a shoulder (sh) at about 965 cm^{-1} which may be attributed to Si-O-Zr asymmetric stretching vibrations (v_{as}), on substitution of Zr^{4+} in the Si-O-Si linkages[26]. However, no such absorption was observed in sample F, Zr-impregnated Sil-1 or amorphous Zr-silica. A similar band near 960 cm^{-1} has been reported for the SiO_2/TiO_2 and titanium silicates (TS-1 and TS-2) typically representing the asymmetric stretching vibrations of Si-O-Ti linkages[27-30]. For well dispersed zirconia on silica, Dang et al.[31] have observed a band at 945 cm^{-1} from difference IR spectra and attributed this vibration to the possible formation of Si-O-Zr linkages in their samples. Additionally, a band (sh) at 877 cm^{-1} was observed probably due to stretching vibrations (v_s) of Zr=O species for higher Zr content (sample C)[32,33]. A nearly linear decrease in the position of main T-O-T vibrations (v_{as}) at about 1100 cm^{-1} is observed (Table 2.3) with increasing Zr content in the MFI framework[13].

(ii) Determination of acid sites

In Figure 2.12(A), the IR spectrum of a typical Zr-Sil-1 sample B (Si/Zr = 200) in the hydroxyl stretching region shows a strong band at 3720 cm^{-1} which is due to the presence of terminal silanol (Si-OH) groups on the external crystal surface. A broad band of low intensity at 3683 cm^{-1} can be assigned to Zr-OH groups[34]. In Figure 2.12(B), the infrared spectra of pyridine adsorbed on sample B after evacuation at 373, 473 and 573 K (curves a to c, respectively) are given. The spectra show strong bands at 1600 and 1450 cm^{-1} due to pyridine coordinately bound to Lewis acid sites (v_s modes)[35]. A weak band at 1545 cm^{-1} is assigned to the pyridinium ion, which provides a measure of Brönsted acid sites. However, the desorption of pyridine at increasing temperatures (> 473 K) resulted in preferential removal of pyridine bound to Brönsted relative to Lewis acid sites. A band of
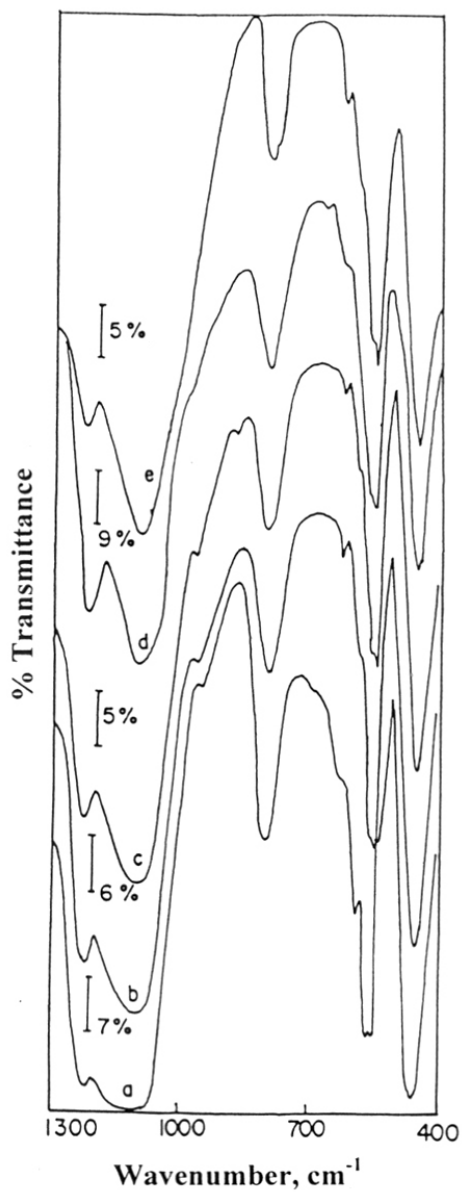
Figure 2.11: Framework FT-IR spectra of Zr-Sil-1 samples A to D (**curves a to d**) and sample F (**curve e**), respectively
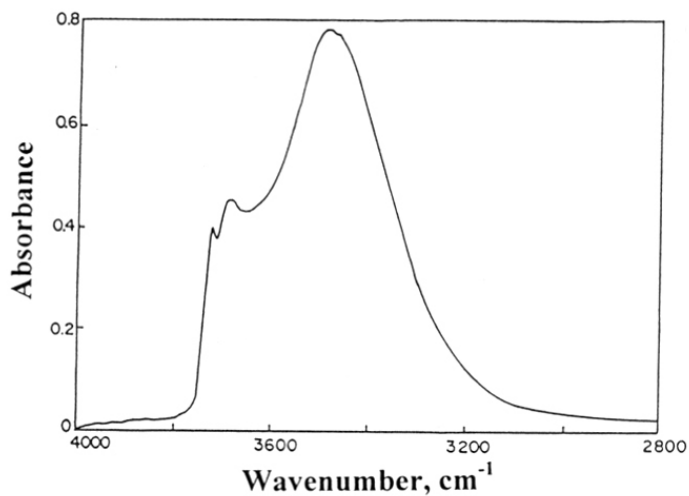
Figure 2.12(A): Infrared spectra of Zr-Sil-1 sample B in the hydroxyl stretching region, after evacuation at 673 K.
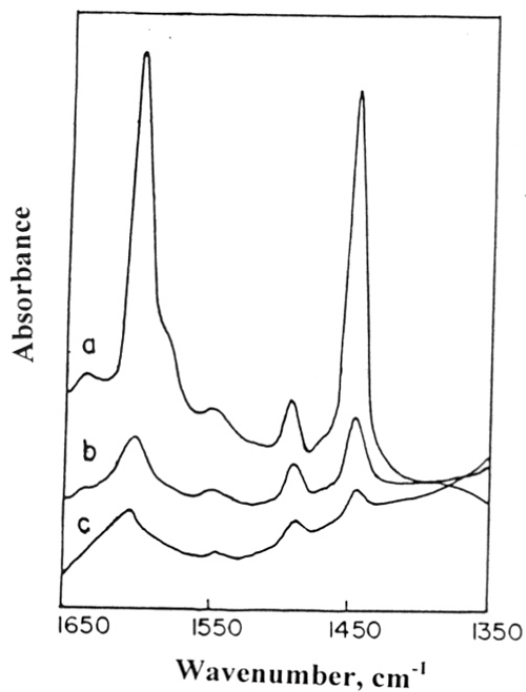
Figure 2.12(B): Infrared spectra of pyridine adsorbed on Zr-Sil-1 sample B after evacuation at 373 K **(a)**, 473 K **(b)** and 573 K **(c)**.

medium intensity at 1490 cm^{-1} due to both the coordinated pyridine and pyridine chemisorbed on protonic acid site (i.e. pyridinium ion) is also observed[36]. Therefore, Zr-silicates with MFI structure appear to be more acidic than Sil-1 and may act as a potential catalyst having most of the desirable characteristics of ZrO_2[31] and still be a part of the MFI crystalline structure.

2.3.2.9 Electronic structure calculations

Standard Extended Hückel Molecular Orbital (EHMO) method[37] has been applied to derive the electronic structure of the model systems. Although *ab initio* calculations are desirable to obtain the quantitative results, EHMO calculations have been used, since these are computationally effective to derive qualitative information on the ordering of orbitals. Our interest was to compare the extent of splitting in one-electron energy levels after interaction of pyridine with Zr-Sil-1 compared to that splitting in the absence of interaction. The ionization potential and the orbital exponent values for various elements are given in Table 2.4. The parameters for all I and II row atoms are the default values[38], while for Zr, the parameters reported by Tomanek *et al.* are used[39]. A double- zeta function was used to define the *d* orbitals of Zr (Table 2.4). The eigen values, eigen functions, Mulliken overlap populations between atoms and the net charges on atoms were computed with the mean Wolfsberg-Helmholtz formula[38].

Bond distances and bond angles for the pyridine molecule and the cluster models of ZrO_2 are as derived from X-ray structure. Lattice energy calculations coupled with efficient energy minimization procedures have been performed[40]. The minimum energy crystal structures were calculated for ZrO_2[41] and several dense phases of silicates[40]. These calculations are shown to predict the complex crystal structures correctly and in fact, the force field parameters are optimized to predict the equilibrium crystal structure. Hence, the geometric parameters of cluster models of ZSM-5 are adopted from the crystal structure reported by Olson *et al.*[42]. There are12 crystallographically distinct Si sites in the crystal structure of ZSM-5. The calculations have been carried out on a cluster model $TO_4[T(OH)_3]_4$ (pentamer), where T = Si or Zr, whose suitability to study the properties of zeolites have been evaluated and established elsewhere[43]. In this pentameric cluster model, the central TO_4 tetrahedral unit is linked to four more TO_4 tetrahedra by corner sharing of oxygen atoms. The valencies of the peripheral oxygen atoms are saturated by bonding to hydrogen atoms, whose positions are same as 'T' sites in the crystal lattice. $SiO_4[Si(OH)_3]_4$

Table 2.4: The parameters used in the EHMO calculations

Orbital		H_{ii} (eV)	$\zeta_1{}^a$	$\zeta_2{}^a$	$C_1{}^b$	$C_2{}^b$
H	1s	-13.600	1.300	–	–	–
C	2s	-21.400	1.625	–	–	–
	2p	-11.400	1.625	–	–	–
N	2s	-26.000	1.950	–	–	–
	2p	-13.400	1.950	–	–	–
Si	3s	-17.300	1.383			
	3p	- 9.200	1.383	–	–	–
Zr	5s	- 6.950	1.817	–	–	–
	5p	- 4.930	1.776	–	–	–
	4d	- 8.610	3.835	1.505	0.636	0.593

[a] = orbital exponent

[b] = contribution factors in the double- ζ functions.

cluster model was used to study the properties of all siliceous MFI structure. The central 'T' site was substituted by Zr, while the four peripheral $T(OH)_3$ groups are $Si(OH)_3$, thus leading to a cluster model of $ZrO_4[Si(OH)_3]_4$. This model shown in Figure 2.13 (a) and (b) is used to represent the isomorphously substituted Zr^{4+} in the place of Si^{4+} ions in the ZSM-5 structure.

The quantity and location of isomorphously substituted metal ions depends on the local geometry of different crystallographic sites and the extent of relaxation due to their possible substitution in place of silicon in the lattice. Hence, the ease of zirconium substitution at the 12 crystallographically distinct sites in the MFI structure has been calculated as substitution energy values. The substitution energy at different sites had similar values with slight preference for Zr^{4+} substitution at sites 2 and 12, where the Si-O distances are the largest and Si-O-Si bond angle values are the smallest. The sites 2 and 12 are common to both straight and sinusoidal channels. The sites 8 and 11 are the least preferred sites for the substitution of Zr^{4+} ions. The sites 8 and 11 never occur in the sinusoidal channel but occur only in the straight channel and hence statistical distribution of Zr in the sinusoidal channel is expected to be higher, as shown in Figure 2.14. However, the ordering of the molecular orbitals remains the same independent of the small variations in the geometry of different crystallographic sites. The energy minimization procedures performed with interatomic potential of central-force ionic models lead to uniform geometries for all the cluster models representing several crystallographic sites. Thus these results bring out the fact that the nature of the acid sites and their interaction with basic molecules such as pyridine are not dependent on the crystallographic location of Zr^{4+} ions in the zeolite lattice.

The interaction of pyridine with Zr^{4+} in the monoclinic phase of ZrO_2 was calculated by analyzing the electronic structure of suitable cluster models shown in Figure 2.13 (c) and (d). The coordination of Zr^{4+} ions in ZrO_2 is seven-fold while it is four-fold coordination (tetrahedral symmetry) in the Zr-Sil-1. The net charges on the atoms are in correspondence with this as given by Mulliken population values. The Lewis acidity of the isolated Zr surrounded by SiO_4 tetrahedra in Zr-Sil-1 sample is stronger than that of Zr in ZrO_2 lattice. This trend is predicted in the terms of binding energy of pyridine, as shown in Figure 2.13. In this Figure, a typical pentameric cluster model is centered at T2 site of the MFI structure wherein pyridine is coordinately bound to Lewis acid site (a) (binding

Zr-Silicalite-1

(a) Pyridine → Lewis acid site

(b) Pyridine → Brönsted acid site

ZrO₂

(c) Pyridine → Lewis acid site

(d) Pyridine → Brönsted acid site

Si
Zr
O
N
C
H
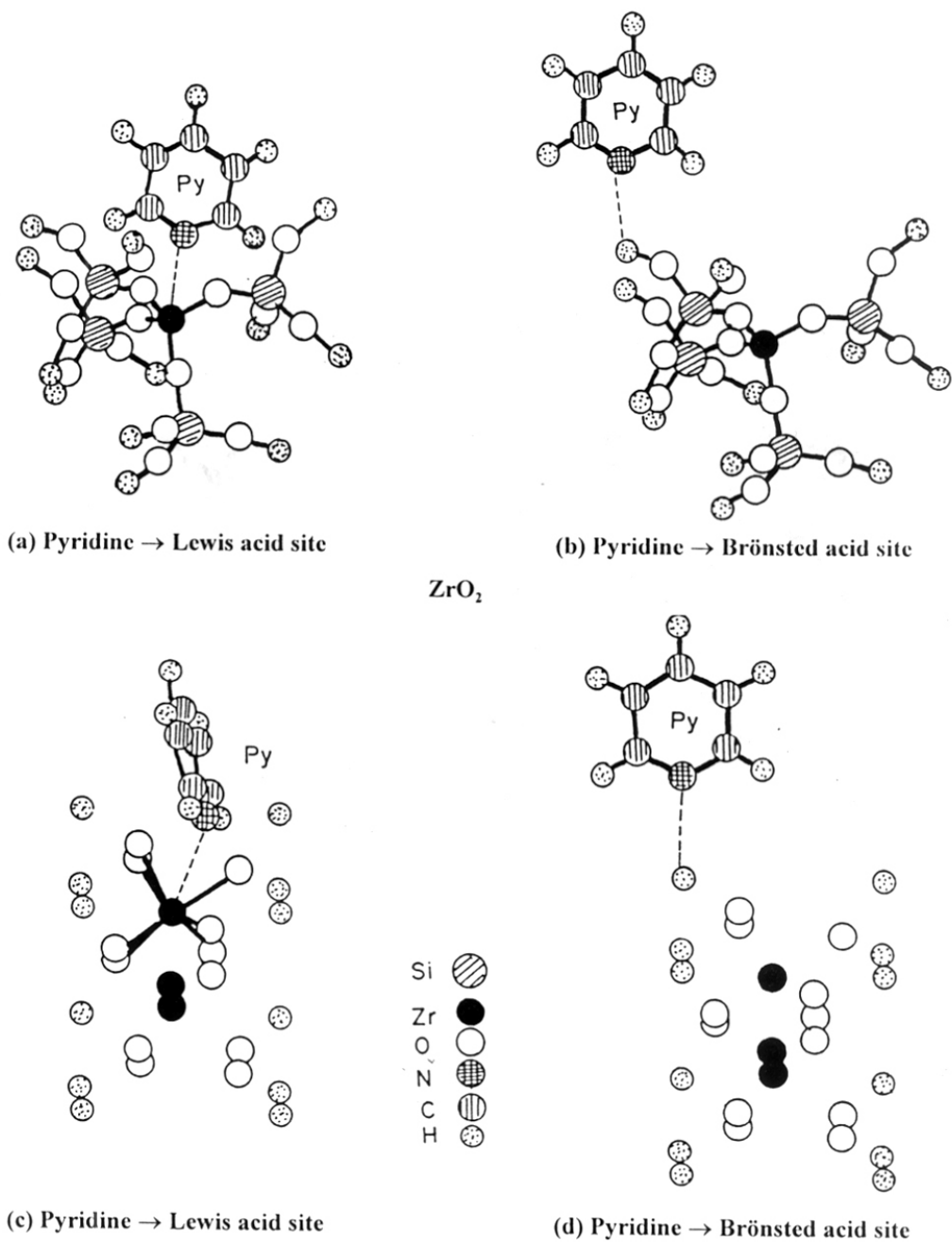
Figure 2.13: The cluster models used in the EHMO calculations. A typical pentameric cluster model centered at T2 site of MFI structure.
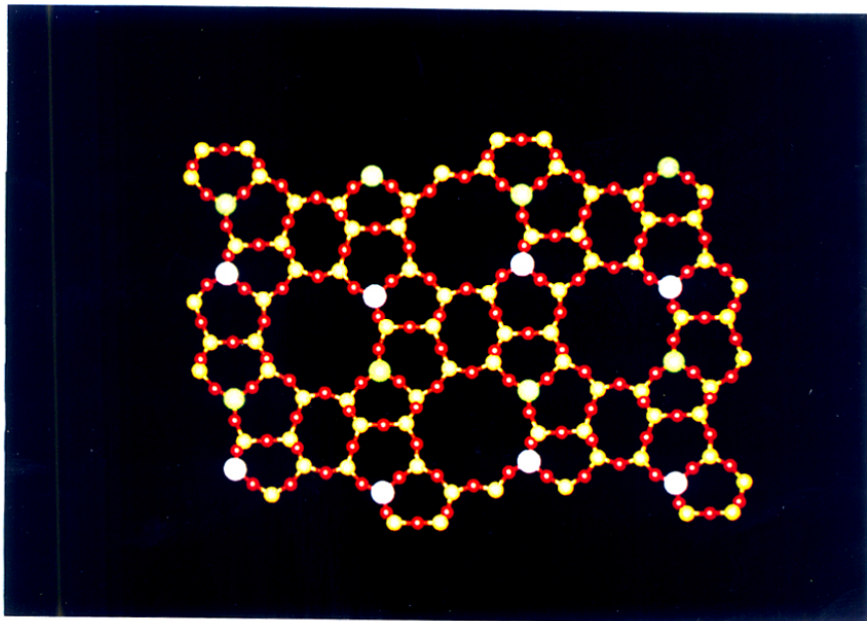
Figure 2.14: Possible location of Zr at the T2 (white) and T12 (green) crystallographically distinct sites of MFI structure.

energy = - 4.37 eV) and bound to a Brönsted acid site (b) as pyridinium ion (binding energy = - 1.79 eV). In the cluster model of monoclinic ZrO_2, pyridine is coordinately bound to Lewis acid site (c) (binding energy = - 2.03 eV) and bound to a Brönsted acid site (d) as pyridinium ion (binding energy = - 1.88 eV). The bonding of pyridine to Zr in ZrO_2 is also hindered due to its relatively crowded coordinations compared to the situation in Zr-Sil-1. The pyridinium ion formation on the surface -Zr-OH groups in ZrO_2 and with the silanol groups in Zr-Sil-1 sample was studied. The binding energy of pyridine with surface hydroxyl groups (Figure 2.13 (b) and (d)) is less when compared to that of binding energy of pyridine coordinated to Zr^{4+} ions (Figure 2.13 (a) and (c)). In the former case, the interaction of lone pair of pyridine is with the hydrogen 1s orbital, while in the latter case, it is with the Zr 4d orbitals. Although, LUMO band is a composite of H 1s and Zr 4d orbitals, the low lying orbitals get more contribution from the 4d orbitals of Zr. The dependence of the stabilization of 4d orbitals on the coordination is also brought out from the results of the calculations on the cluster models shown in Figure 2.13 (a) and (b). The stabilization of e_g orbitals in the tetrahedral coordinations is the cause of stronger Lewis acidity of Zr-Sil-1 samples.

2.3.3 Catalytic reactions

2.3.3.1 Oxidation reactions: Hydroxylation of phenol

Traditionally, hydroquinone was manufactured by oxidation of aniline over stoichiometric amounts of manganese dioxide and strong mineral acid such as H_2SO_4, $HClO_4$ to give p-benzoquinone, followed by reduction with iron and hydrochloric acid (Rhone-Poulenic)[44]. Later on, this process was modified to reduce the formation of by-products. It involved the use of catalytic oxidation of p-diisopropylbenzene followed by acid-catalyzed rearrangement of the bishydroperoxide using Fenton reagent $Fe^{2+}.H_2O_2/CF_3COOH$ (Birchima)[45]. In contrast to these processes, a more cleaner route to hydroquinone was reported using a heterogeneous catalyst such as TS-1 in the presence of aqueous H_2O_2. It catalyzed the hydroxylation of phenol to a mixture of catechol and hydroquinone with 90% H_2O_2 selectivity. The use of H_2O_2 as oxidant offered some advantages such as low cost per oxygen atom and the absence of harmful by-products.

This process has been commercialized by Enichem[46]. The reaction scheme is as follows:
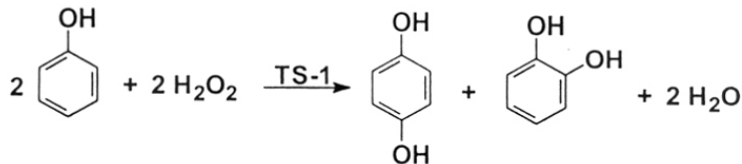
This reaction also provides information about the framework location of substituted heteroatom in the silicalite structure[47,48]. The formation of isolated active centers in the crystal lattice is presumably an important prerequisite for the selective oxidation reactions. Therefore it is also attempted over Zr-Sil-1 samples to study the effect of their intrinsic zirconium (IV) atoms in the hydroxylation of phenol.

(i) Effect of H_2O_2 addition on product distribution

The course of hydroxylation of phenol at 348 K was followed for 24 h with slow addition of H_2O_2 (30 % aqueous) for the initial 1h. Figure 2.15 shows that in the beginning of the reaction, the product selectivities to parabenzoquinone and catechol are quite high and then decrease drastically with time. Upto almost 4 h, a negligible conversion of phenol to hydroquinone is obtained, due to the formation of parabenzoquinone and catechol predominantly. The formation of desired product, hydroquinone increased rapidly after about 6 h and reached to a maximum level at 10 h and then leveled off. A negligible amount of tar was formed during the reaction.

(ii) Effect of intrinsic Zr (IV) sites

The conversions of phenol and H_2O_2 selectivity increase with intrinsic Zr content in the samples up to 0.6 Zr per unit cell. Beyond this limit, again conversion decreases but the selectivity remains the same. These results confirmed that Zr(IV) active centers are uniformly dispersed in Zr-Sil-1 samples. A marginal difference in the product distribution is observed with the increase in Zr content.

The samples showed 34% H_2O_2 selectivity with turn over number (TON) of 112 (Table 2.5). A catechol to hydroquinone ratio of 1.0 - 1.4 for the Zr-Sil-1 samples indicates a certain degree of shape selectivity. A catechol to hydroquinone ratio of 0.9 to 1.3 has been reported for the titanium silicates and vanadium silicates[48]. These results indicate that in addition to being well dispersed, the Zr^{4+} ions are probably located within the channels of MFI structure as active sites.
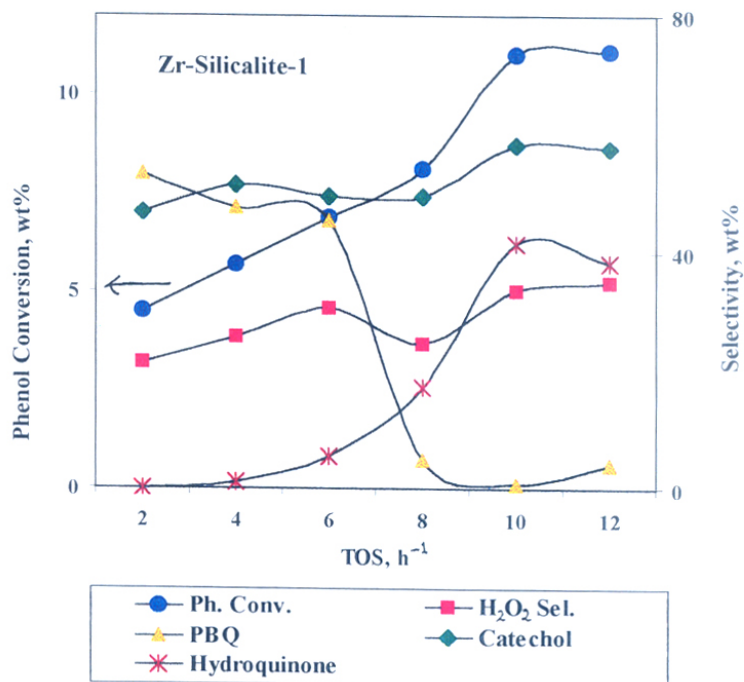
Figure 2.15: A plot of phenol conversion and product selectivities at different time on streams (TOS), h^{-1} in the hydroxylation of phenol over Zr-Sil-1 catalyst.

Table 2.5: Hydroxylation of phenol[a]

Catalyst	TON[b]	H$_2$O$_2$ Sel.	Product distribution (wt.%)[c]		
			PBQ[d]	CAT[d]	HQ[d]
Zr-Sil-1(188)[e]	98.6	24.6	1.3	49.3	49.4
Zr-Sil-1(158)	112.0	33.5	0.8	58.2	41.0
Zr-Sil-1(105)	62.2	27.9	1.3	43.3	54.9
Zr-Sil-1(160)[f]	8.3	2.6	8.2	61.9	29.9
Zr/Sil-1[g]	-	3.0	38.5	58.2	3.3
Amorphous Zr-silica	-	2.4	35.5	62.6	1.9
Sil-1	-	8.5	51.7	47.4	0.9

[a]Reaction conditions: catalyst = 0.5 g; solvent = 10 g; phenol/H$_2$O$_2$ (mol) = 3 ;
reaction duration = 10 h; temperature = 353 K.

[b]Turn over number = Mole of phenol converted per mole of Zr atom.

[c]For formation of parabenzoquinone (PBQ), catechol (CAT) and hydroquinone
(HQ), excluding tar.

[d]PBQ = parabenzoquinone, CAT = catechol and HQ = hydroquinone.

[e]Si/Zr molar output ratio in the parentheses.

[f]Sample synthesized in HF/CH$_3$NH$_2$ medium.

[g]Zr-impregnated Sil-1 (SiO$_2$/ZrO$_2$ = 102).

In order to check the catalytic behaviour of Zr-Sil-1, blank reactions were carried out on Zr-impreg.Sil-1, amorphous Zr-silica sample and Sil-1 samples under identical conditions and were found to have negligible activity in the reaction. Apparently, only those zirconium ions present in the silicalite framework are active in the reaction.

A slight deactivation of the catalyst due to deposition of high molecular weight carbon compounds (tar) after 12 h was observed. After regeneration of the catalyst, original activity for the reaction was found.

(iii) Effect of Crystallite size

The samples synthesized in HF/CH$_3$NH$_2$ medium showed negligible catalytic activity (Table 2.5, sample F) but the product selectivity (catechol/hydroquinone = 2) was different as compared to blank reactions. It is probably due to their bigger crystallite size, which limits the intraporous diffusion.

(iv) Nature of active sites

It is well known in the literature[49] that Group IV-VI transition metals containing-peroxo-species are formed by the reaction of metal oxides or metal complexes with either organic hydroperoxides or hydrogen peroxide. These species have structure (I) and/or structure (II) has been proposed as intermediates or as active centers in several oxidation reactions with hydroperoxides (R = alkyl, aryl) or H$_2$O$_2$ (R = H) as the oxidant.
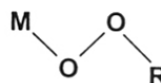
(I) Peroxo- species   (II) Hydroperoxo- species

When these tetravalent metal ions like Ti^{4+}, Zr^{4+}, etc. are incorporated in the silicalite framework, the resulting metallo-silicates are neutral in nature. The origin of activity of these metallo-silicates in the selective oxidation reactions using aqueous H$_2$O$_2$ is believed to be due to the stability of the corresponding metal-peroxo species[50]. The active species and reaction mechanism in the oxidation reactions have been proposed for Ti-containing molecular sieves, on the basis of ESR and EXAFS studies. In this case, a five-membered cyclic hydrogen bonded structure with a titanium hydroperoxo moiety, Ti-OOH, and a protic solvent molecule e.g. water is proposed as active species, as shown below:
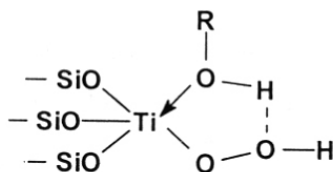
Similarly, it is evident from the structural investigations that Zr-Sil-1 samples contain an appreciable amount of isolated Zr^{4+} *active centers*, which are uniformly distributed within the crystals. Two probable structures have been proposed for these isolated zirconium active centers incorporated in the silica matrix of MFI framework, (I) the zirconyl ($Zr = O$) form and/or (II) the tetrahedrally coordinated forms as shown below:
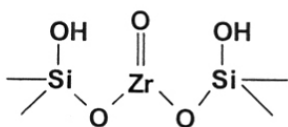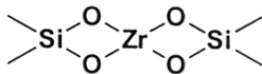
(I)   (II)
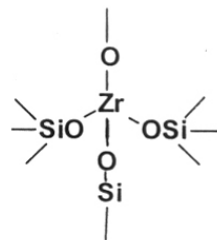
Although FTIR and XPS studies showed the presence of $Zr = O$ species, such type of absorptions ($Zr-O-Zr$ or $Zr = O$) were absent in the UV-visible spectra of Zr-Sil-1 samples. This supports the presence of tetrahedrally coordinated isolated zirconium active sites in the form of Si-O-Zr linkages. Thus, each Zr atom is surrounded by silicon and is isolated from other zirconium atoms by long -Si-O-Si-O- linkages. This isolation of the Zr^{4+} centers is presumed to be a prerequisite for the high H_2O_2 selectivity of Zr-Sil-1 samples in comparison to the Zr-impregnated Sil-1 sample. The precise catalytic reaction mechanism associated with these isolated zirconium active centers is not yet understood. But the key events may be the interaction of H_2O_2 and a protic solvent, water with Zr active site and the transfer of a peroxide oxygen species to the phenol to be oxidized. The reactive intermediate species of these interactions are investigated using ESR and UV-visible techniques and are described in comparison to Zr-Silicalite-2, in Chapter 3 of the thesis.

2.4 CONCLUSIONS

The synthesis of zirconium silicates with different Si/Zr ratios through the two different synthetic routes is carried out. The dependence of the physico-chemical, structural and catalytic properties of samples prepared through the two routes is discussed. Incorporation of Zr^{4+} in the place of Si^{4+} in MFI framework causes an increase in unit cell volume. There seems to be an upper limit on the extent of incorporation of Zr^{4+} in the framework limiting it to 0.6 Zr/unit cell (unit cell volume expansion of 5321-5342 $\mathring{A}^3$). The absence of amorphous matter is confirmed by XRD and SEM studies. The framework IR spectra showed the presence of Si-O-Zr linkages as well as Zr = O type species. The IR spectra in the hydroxyl stretching region showed the presence of Si-OH and Zr-OH groups on the surface. The IR spectra of the adsorbed pyridine showed the presence of strong Lewis and weak Brönsted acid sites. The pyridinium ion at the Brönsted acid sites are weakly bound in correspondence with the Si-OH and Zr-OH type weak Brönsted acid sites predicted earlier. Further, a characteristic absorption at 212 nm in the UV-visible spectrum and the two peaks with binding energy values at 184 and 186 eV for $3d_{5/2}$ and $3d_{3/2}$, respectively in the XPS spectrum support the presence of Zr in tetrahedral coordination.

The catalytic activity based on the hydroxylation of phenol is quite high (TON = 112) for the samples prepared in alkaline medium than those prepared in HF/CH_3NH_2 medium (TON = 8.3). The product selectivity obtained in the reaction indicates the presence of Zr^{4+} in the channels, rather than on the surface. The ordering and shift in the molecular orbitals are not significantly different for monoclinic zirconia and orthorhombic zirconium silicate structures, as derived from the cluster calculations. However the binding energy of pyridine is significantly higher when it is coordinated to zirconium in comparison to the pyridinium ion formation with surface hydroxyl groups.

2.5 REFERENCES

1.   M. Taramasso, G. Perego and G. Bellusi, US Patent 4,410,501 (1983).

2.   G. Bellussi, A. Carati, M. G. Clerici, A. Esposito, R. Millini and F. Buonomo, Belg. Patent 1,001,038 (1989).

3.   N. K. Mal, V. Ramaswamy, S. Ganapathy and A. V. Ramaswamy, J. Chem. Soc., Chem. Commun. (1994) 1933.

4.   D. A. Young, US Patent 3,329,480 and 3,329,481 (1967).

5.   B. Herbert, L. Heinz, L. Ernst Ingo and W. Friedrich, EP 77, 523 A2 (1983).

6.   G. J. Kim, K. H. Kim, W. S. Ko, D. S. Cho and J. H. Kim, Kinogop Hwahak 5 (1994) 714.

7.   M. K. Dongare, P. Singh, P. Moghe and P. Ratnasamy, Zeolites 11 (1991) 690.

8.   R. Fricke, H. Kosslick, V.A.Tuan, I. Grohmann, W. Pilz, W. Storek, and G. Walther, Stud. Surf. Sci. Catal. 83 (1994) 57.

9.   G. R. Wang, X. Q. Wang, X. S. Wang and S. X. Yu, Stud. Surf. Sci. Catal. 83 (1994) 67.

10.   M. Costantini, J. L. Guth, A. Lopez, and J. M. Popa, EP 466, 545 (1990); US Patent 5399336 (1995).

11.   B. Rakshe, V. Ramaswamy, S. G. Hegde, R. Vetrivel and A. V. Ramaswamy, *Catal. Lett.* 45 (1997) 4.

12.   R. von Ballmoos and J. B. Higgins, *Collection of simulated XRD powder patterns for zeolites*, Second Revised Edition (Princeton, 1990).

13.   R. M. Barrer, *Hydrothermal Chemistry of Zeolites* (Academic Press, London, 1983).

14.   G. Engelhardt and D. Michel, *High resolution solid state NMR of silicalite and zeolites* (John Wiley, New York. 1987).

15.   R. M. Barrer, Chem. Br. (1966) 380.

16.   G. Booxhorn, O. Sudmeijar, and H. G. van Kasteren, J. Chem. Soc. Chem. Commun. (1983) 1416.

17.   R. Kumar, A. Bhaumik, R. Ahedi and S. Ganapathy, Nature 381 (1996) 298.

18.   R.D. Shannon, Acta Cryst. A 32 (1976) 751.

19.   F. Crea, A. Nastro, J. B. Nagy and R. Aiello, Zeolites 8 (1988) 262.

20.   S. Sinha, S. Badrinarayananan and A.P.B. Sinha, J. Less - Common Metals 125 (1986) 85.

21.   G. L. Marra, G. Tozzola, G. Leofanti, M. Padovan, G. Petrini, F. Genoni, B. Venturelli, A. Zecchina, S. Bordiga and G. Ricchiardi, Stud. Surf. Sci. Catal. 84 (1994) 559.

22.   T. J. Bastow, M. E. Smith and S. N. Stuart, Sci. Technol. Zirconia V, 5th Int. Conf. (1993) 171.

23. T. J. Bastow, M. E. Hobday, M. E. Smith, S. N. Stuart and H. J. Whitfield, Solid state Nucl. Magn. Reson. 5 (1996) 293.

24. K. W. Terry, C. G. Lugmair and T. D. Tilley, J. Am. Chem. Soc. 119 (1997) 9745.

25. J. S. Reddy, R. Kumar and P. Ratnasamy, Appl. Catal. 58 (1990) L1.

26. R. Szostak, *Molecular Sieves: Principles of Synthesis and Identification* (van Nostrand Reinhold, New York, 1989) p. 317.

27. P.J. Dirken, M.E. Smith and H.J. Whitfield, J. Phys. Chem. 99 (1995) 395.

28. D. Scarano, A. Zeechina, S. Bordiga, F. Geobaldo, G. Spoto, G. Petrini, G. Leofanti, M. Padovan and G. Tozzola, J. Phys. Chem. 89 (1993) 4123.

29. Z. Liu. and R. L. Davis, J. Phys. Chem. 98 (1994) 1253.

30. J. R. Sohn, H. J. Jang, E. H. Park and S. E. Park, J. Mol. Catal. 93 (1994) 149.

31. Z. Dang, B.G. Anderson, Y. Amenomiya and B. A. Morrow, J. Phys. Chem. 99 (1995) 14437.

32. K. Dehnicke and J. Weidlein, Angew. Chem. Inter. Edn. 5 (1966) 1041.

33. D. C. Bradly and P. Thronton, *Comprehensive Inorg. Chem.*, Vol. 3 (Pregamon Press Ltd., 1973).

34. T. Yamaguchi, Catal. Today 20 (1994) 199.

35. C. Morterra and G. Cerrato, Langmuir 6 (1990) 1810.

36. K. Ebitani, H. Hattori and K. Tanabe, Langmuir 6 (1990) 1743.

37. R. Hoffmann, J. Chem. Phys. 39 (1963) 1397.

38. C. J. Ballhausen and H. B. Gray, *Molecular Orbital theory* (W. A. Benjamin Inc, New York, 1965).

39. D. Tomanek, R. Hauert, P. Oelhafen, R. Schlogl and H. J. Guntherodt, Surf. Sci.160 (1985) L 493.

40. C.R.A. Catlow, P. A. Cox, R.A. Jackson, S. C. Parker, G. D. Price, S. M. Tomlinson and R. Vetrivel, Molecular Simulation 3 (1989) 49.

40. V. Butler, C.R.A. Catlow, B.E.F. Fender and J. H. Harding, Solid State Ionics 8 (1983) 109.

41. D. H. Olson, G. T. Kokotailo, S. L. Lawton and W. M. Meier, J. Phys. Chem. 85 (1981) 2238.

42. A. Chatterjee and R. Vetrivel, Micropor. Mater. 3 (1994) 211.

43. F. Bourdin, M. Costantini, M. Jouffret and G. Lartigan, Ger. Patent DE 2,004,497 (1971).

44. P. Maggioni, US Patent 3,580,956 (1972).

45. B. Notari, Stud. Surf. Sci. Catal. 37 (1988) 413.

46.   A. Esposito, C. Neri, F. Buonomo and M. Taramasso, UK Patent 2,116,974 (1983).

47.   G. Perego, G. Bellusi, C. Corno, M. Taramasso, F. Buonomo and A. Esposito, Stud. Surf. Sci. Catal. 28 (1986) 129.

48.   A.V. Ramaswamy and S. Sivasanker, Catal. Lett. 22 (1993) 239.

49.   J. A. Connor and E. A.V. Ebsworth, *Advances in Inorganic Chemistry and Radiochemistry* (H. J. Emeleus and A. G. Sharpe, Eds.), Vol. 6 (Academic Press, New York, 1964) p. 279.

50.   G. Bellusi, A. Carati, M. G. Clerici, G. Maddinelli and R. Millini, J. Catal. 133 (1992) 220.

CHAPTER 3

Crystalline, microporous Zr-silicate molecular sieves with MEL structure (Zr-Silicalite-2)
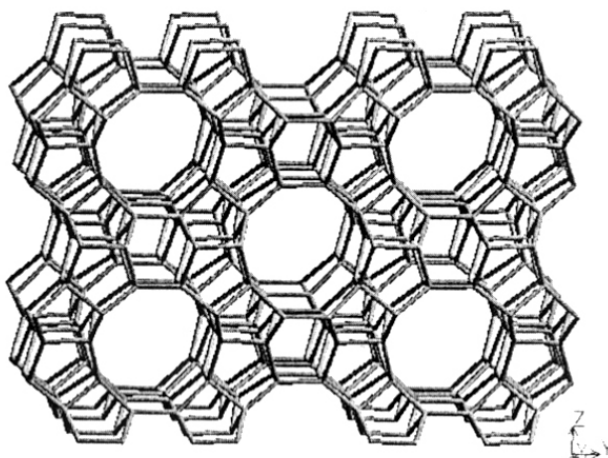
This chapter deals with synthesis and characterization of medium pore, crystalline and microporous Zr-silicate molecular sieves with MEL structure (Zr-Silicalite-2). Their catalytic properties are investigated in the hydroxylation of phenol, decomposition of isopropanol and oxidative dehydrogenation of ethanol.

3.1 INTRODUCTION

The isomorphous substitution of Si^{4+} by Ti^{4+}, V^{4+} and Sn^{4+} in the Silicalite-2 (ZSM-11, MEL) framework has been the subject of some recent reports[1-4]. We have attempted for the first time to substitute Zr^{4+} in the MEL framework[5]. As discussed in chapter 2, it is presumed on the basis of unit cell volume expansion of about 21 $Å^3$ that only 0.6 Zr atom per unit cell of MFI could be incorporated. In this chapter, we have described the synthesis, structural investigations and catalytic properties of similar medium-pore, pentasil silica polymorph with MEL structure. X-ray diffraction, FTIR, diffuse reflectance UV-visible and extended X-ray absorption fine structure measurements elucidate the presence of zirconium in the MEL framework. The acid sites of all the samples are determined by pyridine adsorption studies. Its catalytic activity is tested in the hydroxylation of phenol, using aqueous hydrogen peroxide as oxidant. The reactive intermediates formed in the reaction are compared to those of Zr-Silicalite-1 sample using electron spin resonance and diffuse reflectance UV-visible spectral techniques. As it is well known that ZrO_2 has both acidic and basic properties[6], the effect of possible acid-base properties due to zirconium incorporated in the silicalite lattice is investigated in the decomposition of isopropanol and oxidative dehydrogenation of ethanol.

3.2 EXPERIMENTAL METHODS

3.2.1 Hydrothermal synthesis

Zirconium containing medium pore, Al-free molecular sieves with MEL structure (Si/Zr = 60 - 300) have been synthesized using tetrabutylammonium hydroxide. For comparison, a *Silicalite-2* sample and a *Zr-impregnated Silicalite-2* sample (Si/Zr = 100) were prepared. An *amorphous Zr-silica* sample (Si/Zr = 100) was also prepared from the precursor gel solution which was not subjected to autoclaving and crystallization.

The Zr-Silicalite-2 samples synthesized using two different sources of zirconium, viz., zirconium tetrachloride ($ZrCl_4$) and zirconium tetra-acetylacetonate ($Zr(acac)_4$) are referred to as Zr-Sil-2(A) and Zr-Sil-2(B), respectively.

The hydrothermal synthesis of Zr-Sil-2(A) was carried out using the following molar composition of the gel: 1.0 SiO_2 : x ZrO_2 : 0.4 TBAOH : 30 H_2O, where x = 0.0033 to 0.015. In a typical synthesis, a solution of 25.95 g of tetrabutylammonium hydroxide (TBAOH) (Aldrich, 40% aqueous) was added dropwise to 21.25 g of tetraethyl

orthosilicate (TEOS) (Aldrich, 98%). This mixture was stirred for 30 min. at 298 K in order to complete the hydrolysis of TEOS. To the above mixture, a solution of 0.24 g of ZrCl$_4$ (Merck, 99%) in 5 g of distilled water was added slowly. The resulting mixture was stirred for about 30 min. to get a homogeneous solution. Finally, the remaining volume of water was added and after stirring for 1 h, the liquid gel (pH = 12.20) was transferred to a stainless steel autoclave. The crystallization was conducted at 443 K for three days, under static condition. After the crystallization, the solid product was filtered, washed with deionized water thoroughly until free of chloride ions, dried at 383 K and calcined in air at 823 K for 16 h. The product yield was 80 wt.%. Four such samples having different Si/Zr ratios (60 to 300) were prepared. All the zirconium silicate samples were treated with 1M ammonium acetate solution to remove alkali metal impurities, if any and then further calcined at 773 K in air for 8 h.

3.2.1.1 Effect of different Zr precursors

To achieve greater homogeneity in the gels, several modified sol-gel procedures have been adapted such as prehydrolysis of silicon precursor[7] and retardation of the rate of hydrolysis for the zirconium precursor via incorporation of chelating ligand[8]. Here, we have attempted to study the effect of a different Zr source, Zr(acac)$_4$ on the synthesis gel as well as the crystalline product of Zr-Sil-2 molecular sieves.

The hydrothermal synthesis of Zr-Sil-2 was carried out using Zr(acac)$_4$ (Aldrich, 99%). In a typical synthesis, a solution of 0.48 g of Zr(acac)$_4$ in 50 g of acetone was added to 21.25 g of TEOS. After stirring for 30 min., 25.95 g of TBAOH was added dropwise. The solution thus obtained was kept under stirring for 1 h. Finally, required amount of water was added to it. After stirring for another 30 min., the clear gel (pH = 12.3) was transferred to a teflon-lined autoclave and crystallized under similar conditions as those of Zr-Sil-2 (A). The resultant material was filtered, washed with deionized water, dried at 383 K and calcined at 823 K for 16 h.

3.2.2 Post-synthesis method: Zr- impregnated Silicalite-2

In a typical synthesis of *Zr-free Silicalite-2 (Sil-2)*, a solution of 25.95 g of TBAOH (Aldrich, 40% aqueous) was added dropwise to 21.25 g of TEOS (Aldrich, 98%). The stirring was continued for 30 min. After addition of 19 g of deionized water, the mixture was further stirred for 1 h. Finally, the liquid gel (pH = 12.20) was transferred to a stainless steel autoclave. The crystallization was conducted at 443 K for three days, under static condition. After the crystallization, the solid product was filtered, washed with

deionized water, dried at 383 K and calcined in air at 823 K for 16 h.

For the preparation of *Zr-impregnated Silicalite-2 (Zr-impreg. Sil-2)*, 2 g of this Sil-2 sample was mixed with 0.17 g of $ZrCl_4$ in ~ 5 g of deionized water and made into a fine slurry with stirring for 30 min. The resultant mixture was dried at 383 K. Finally, the dried powder was again mixed in a mortar to obtain a homogeneous mixture. Then it was calcined in air 773 K for 8 h to get 3.2 wt.% Zr loading on Silicalite-2.

3.2.3 ^{29}Si liquid NMR spectroscopy of the synthesis gels

In order to understand the nature of silicate species in the presence of two different zirconium sources, viz., $ZrCl_4$ and $Zr(acac)_4$, ^{29}Si liquid NMR studies of the gels were carried out. The methods of gel preparation for both the methods are summarized in the schematic diagram, Figure 3.1.

^{29}Si liquid NMR (59.6 MHz) measurements were carried out in a Bruker MSL 300 FT-NMR spectrometer at 293 K, using $30°$ pulse with a 5s recycle delay time. The chemical shifts were recorded with reference to tetramethyl silane (TMS).

3.2.4 Characterization

The calcined samples were characterized by powder X-ray diffraction, scanning electron microscopy, diffuse reflectance UV-visible spectroscopy, FTIR, NMR, ESR and EXAFS spectral techniques. The elemental analysis was performed using ICP emission spectroscopy and X-ray fluorescence spectroscopic methods. The micropore areas and micropore volumes were determined from the N_2 adsorption isotherms at liquid nitrogen temperature.

3.2.4.1 Powder X-ray diffraction

Powder XRD patterns of the calcined Zr-Sil-2 samples were obtained on a Rigaku diffractometer (model D-MAX III VC), using Ni filtered CuKα radiation and graphite crystal monochromator. The patterns were recorded in 2θ range of 5° - 50° at a scan rate of $1°min^{-1}$. The samples were subjected to a continuous rotation during the scanning. Silicon was used as an internal standard. The phase purity of all the samples was checked by comparing the X-ray data available in the literature for silica polymorph with MEL topology. The degree of crystallinity of the calcined samples was determined with reference to a highly crystalline Zr-free Silicalite-2 sample (prepared under similar conditions). The unit cell parameters were calculated from the corrected *d* values and refined by using least squares fitting. In order to determine the extent of isomorphous

Molar Composition of the gel
1.0 SiO_2 : 0.0033 - 0.015 ZrO_2: 0.4 TBAOH: 30 H_2O

Method A

Method B

TEOS + TBAOH (40 % aq.)

TEOS + $Zr(acac)_4$ in acetone

Stirring for 30 min.

$ZrCl_4$ in water

TBAOH

Stirring for 30 min.

H_2O

H_2O

Stirring for 60 min.

Zr-Silicalite-2 synthesis gel
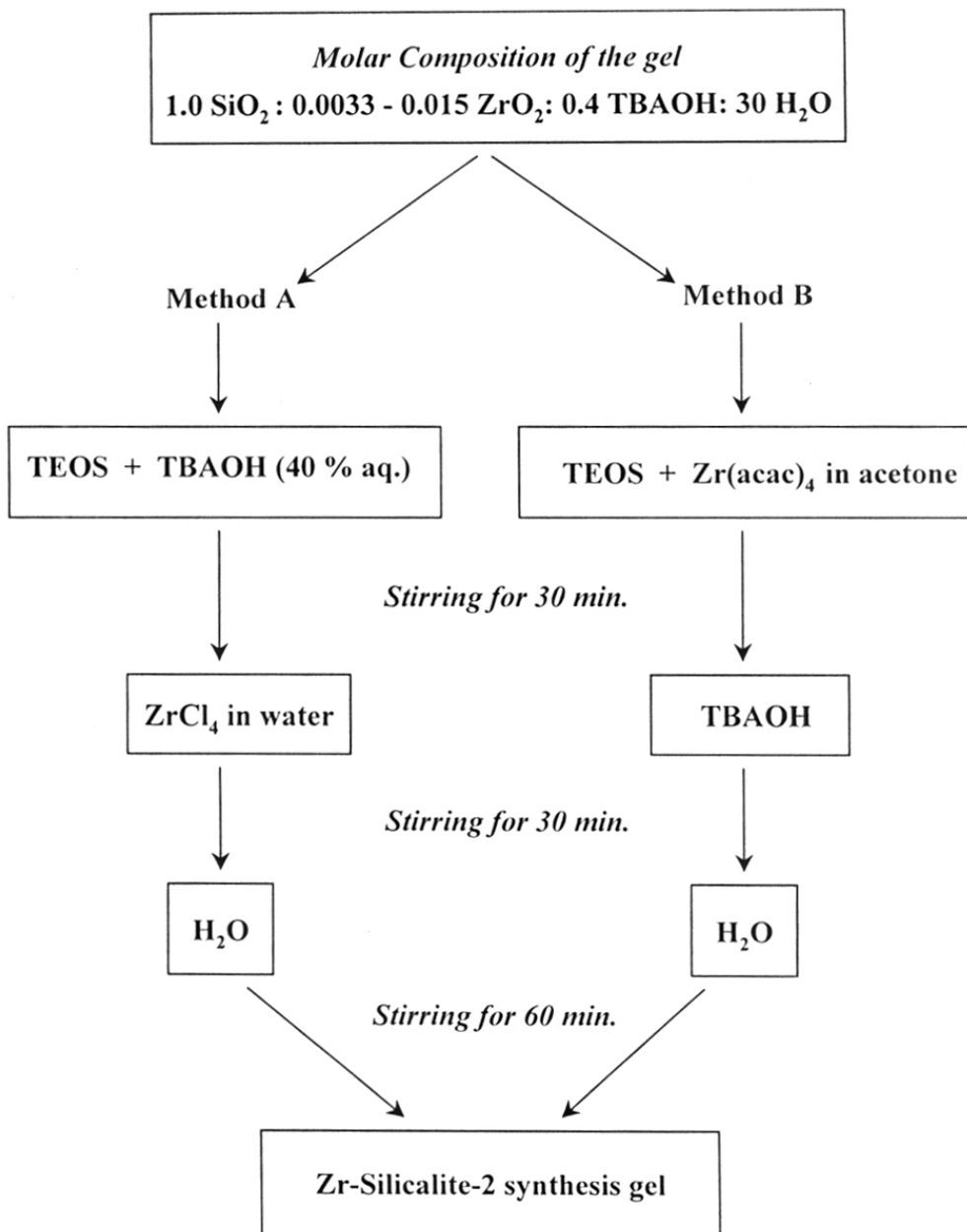
Figure 3.1: Two different methods during the gel preparation of Zr-Sil-2 molecular sieves

substitution in the Zr-Silicalite-2 samples, the calculated values of unit cell volume (UCV).

3.2.4.2 Scanning electron microscopy

The morphology and particle size were determined using a Leica Stereoscan 440 scanning electron microscope. The samples were finely dispersed in a organic liquid, ethyl alcohol on the surface of a metallic sample holder. Then these samples were sputtered with a thin layer of silver paint to prevent surface charging and to protect any thermal damage due to the electron beam.

3.2.4.3 Chemical analysis

In a typical analysis, around 100 mg of sample was heated in a Pt crucible until a constant weight of the dry sample was recorded. This anhydrous sample was treated with hydrofluoric acid (HF, 40% aqueous) to remove silicon by evaporation. The loss in the weight of the sample on ignition was determined to calculate the content of silica. The residue thus obtained was dissolved in 2-3 drops of concentrated sulphuric acid + 10 mL of HF and then transferred to a Teflon container equipped with a tight lid. This solution was heated at 383 K for 6 h. After cooling, the solution was diluted to 100 mL and then analyzed with *inductively coupled plasma* (ICP) spectrometer (model Jobin Yuon-38 VHR) (3600 lines/mm).

The Si/Zr molar ratios of the calcined samples were determined by *X-ray fluorescence* spectrometer (Rigaku, model 3070) using $CuK\beta$ radiation.

3.2.4.4 Diffuse reflectance UV-visible spectroscopy

Diffuse reflectance (DR) UV-visible spectra of fine powder samples (about 0.5-0.7 g) were recorded on a Shimadzu spectrophotometer (model UV-VIS 2101 PC). $BaSO_4$ was used as an external standard to correct the baseline in the spectra.

As this technique is an important tool to get the information on the chemical changes occuring in the first coordination sphere of transition metal ions, we have attempted to monitor the species formed in the samples upon interactions with water and hydrogen peroxide by this technique.

3.2.4.5 Adsorption methods

The micropore areas and micropore volumes ($p/p_o = 0.05$) were calculated from the N_2 adsorption isotherms using a 100CX Omnisorp system (Coulter), at liquid nitrogen temperature. The monolayer volumes were taken at, where all micropores are filled up. The mesopore areas were obtained from the t-plots of N_2 adsorption data at higher partial

pressures.

The amounts of water, n-hexane and cyclohexane adsorbed by the calcined samples were measured gravimetrically at a fixed $p/p_o = 0.5$ at 293 K on a Cahn (2000 G) electrobalance. The samples were equilibrated for 5 h at 673 K prior to the adsorption experiments.

3.2.4.6 ^{29}Si MAS NMR spectroscopy

The solid state ^{29}Si MAS NMR spectra of the samples were obtained at room temperature in a Bruker MSL-300 MHz spectrometer at a resonance frequency of 59.6 MHz. The chemical shifts (in ppm) were recorded with reference to TMS in an external magnetic field of 7.0 Tesla.

3.2.4.7 Fourier transform infra-red spectroscopy

The framework IR spectra were recorded in the region of $400 - 1300$ cm^{-1} using a 60 SXB Nicolet FTIR spectrophotometer. The samples were prepared by KBr pellet (1:300 mg) technique.

The *in situ* IR spectra of adsorbed pyridine were recorded (resolution 2 cm^{-1}) on a Digilab FTS-60 spectrometer after evacuation of the self supported Zr-silicate samples at 773 K for 16 h, adsorption of pyridine at room temperature and subsequent evacuation at 348 - 473 K.

3.2.4.8 Extended X-ray absorption fine structure

Extended X-ray absorption Fine structure (EXAFS) measurements were performed at the Swiss Norwegian Beamline (BM01) at the European Synchrotron Radiation Facility (ESRF), BP 220, F- 38043, Grenoble Cédex, France. The absorption was measured by means of ionization chambers. The beam was unfocussed and a gold mirror was used to reject harmonics.

Prior to these experiments, the samples were pressed into a self-supporting wafer in a special EXAFS cell and it was treated at 673 K in a He flow for 3 h. It was then left in the cell under Helium atmosphere. During the measurement the sample was cooled to liquid nitrogen temperature. The three scans were averaged to obtain a good signal to noise ratio. K-range used for the analysis was $3.00 - 19.00$ Å^{-1}. A Zr-edge EXAFS spectrum of Zr-Sil-2 sample was compared to that of zirconia. XDAP program (MS-DOS version, developed by M. Vaarkamp and D. C. Köningsberger) was used to analyze the experimental data.

3.2.4.9 *Electron spin resonance spectroscopy*

Electron spin resonance (ESR) spectra were recorded at room temperature using Bruker EMX, X-band ESR spectrometer. The calcined powder samples were taken in a quartz cell, suitably designed for in-situ evacuation treatments. Prior to the experiments, the samples were evacuated for 5 h at 673 K and then cooled down to the room temperature. Then it was flushed with H_2 in presence of inert atmosphere (Argon) and then was allowed hydrogen flow in a cell for 5 minutes to adsorb on the sample. It followed by UV-irradition of the samples using UV-lamp (200 – 400 nm) in reduced atmosphere and immediately the ESR spectrum was recorded.

In the case of experiments with aqueous H_2O_2, a freshly calcined sample was contacted with aqueous H_2O_2 at room temperature and then spectra recorded in the presence of different solvents such as water, methanol and acetonitrile. The same sample was then heated at 373 K for 1 h and the spectra were again recorded. The signal to noise ratio was improved by averaging the results of 10 repeated scans.

3.2.5 Catalytic properties

3.2.5.1 Hydroxylation of phenol

The hydroxylation of phenol was carried out, using H_2O_2 (Aldrich, 30 % aqueous) as oxidant. In a standard run, 5 g of phenol, 10 g of water and 0.5 g of catalyst were taken in a 50 mL round bottomed flask and heated to 353 K in an oil bath. 2.13 g H_2O_2 (phenol / H_2O_2 mole ratio = 3) was added to the reaction mixture and the reaction continued for 10 h. The products were analyzed by GC (HP- 5880A) equipped with methyl-silicon gum capillary column and a flame ionization detector. The content of tar obtained in the reaction products was analyzed by thermogravimetric method in an inert atmosphere. H_2O_2 selectivity was calculated by assuming that the formation of phenol and parabenzoquinone are consecutive reactions and hence considering that 1 mole of parabenzoquinone consumes 2 moles of H_2O_2.

Further studies were carried out to locate the reactive intermediate species during the reaction using ESR and UV-visible spectroscopic techniques.

3.2.5.2 Catalytic decomposition of isopropanol

Catalytic decomposition reactions were performed in a down-flow quartz reactor using 1.7 g of Zr-Sil-2 catalyst and isopropanol as a feed (4 mL h^{-1}) at the different temperatures of 398 to 573 K. The gas products (acetone and propene) as well as liquid

products (water, acetone and isopropanol) were analyzed by GC equipped with a 2 m long Porapak-N column and a thermal conductivity detector (TCD). The steady-state catalytic activity was determined at 3 h. The reactions over Zr-impreg. Sil-2 and Zr-free Sil-2 were also performed at 473 K, for comparison.

3.2.5.3 Oxidative dehydrogenation of ethanol

This vapour phase reaction was carried out in a bench top reactor system (BTRS, Autoclave engineers U.S.A.), which is a fixed-bed continuous down-flow stainless-steel reactor (5 cc) under steady-state conditions. The reactions were performed under oxidative conditions to avoid rapid deactivation of catalysts. Ethanol (doubly distilled, 99%) was fed through a HPLC liquid injection pump (Alcott, Model 760) and air (5.3 cc/170 cc) was passed using a mass flow controller (Brooks, Model 5896). The reactants were mixed and vaporized in a preheated oven maintained at 393 K and passed through the reactor (6 mm i.d.). The temperature around the reactor was maintained by a temperature-controlled furnace. The outlet of the reactor was connected to a gas chromatograph (HP-5890 Series II) through a heated transfer line which was maintained at 393 K. An eight-port sampling valve in BTRS was used to inject a known amount of the product sample or reactant (250 μL) to the GC using nitrogen as a carrier gas. The products were analyzed using a capillary column (crosslinked methyl silicone gum, 50 m × 0.2 mm) and a flame ionization detector (FID).

3.3 RESULTS AND DISCUSSION

3.3.1 ^{29}Si liquid NMR spectroscopy of the synthesis gels

High resolution ^{29}Si NMR has been the most successful technique to identify the nature and concentration of the silicate species in the solution phase. The hydrothermal synthesis of Zr-Sil-2 molecular sieves was carried out using two different methods. The method A is addition of $ZrCl_4$ to TEOS after its complete hydrolysis by TBAOH and method B is addition of $Zr(acac)_4$ to TEOS, followed by its hydrolysis, as shown in Figure 3.1. These methods were distinguished by ^{29}Si NMR studies during the gel preparation prior to the hydrothermal synthesis.

The ^{29}Si liquid NMR spectrum of TEOS showed a signal at about - 82.5 ppm which is characteristic of silicate monomers (Q^0) (Figure 3.2 a). Addition of TBAOH to TEOS solution under stirring for 5 min., induced hydrolysis of $Si(OEt)_4$ immediately. It resulted in the rapid transformation of Q^0 (- 75.0 ppm) species to Q^1 (- 78.0 ppm), Q^2

(- 87.1 ppm), Q^3 (- 101.1 ppm) and Q^4 (-108.4 ppm) as evidenced in Figure 3.2 b. The trend was as follows:

$$Q^3 > Q^4 > Q^2 \approx Q^1 > Q^0$$

Once the monomeric species are formed, they immediately react further to combine with other monomeric species to form Q^1 - Q^4 species. Therefore, it was quite difficult to locate the exact time at which only monomeric species are likely to be present in the gels during the hydrolysis of TEOS by TBAOH. Moreover, ^{29}Si NMR clearly shows that the relative concentration of Q^3 species increases with time. On further stirring of the reaction mixture for 30 min., Zr source was added to the gel solution and then ^{29}Si signals were monitored for both the modes of addition. The values of signals of the silicate species detected by ^{29}Si liquid NMR are given in Table 3.1.

In method A, after the addition of $ZrCl_4$, a broad peak of Q^3 species at - 98.8 ppm was observed with a small fraction of Q^4 species. However Q^2 (- 88.8 ppm) is predominant over Q^4 (- 108.1ppm) species (Figure 3.2 c). As Q^4 species appeared, the Q^0 species almost disappeared. The trend in the concentrations of the silicate species was as follows:

$$Q^3 > Q^2 > Q^4 > Q^1$$

Further stirring for 60 min. did not cause any significant change in the Si species present in the gel. All the signals were quite sharp and well resolved. (Figure 3.2 d).

In method B, after the addition of $Zr(acac)_4$ in acetone, the spectrum showed the presence of a small amount of Q^0 species (Figure 3.3(A), curve a). On further stirring for 60 min., it was observed that Q^3 (-98.2 ppm) is predominant over Q^4 species (-107.6 ppm) (Figure 3.3(A), curve b). These Q^4 species are not well resolved and are present as a shoulder of Q^3 peak. In presence of TBAOH, $Zr(acac)_4$ first hydrolyzes to give the rather unstable $Zr(OH)_4$ species. However, the formation of Zr-O-Zr bridges and thus ZrO_2 formation is prevented by the lower concentration of zirconium in the gel (< 1 mol %). After the addition of TBAOH, ^{29}Si NMR shows that Q^2 (-90.0 ppm) and Q^3 species are predominant. The trend in the concentrations of the silicate species was as follows:

$$Q^3 > Q^2 \approx Q^4 > Q^1 > Q^0$$

In this method, all the signals were broad, less intense along with a slight shift in Q^3 and Q^4 signals at lower fields, in comparison to method A. For method B, $Zr(acac)_4$ was first mixed with acetone to allow the dilution of Zr source in acetone. To find out whether
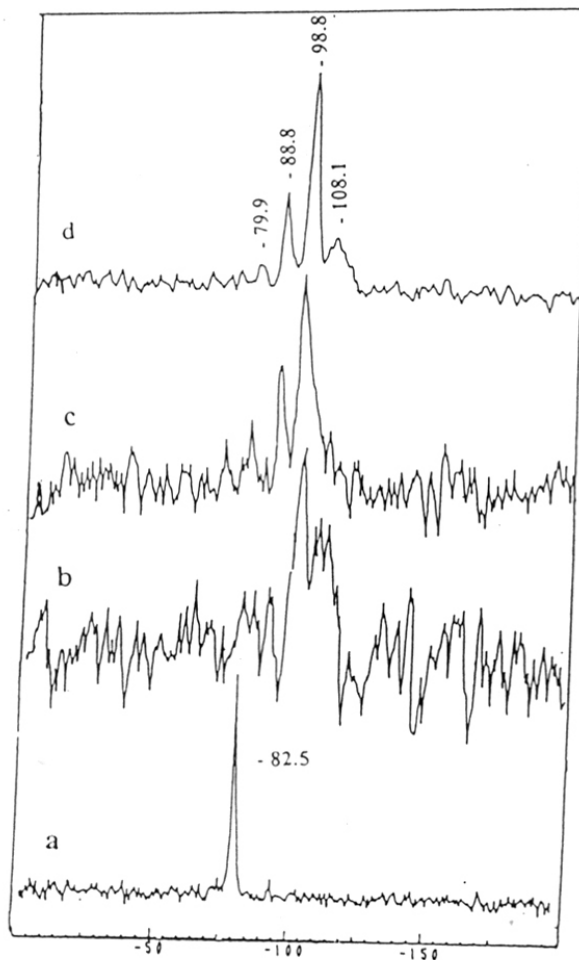
Figure 3.2: ^{29}Si liquid NMR spectra of (**curve a**) TEOS; [1.0 TEOS: 0.4 TBAOH] stirred for 5 min. (**b**); [1.0 TEOS: 0.4 TBAOH] stirred for 30 min. and then 0.01 M ZrCl$_4$ in water was added and the spectra recorded immediately (**c**); after stirring the gel (c) for another 1 h (**d**), respectively.
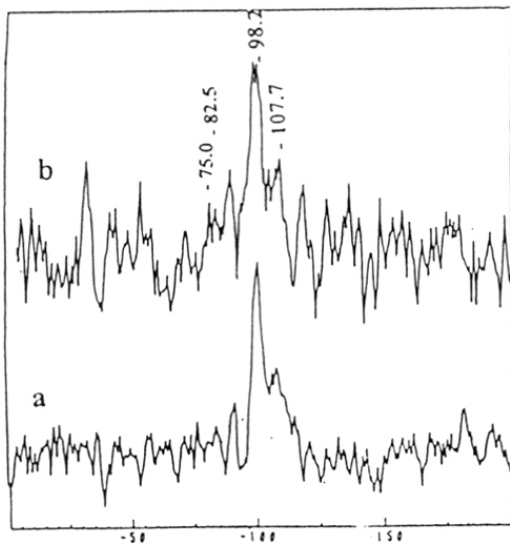
Figure 3.3 (A): ^{29}Si liquid NMR spectra of: [1.0 TEOS: 0.4 TBAOH] stirred for 30 min. and 0.01 M Zr(acac)$_4$ in acetone was added and the spectra recorded immediately (curve a); after stirring the gel **(a)** for another 1 h **(b)**, respectively.
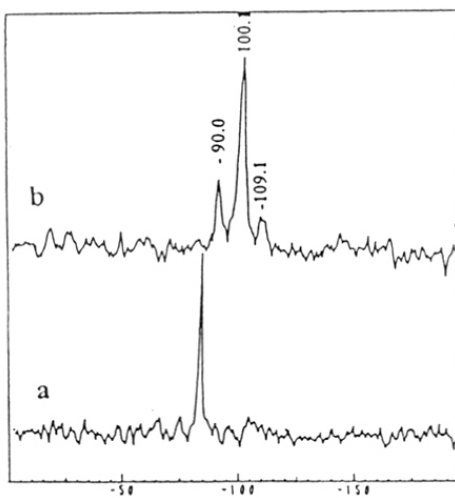
Figure 3.3(B): ^{29}Si liquid NMR spectra of: [TEOS + acetone] **(a)** and [1.0 TEOS: 0.4 TBAOH] stirred for 30 min. and acetone was added and further stirred for 1 h **(b)**, respectively.

86

Table 3.1: The silicate species in the synthesis gels detected by ^{29}Si liquid NMR

Silicate Species	Signal (ppm)		Identification
	Method A	Method B	
1. Si(OEt)$_4$	- 82.5	- 82.5	TEOS
2. Si(OH)$_4$	- 75.0	- 72.0	Q^0 (monomer)
3. (OH)$_3$-Si-O-M(OH)$_3$	- 79.9	- 80.2	Q^1
4. (OH)$_2$Si-[OM(OH)$_3$]$_2$	- 88.8	- 90.0	Q^2
5. (OH)Si-[OM(OH)$_3$]$_3$	- 98.8	- 98.2	Q^3
6. Si[OM(OH)$_3$]$_4$	- 108.1	- 107.7	Q^4

M = Zr or Si; Method A = ZrCl$_4$ source; Method B = Zr(acac)$_4$ source.

there is any effect of acetone addition in the distribution of silicate species, we recorded the spectra for the gels with the addition of only acetone to TEOS (Figure 3.3(B), curve a), before its hydrolysis and also after the complete hydrolysis of TEOS by TBAOH (Figure 3.3(B), curve b). These spectra were marginally similar to those observed in method A. Thus this downfield shift may be due to the presence of Zr(acac)$_4$ in the gel. A similar observation is reported in the case of Silicalite-1 solid sample. On addition of acetylacetone, ^{29}Si MAS NMR spectrum of this sample showed a small shift by a few ppm, in the individual peaks. It was claimed that these changes were induced by acetylacetone[9].

Thus, the samples synthesized using ZrCl$_4$ as zirconium source, *i.e.*, method A was found to be better than those synthesized using Zr(acac)$_4$ source *i.e*, method B. For preparations where x > 0.01, there was no clear gel formation and the excess zirconium precipitated as ZrO$_2$. However, in the Zr-Sil-2(B) samples, there was a clear gel formation up to a metal concentration (x) of 0.0125, which may enhance the metal incorporation beyond 1 Zr atom/unit cell in the framework without any precipitation of ZrO$_2$.

The Zr-Sil-2(A) samples were crystallized at 443 K, in 1-2 days with yields of 86%. The oligomers are formed probably through –Si-O-Zr-O-Si- linkages. The samples synthesized by method B, were crystallized at 443 K, after 3 days with low yields of 60%.

3.3.2 Characterization

3.3.2.1 Powder X-ray diffraction

The XRD profiles of the calcined Zr-Sil-2 samples (Figure 3.4 A) are similar to that of Sil-2[10] and exhibit a high crystallinity, without any impurity phase. The interplanar *d* spacings of Sil-2 shift to higher values due to the incorporation of the larger zirconium ions. The unit cell parameters for a tetragonal crystal system were refined by least-squares fitting. Although the fitting makes use of selected reflections only, yet a reasonable standard deviation and a correlation coefficient (~ 0.91) are obtained. The unit cell volume (UCV) is found to increase linearly as a function of zirconium content. It is reasonable to consider that this expansion in UCV from 5341 – 5375 Å^3 corresponds to isomorphous substitution of zirconium in the silicalite framework. Figure 3.4(B) compares the experimental UCV with that calculated assuming replacement of Si^{4+} by Zr^{4+} in tetrahedral positions. A very good agreement between the two, within the experimental errors (shown by error bars) up to a metal concentration (x) of 0.01 (Si/Zr = 102) is observed. However, in the case of the sample with Si/Zr = 61, the UCV is nearly equal to
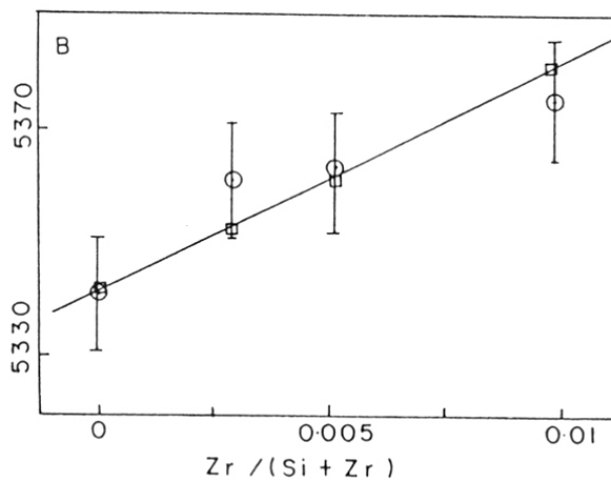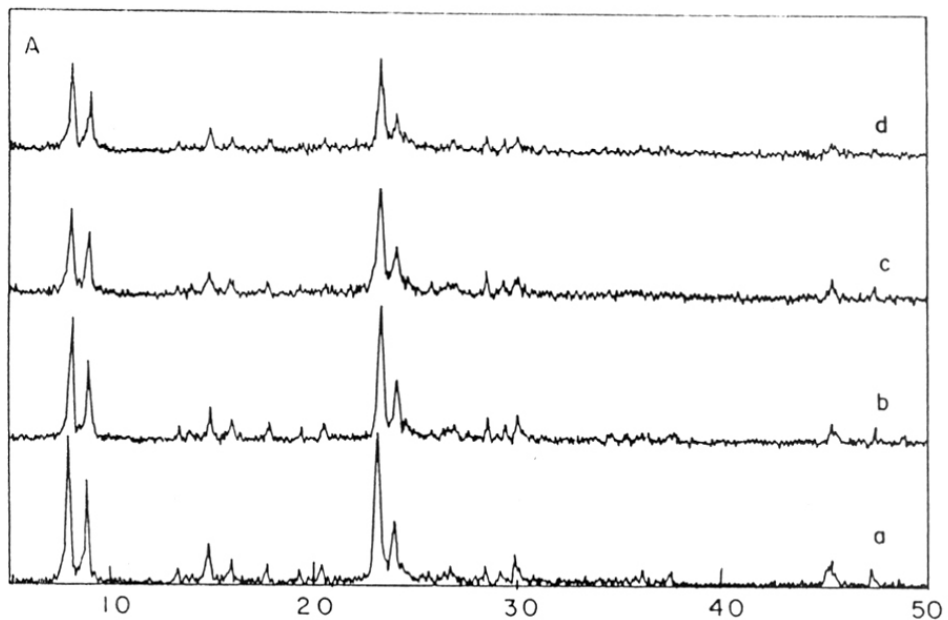
Figure 3.4(A): X-ray diffraction profiles of calcined Silicalite-2 (MEL) sample **(curve a)** and Zr-Sil-2 samples prepared by hydrothermal synthesis with Si/Zr molar ratios of 345, 205 and 102 **(curves b to d)** respectively.

  (B): Increase in unit cell volume (Experimental (o) Theoretical (□) with Zr content in the samples.
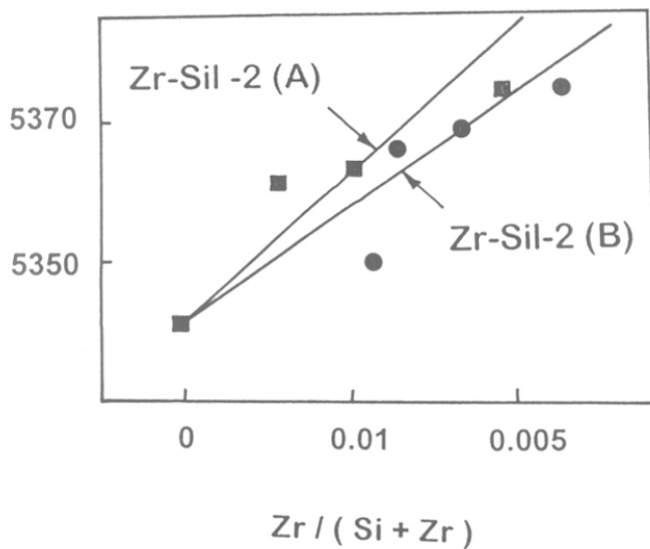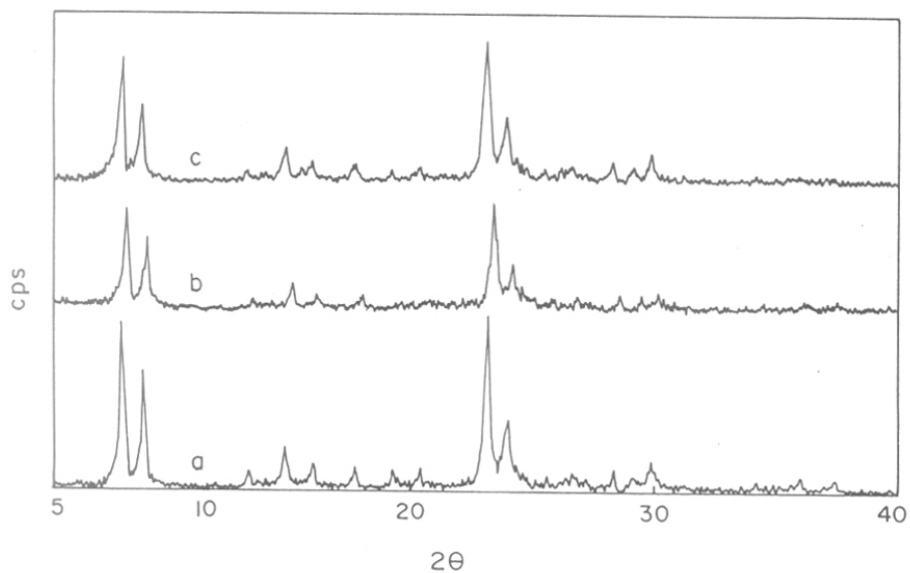
Figure 3.5(A): XRD profiles of calcined Silicalite-2 **(curve a)**, Zr-Sil-2(A) and Zr-Sil-2(B) (Si/Zr = 102 and 118) samples. **(b to c)**, respectively.

(B): Expansion of the unit cell volume (UCV) with the zirconium content for Zr-Sil-2 samples of (A) and (B) series.

Table 3.2: Unit cell parameters of Zr-Silicalite-2 samples

Sample	Si/Zr (molar ratio)		Zr/uc[a]	Unit cell parameters (Å)		UCV(Å^3)
	gel	product		a	c	
Silicalite-2		-	-	19.9971	13.3574	5341
	300	345	0.28	20.0277	13.3658	5361
Zr-Sil-**2**(A)[b]	200	205	0.50	20.0198	13.3816	5363
	100	102	0.94	20.0110	13.4218	5375
	60	61	1.57	20.0000	13.3675	5347
	200	173	0.55	20.0013	13.3735	5350
Zr-Sil-**2**(B)[c]	150	154	0.62	20.0280	13.3774	5366
	100	118	0.81	20.0391	13.3706	5369
	80	87	1.09	20.0497	13.3664	5373

[a]Total amount of Zr (in moles) in the product per unit cell.
[b]Zr-Sil-2 samples synthesized using $ZrCl_4$ source.
[c]Zr-Sil-2 samples synthesized using $Zr(acac)_4$ source.

that of Sil-2 sample which may be due to the presence of extraframework zirconium, at higher concentrations of zirconium. Similar observations were found for Zr-Sil-2 samples of (B) series, as well. (Table 3.2).

3.3.2.2 Scanning electron microscopy

Scanning electron micrographs confirm the absence of any amorphous material around Zr silicate crystals. The particle size of pure silicalite sample is about 6 μm while Zr-Sil-2 samples showed 1.5-2.0 μm cuboid crystals in the form of spherical aggregates. The samples of (B) series are composed of oval shaped uniform crystals of about 0.4 - 0.5 μm without any aggregates (Figure 3.6).

3.3.2.3 Diffuse reflectance UV-visible spectroscopy

The diffuse reflectance UV-visible spectrum of Zr-Sil-2 (100) sample of (A) series (Figure 3.7, curve c) shows a characteristic absorption at about 210 nm attributable to a charge transfer (CT) transition involving the Zr (IV) (tetrahedral configuration) sites[11]. This absorption is absent in the spectra of amorphous Zr-silica and Zr-impregnated Sil-2 samples (curves a and b, respectively). These electronic transitions are clearly distinguishable from those in pure ZrO_2 (monoclinic symmetry) which shows strong absorption at about 240 and 310 nm (Figure 3.7, curve d).

3.3.2.4 Adsorption methods

The N_2 adsorption isotherms of Zr-Sil-2 samples are characteristic of microporous materials (Figure 3.8). The micropore areas are in the range of 385 - 481 m^2g^{-1} in comparison to a value of 301 m^2g^{-1} obtained for Sil-2 (Table 3.3A). The smaller crystals of Zr-Sil-2(B) samples are responsible for the higher surface area (450 m^2g^{-1}) in comparison to a value of 400 m^2g^{-1} obtained for Zr-Sil-2(A) samples with Si/Zr = 100 (Table 3.3B). Due to higher external surface area, the sample showed a very less amount of hydroquinone in the hydroxylation of phenol. Due to this, this sample was excluded for further structural investigations.

The amounts of water, n-hexane and cyclohexane probe molecules adsorbed on the samples are compared to that by pure Sil-2 (Table 3.3). The sorption capacities of Zr silicates indicate the absence of any pore blockage due to occluded or amorphous material in the microporous structure.
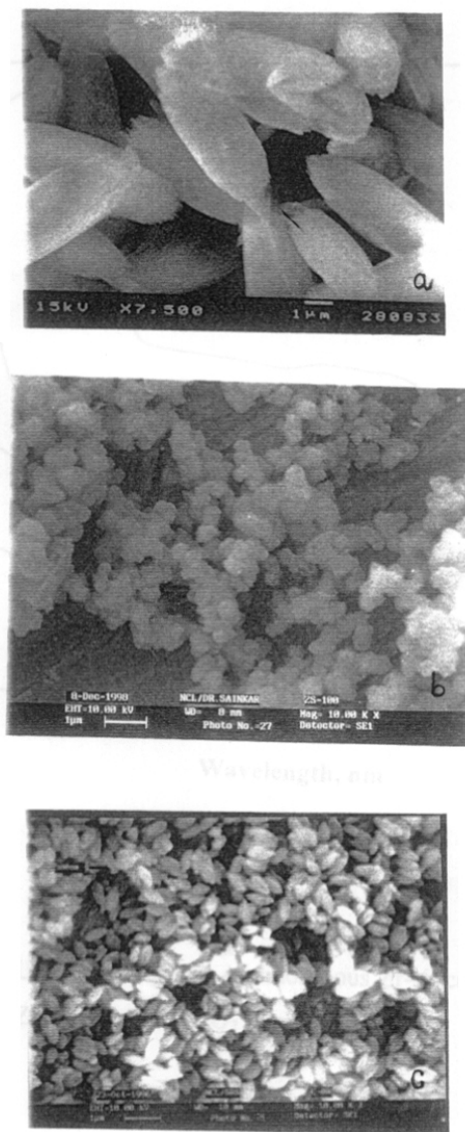
Figure 3.6: Scanning electron micrographs of Sil-2 (**a**) and Zr-Sil-2(A) and Zr-Sil-2(B) samples (Si/Zr = 102 and 118) (**b and c**), respectively.
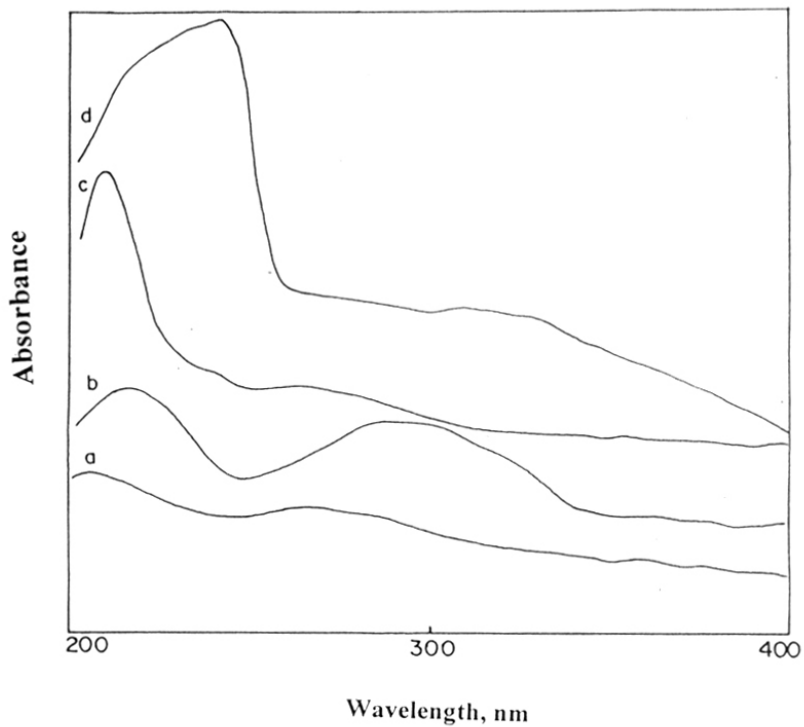
Figure 3.7: DR UV-visible spectra of amorphous Zr-silica (**curve a**), Zr-impreg. Sil-2 (**b**), Zr-Sil-2 (**c**) and ZrO_2 samples (**d**).
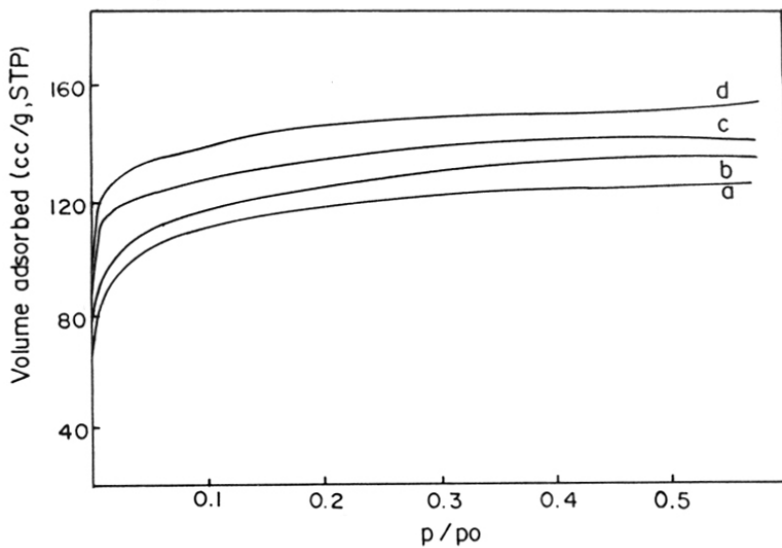
Figure 3.8: Nitrogen adsorption isotherms at 77K of Sil-2 (**curve a**), Zr-Sil-2(A) with Si/Zr = 205 (**b**) and 102 (**c**) and Zr-Sil-2(B) sample with Si/Zr = 118 (**c**), respectively.

Table 3.3(A): Physico-chemical properties of Zr-Sil-2 samples

Sample	Sorption capacities (wt.%)[a]			Surface area area[b], $m^2.g^{-1}$	Micro-pore vol., $mL.g^{-1}$	Meso-pore area, $m^2.g^{-1}$
	water	cyclo-hexane	n-hexane			
Silicalite-2	7.4	7.0	12.5	301	0.12	*
Zr-Sil-2(345)[c]	7.9	9.0	13.3	460	0.13	*
Zr-Sil-2 (191)	8.0	8.7	13.6	481	0.14	*
Zr-Sil-2 (102)	8.2	9.5	14.0	400	0.12	54
Zr-Sil-2 (61)	7.6	9.0	13.2	385	0.13	65

[a]Gravimetric adsorption at p/p_o = 0.5 and at 298 K.

[b]Volumetric adsorption at p/p_o = 0.05 and at 77 K.

[c]Si/Zr molar output ratio in the calcined samples, given in parentheses; *Negligible.

Table 3.3(B): Surface areas of Zr-Sil-2 samples prepared by two different methods

Sample	Si/Zr[a]	Surface area[b] $m^2.g^{-1}$	Micro-pore vol. $mL.g^{-1}$
Silicalite-2	-	301	0.12
	345	460	0.13
Zr-Sil-2(A)[c]	191	481	0.14
	102	400	0.12
	173	390	0.13
	154	352	0.14
Zr-Sil-2(B)[d]	118	450	0.15
	87	413	0.15

[a]Si/Zr molar output ratio; [b]Volumetric adsorption at p/p_o = 0.05 and at 77 K.

[c]Zr-Sil-2 samples synthesized using $ZrCl_4$ source.

[d]Zr-Sil-2 samples synthesized using $Zr(acac)_4$ source.

3.3.2.5 ^{29}Si MAS NMR spectroscopy

^{29}Si MAS NMR analysis of Zr-Sil-2(A) samples exhibited predominately an intense and broad signal at around - 113 ppm, which was assigned to $Q^4[Si(OSi)_4]$ species. The broadening of this resonance line as well as a marginal shift to the lower field (- 113.7 to - 112.6 ppm) were observed with an increase in Zr content. This is likely due to the distorted Si environment due to Si-O-Si or Si-O-Zr linkages (Figure 3.9). These results indicated that Zr^{4+} ions are probably linked to the defect silanol groups in tetrahedral coordinations.

3.3.2.6 FTIR spectroscopy

(i) Isomorphous substitution

The framework FTIR spectrum of Zr-Sil-2 (Figure 3.10, curve a) indicates a shoulder (sh) at about 960 cm^{-1} which may be attributed to Si-O-Zr asymmetric stretching vibrations (ν_{as}), from the possible substitution of zirconium in the Si-O-Si linkages. However, no such absorption was observed in Zr-impreg. Sil-2 and Zr-amorphous silica samples (curves b and c, respectively).

(ii) Determination of acid sites

In Figure 3.11, the infrared spectrum of pyridine adsorbed on Sil-2 (curve a) is compared with those of Zr-Sil-2 samples with Si/Zr molar ratios of 102, 205 and 345 (curves b, c and d, respectively) after evacuation at 348, 383 and 473 K. The spectra of the Zr-Sil-2 samples show strong bands at 1620 and 1450 cm^{-1} due to the pyridine coordinatively bound to Lewis acid sites (ν_s modes). A weak band at 1545 cm^{-1} is assigned to the pyridinium ion which is absent in the spectrum of Sil-2. These weak Brönsted acid sites may be due to the interaction between pyridine chemisorbed on Lewis acid sites and a nearby surface OH group. However, the desorption of pyridine at increasing temperature (> 473 K) resulted in preferential removal of Brönsted bound pyridine relative to Lewis bound pyridine. A band at 1490 cm^{-1} due both to the coordinated pyridine and pyridine chemisorbed on protonic acid sites (*i.e.*, pyridinium ion) is also observed. It is observed that Sil-2 sample has no coordination sites at increasing temperature to interact with gaseous pyridine. Therefore, Zr-Sil-2 appears to be more acidic than Sil-2. The Si-O$^{\delta-}$... $Zr^{\delta+}$ bridges, because of their strong polarization, may be the preferable sites for the adsorption of polar molecules. These IR results could be interpreted as an indication that the tetrahedral Zr in the silicalite lattice bears a δ^+ charge so that the O$^{\delta-}$... $Zr^{\delta+}$ bond may
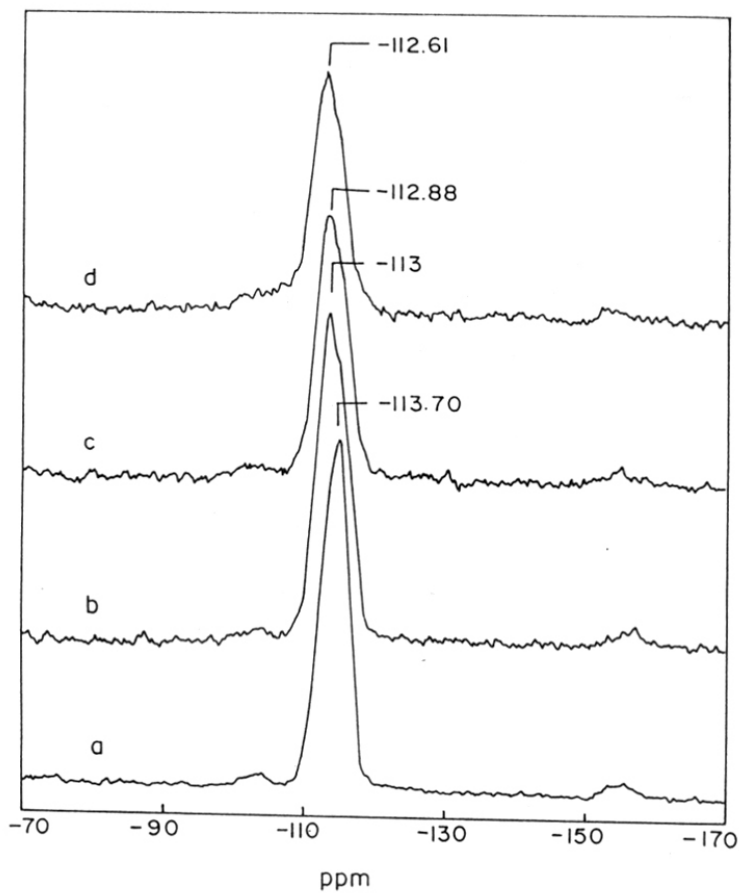
Figure 3.9: ^{29}Si MAS NMR spectra of Sil-2 **(curve a)** and Zr-Sil-2 samples A to C with Si/Zr = 345 – 102 **(curves b to d)**, respectively.
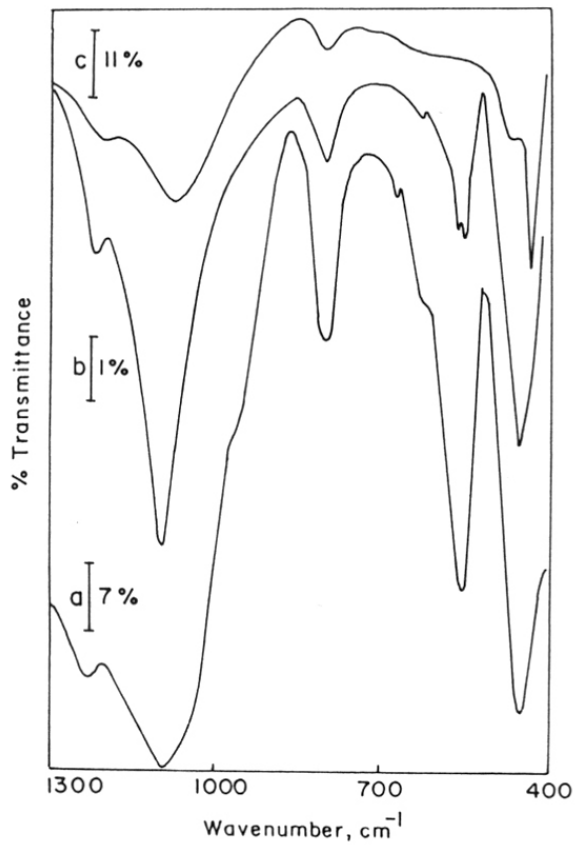
Figure 3.10: Framework FT-IR spectra of Zr-Sil-2(A), Zr-impreg. Sil-2 and amorphous Zr-silica samples **(curves a to c)**, respectively.
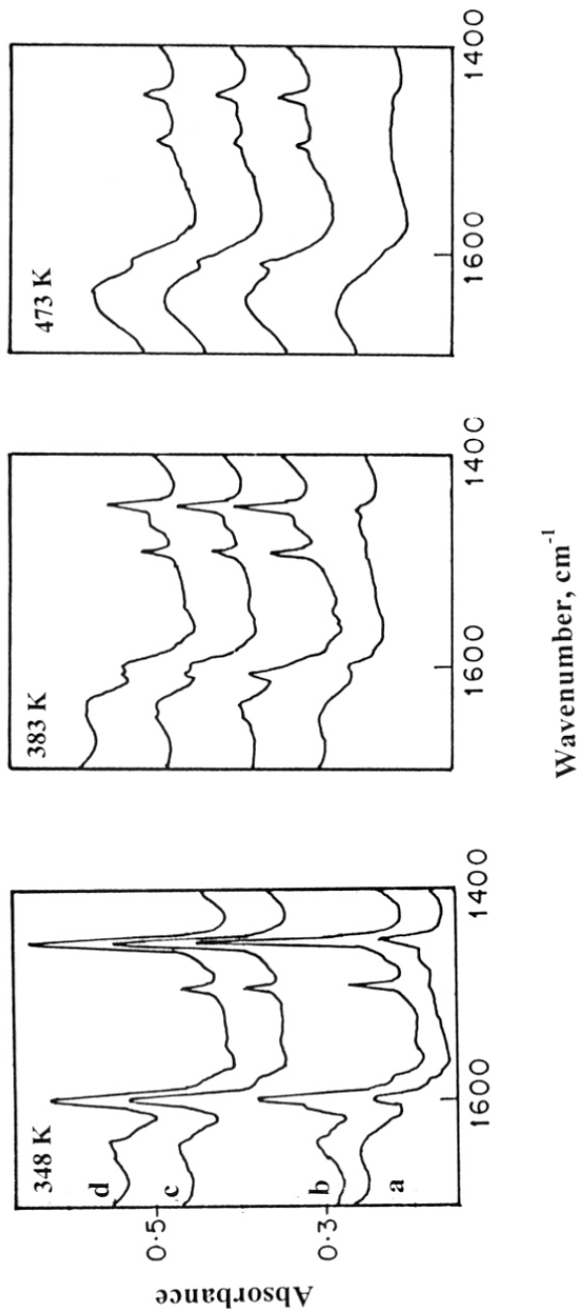
Figure 3.11: Infrared spectra of pyridine adsorbed on Sil-2 sample (**curve a**) and Zr-Sil-2(A) samples with Si/Zr molar ratios of 102, 205 and 345 (**curves b to d**), respectively) after evacuation at (**I**) 346 K. (**II**) 383 K and (**III**) 473 K.

be viewed as a Lewis acid-base pair. A similar interpretation has been given for the origin of Lewis acid sites in titanium silicalites[12].

3.3.2.7 Extended X-ray absorption Fine structure

In the case of Ti-silicalites, attempts have been made to clarify the substitution of Ti in the framework position by EXAFS[13,14]. However, for other tetravalent metal ions such as Sn and Zr, it is quite difficult to prove their incorporation in the zeolite lattice. A similar study has been performed over zirconia dispersed on silica[15] and Zr-exchanged beidellite[16]. In our studies, we have selected a sample of Zr-Sil-2(A) with optimum Zr content (Si/Zr = 102) in the framework as proved by other characterization techniques.

Even though there is a large difference between the ionic radii of Si^{4+} (0.26 Å) and Zr^{4+} (0.59 Å), due to the flexibility of the zeolite framework structures, such a large cation is likely to have occupied framework position (tetrahedral site) in zeolite lattice. The existence of Zr^{4+} in T positions has been supported based on the XRD, FTIR and UV-visible data. These results are also supported by more powerful tool such as X-ray absorption technique, EXAFS. We compared the EXAFS spectra of the sample with monoclinic zirconia with seven-fold coordinations as a standard because of the lack of tetrahedral Zr-oxide compounds. The fitting parameters given in Table 3.4 (3.9 = ~ 4.0 oxygens at 1.94 Å) are consistent with a structure where Zr(IV) is uniformly substituted in

Table 3.4: Fitting parameters calculated for Zr-Sil-2 sample

Coordination Shell	Backsc	N-cor	$\Delta\sigma^2$ [Å^2]	R[Å]	E_0-corr [eV]
1	Zr-O	3.9	-0.00074	1.94	4.95
2	Zr-Si	1.2	-0.00217	3.35	-12.99

N = no. of atoms coordinated to Zr atom; σ^2 = disorder factor;
R = nearest neighbour position; E_0 = threshold energy.

the place of Si(IV) in the framework, assuming a tetrahedral oxygen coordination sphere. A σ^2 value of the order of 10^{-5} Å^2 indicates a highly ordered structure in the first coordination shell. Figure 3.12(A) shows the plot of $k^3\chi(k)$ *versus* $k(A^{-1})$ wherein, function 'k' is the photoelectron wave factor and 'χ' is the normalized absorption
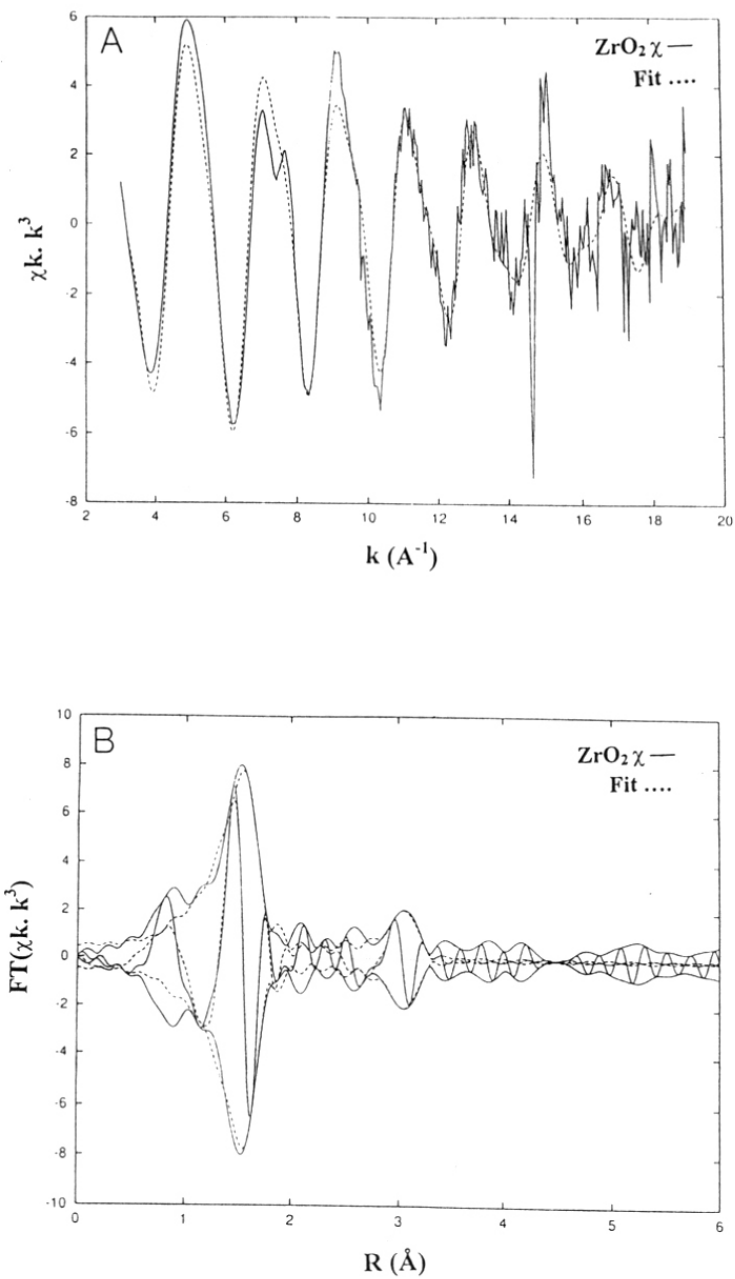
Figure 3.12: EXAFS spectra of Zr-Sil-2: **(A)** The raw $k^3\chi$ (k) data recorded at the Zr-K-edge and **(B)** Fourier transforms of $k^3\chi$ (k) data *versus* R (Å).

coefficient. This experimental curve was obtained after elimination of a high frequency component by Fourier transformation and then fitting of the experimental data. The corresponding Fourier transforms are shown in Figure 3.12(B), a plot of Fourier transformed $k^3\chi(k)$ *versus* R (Å). In this curve, the first peak at 1.94 Å is assigned to the tetrahedral Zr atom linked to four equivalent oxygen atoms, as Zr-O bonds. The second peak at around 3.0 Å may be attributed to the next neighbour, as Zr-Si and/or Zr-Zr bonds. However, for this second peak, R value is of 1.94 Å which is quite different to Zr-Zr distance reported in the literature for monoclinic zirconia (3. 45 Å) and for tetragonal zirconia (3.64 Å)[15], as shown in Scheme I, species (1). Consequently, it is noticeable that

(1)   (2)
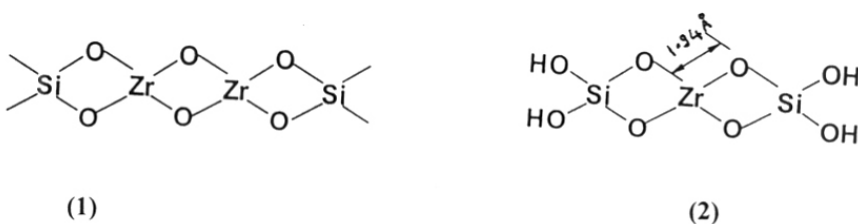
Scheme I (A)

the bond distances at 1.94 Å in the first shell and 3.35 Å in the second shell are due to Zr-O and Zr-Si bonds, respectively. These species are mostly derived from the Si-O-Zr linkages in edge sharing structures (species 2), as shown below, in Scheme I (A).

In the second coordination shell, the N value of 1.2 confirms that this short Zr-Si bond distance is probably due to monomeric (1) or oligomeric (2) Zr species chemically bonded to silicon atom in the form of Si-O-Zr linkages. These structures can be termed as open sites, shown in Scheme I (B).

(1)   (2)

Scheme I (B)

103
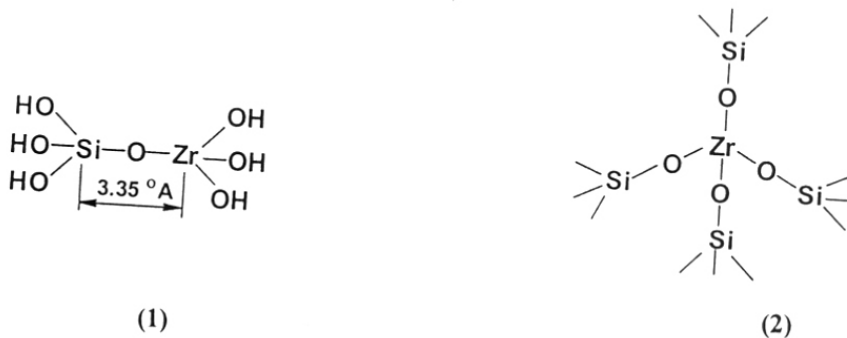
This Zr-edge EXAFS spectral analysis inferred that Zr is in the tetrahedral coordinations along with the presence of Si-O-Zr linkages.

3.3.2.8 Electron spin resonance spectroscopy

The characterization of most of the metallosilicates by electron spin resonance spectroscopy is always limited due to their stable tetravalent oxidation states, which are ESR inactive. However, a trivalent cation for example, Ti^{3+}, Zr^{3+}, etc. with d^1 electron configuration has characteristic ESR signals dependent on their coordination geometry. The low stability of these trivalent ions at room temperature again makes it difficult to monitor the ESR signals. Therefore, in order to study such species using ESR technique, several methods are used to reduce transition metal ions in the molecular sieves[17-19] as follows:

♦ Thermal treatment at high temperature

♦ Treatment with H_2/CO at moderate to high temperature

♦ UV or γ-ray irradiation

A distortion in the environment of the paramagnetic ion causes the increase of the g values and consequently, of the relaxation time, the spectra become easily observable even at room temperature[20]. This is in agreement with the observed ESR signals at g = 2.04 and 1.97, in Zr-Sil-2 as well as Zr-impreg. Sil-2 samples, respectively, on photoreduction of Zr (IV) at room temperature, as shown in Figure 3.13. These signals are assigned to Zr^{3+} ions formed on the interaction of Zr^{4+} ions with H_2 molecules as a consequence of the reductive process. The difference in g values of both the samples are due to a significant variation in the coordination sphere around the Zr(IV) center to which the superoxide ion is binding. Thus it is apparent that the crystal field associated with these samples is different from each other. The thermal treatment of the samples in the flowing air did not show any signal in the spectra. These reversible changes occurred due to the reoxidation of Zr(III) → Zr(IV) species. It proves the redox nature of Zr(III) → (IV) ions in the silicalite framework and its applicability in the oxidation reactions.

3.3.3 Catalytic properties

3.3.3.1 Hydroxylation of phenol

As discussed in Chapter 2, Zr-Silicalite-1 samples showed 33.5 wt.% H_2O_2 selectivity with a catechol/hydroquinone ratio of 1.0 – 1.4 in the products. Here, we have attempted to study the catalytic behaviour of Zr-Silicalite-2 in the hydroxylation of phenol.
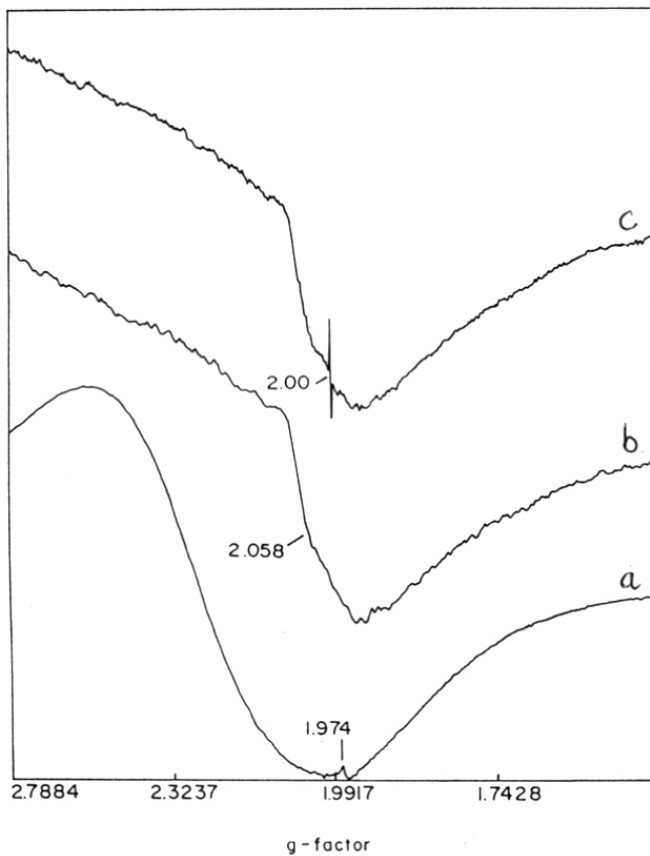
Figure 3.13: ESR spectra recorded on photoreduction in UV light/H_2 atmosphere: Zr-impreg. Sil-2 **(curve a)**, Zr-Sil-2 sample **(b)** in the range of 280-400 nm and **(c)** Zr-Sil-2 in the range of 200-400 nm, respectively.

The initial activity of Zr-Sil-2 samples is much lower as compared to Zr-Sil-1 samples.

(i) Effect of H_2O_2 addition on product distribution

The course of hydroxylation of phenol at 348 K was followed for 24 h with slow addition of H_2O_2 (30 % aqueous) for the initial 1 h. Figure 3.14 shows that in the beginning of the reaction, the product selectivities to parabenzoquinone and catechol are quite high and then decrease drastically with time. Upto almost 4 h, a negligible conversion of phenol to hydroquinone is obtained, due to the formation of parabenzoquinone and catechol predominantly. The formation of hydroquinone increased rapidly after about 6 h and reached to a maximum level at 10 h and then leveled off. We estimated about 10 - 13 wt.% tar formation during the reaction.

(ii) Effect of intrinsic Zr(IV) sites

The Zr-Sil-2 (100) sample showed 25.4% H_2O_2 selectivity with turn over number (TON) (mole of phenol converted per mole of Zr atom) of 71.0 (Table 3.5). In the product distribution, a catechol to hydroquinone ratio of 0.94 for the Zr-Sil-2 (100) sample indicates a certain degree of product shape selectivity. A catechol/hydroquinone ratio of 0.9 to 1.3 has been reported for titanium- and vanadium silicate molecular sieves (TS-2 and VS-2)[21] which are crystalline (MEL type) and microporous, and are similar to Zr-Sil-2 in their properties, having Ti or V in framework positions. These results indicate that in addition to being well dispersed, the Zr^{4+} ions are located within the channels of MEL structure as active sites. In order to check the catalytic behaviour of Zr-Sil-2, the hydroxylation runs were carried out on Zr-impreg. Sil-2, amorphous Zr-silica sample and Zr-free Sil-2 samples under identical conditions and these were found to have negligible activity in this reaction (Table 3.5 A). Apparently, only isolated zirconium ions, which are present in the framework of Silicalite-2, are active in the reaction. The catalytic activity as well as the selectivity for the products, catechol and hydroquinone are comparable to those of Zr-Sil-1 which showed 34.0 wt.% H_2O_2 selectivity (TON = 112) with catechol/hydroquinone ratio of 1.4^5. Although the catalyst can be reused (with marginal loss in activity) after filtration and washing with acetone to remove tar, the original catalytic activity of Zr-Sil-2 can be restored after calcination in air at 773 K for 6-8 h.

A slight deactivation of the catalyst due to deposition of high molecular weight carbon compounds (tar) after 12 h was observed. After regeneration of the catalyst, original activity for the reaction was found.
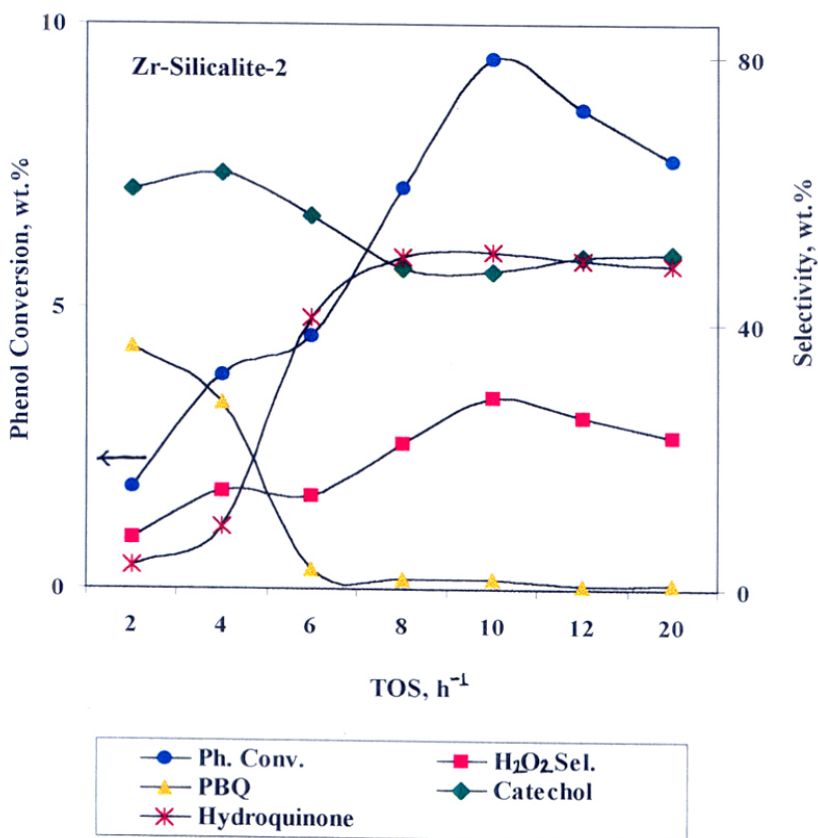
Figure 3.14: A plot of phenol conversion and product selectivities at different time on streams (TOS), h[-1] in the hydroxylation of phenol over Zr-Sil-2 catalyst.

Table 3.5(A): Hydroxylation of phenol[a]

Catalyst	Si/Zr	TON[b]	H_2O_2 sel[c]	Product distribution (wt.%)			
	(molar ratio)			PBQ	CAT	HQ	Tar[d]
Zr-Sil-2(A)[e]	198	42.4	19.2	0.8	46.1	43.0	10.1
Zr-Sil-2(A)	102	71.0	25.4	1.3	41.9	44.6	12.2
Zr-Sil-2 (B)[f]	118	105.4	48.8	1.8	62.2	22.5	13.5
Zr/Sil-2[g]	100	-	3.0	38.5	58.2	3.3	*
Amorphous Zr-silica	100	-	2.4	35.5	62.6	1.9	*
Sil-2	-	-	4.4	58.4	41.4	0.2	*

[a]Reaction conditions: catalyst = 0.5 g; solvent (water) = 10 g; phenol/H_2O_2 (mol) = 3 ; reaction duration = 10 h; temperature = 353 K.

[b]Turn over number = mole of phenol converted per mole of Zr atom.

[c] H_2O_2 utilized for the formation of parabenzoquinone (PBQ), catechol (CAT) and hydroquinone (HQ), excluding tar.

[d]High boiling fractions (> 573 K) estimated from the TG analysis in the products.

[e]Zr-Sil-2 samples synthesized using $ZrCl_4$ source.

[f]Zr-Sil-2 samples synthesized using $Zr(acac)_4$ source.

[g]Zr-impregnated Sil-2, for similar amount of Zr as in the case of Zr-Sil-2 (102).

*Negligible.

(iii) Effect of different Zr precursors

The catalytic activity of Zr-Sil-2(A) samples, synthesized using $ZrCl_4$ is compared to that of Zr-Sil-2(B) sample, synthesized using $Zr(acac)_4$. A significant difference in the product distribution between these two runs is also observed. The catechol to hydroquinone ratios are 0.9 and 1.7 for Zr-Sil-2 (A) and (B) samples, respectively. The turnover numbers of phenol are 62.4 and 105.4 with a H_2O_2 efficiency of 28.9 and 48.9 wt.% for the Zr-Sil-2 samples A and B, respectively. The samples show a nearly two fold activity in the reaction probably due to the smaller particle size. These results indicate that in the case of Zr-Sil-2 (A) samples, the Zr^{4+} ions are well dispersed within the channels of the MEL structure while in the samples of (B) series, the hydroxylation occurs at the external surface as well, where a part of Zr species may be located. For small submicron crystals (<1 μm), external surface sites could be a significant fraction of the total surface area. If the external surface sites are catalytically either the same or more active than the intracrystalline active sites, then the shape selectivity of a zeolite could be changed by these surface sites[20]. Similarly Zr-Sil-2(B) samples showed an external surface area and resulted in a higher catechol formation.

(iv) Nature of the catalyst

In order to show whether the reaction proceeds through heterogeneous or homogeneous catalyst, the catalyst was separated from the reaction mixture by centrifugation after 10 h and the reaction was further continued even after 10 h. However, there was no further change in the product distribution and phenol conversion in the absence of catalyst. The final reaction mixture was analyzed for zirconium using ICP. It was observed that a negligible amount of zirconium was leached out from the Zr-Sil-2 (B) sample during the reaction, which was insufficient to catalyze the reaction. These results confirm that Zr-Sil-2 acts as a heterogeneous catalyst in the reaction.

(v) Effect of different solvents

The results on the use of different solvents such as water, methanol, acetonitrile and acetone under identical conditions in the hydroxylation of phenol on Zr-Sil-2 samples are summarized in Table 3.5(B). The solvents affect both the phenol conversion and H_2O_2 efficiency. Under identical conditions, a maximum conversion of phenol is obtained in water being a highly polar solvent. Whereas negligible conversions are obtained in the other solvents such as methanol, acetone and acetonitrile with a very low selectivity for hydroquinone (1.6 wt.%). A significant selectivity for hydroquinone (11.4 – 22 wt.%) is

109

Table 3.5(B) Effect of different solvents in the hydroxylation of phenol[a]

Solvent	Dielectric constant, (Debye) at 298 K	H_2O_2 sel[c]	Product distribution (wt.%)			TON[b]
			PBQ	CAT	HQ	
water	81	25.4	1.3	41.9	44.6	71.0
acetone	23	2.5	68.2	20.4	11.4	3.2
acetonitrile	38	1.5	59.2	39.2	1.6	2.0
methanol	33	1.0	63.5	34.9	1.6	1.3

[a]Reaction conditions: catalyst = 0.5 g; solvent = 10 g; phenol/H_2O_2 (mol) = reaction duration = 10 h; temperature = 353 K.

[b]Turn over number = mole of phenol converted per mole of Zr atom.

[c]H_2O_2 utilized for the formation of parabenzoquinone (PBQ), catechol (CAT) and hydroquinone (HQ), excluding tar.

observed in acetone, but showed a very less activity (TON = 0.9 – 3.2 wt.%) as well as H_2O_2 efficiency (0.7 – 2.5 wt.%). Thus, a protic solvent, water plays an important role in this selective oxidation reaction.

The decrease in the activity can be explained on the basis of a competitive adsorption between the solvent molecules and H_2O_2 on Zr^{4+} ions. A very low activity was obtained in methanol inspite of its polar nature. Acetonitrile, being a nonpolar solvent also showed similar activity as that of in methanol, irrespective of differences in the polarity of the solvents. Methanol and acetone seem to decrease the activity of reactive intermediate species. The solvent might influence the stability of any of intermediates formed during the reaction and hence the activation of substrate molecule. The reasons for the solvent effects are very intricate, being a function of its polarity, molecular size, diffusion in the pores and interaction of solvent molecules with active centers.

(vi) Interaction of H_2O_2 with Zr-silicates

The catalytic properties of metallosilicates are always dependent on the nature and location of metal in the framework and their accessibility to adsorbates and their coordination with ligands. The spectroscopic features in UV-visible as well as ESR spectra of hydroperoxo- and superoxo- species formed by framework Ti(IV) in titanium silicates in the presence of aq. H_2O_2 have been well studied and reported in the literature[23-25]. A similar study on the formation of the superoxide radical ion on monoclinic zirconia has been reported by Giamello et al.[26].

In the present study, the nature of the intermediate species formed during an interaction of H_2O_2 (30 % aqueous) with Zr-Sil-2(A) sample (Si/Zr = 102) is investigated by ESR and UV-visible spectroscopic techniques. The species formed by the framework Zr(IV) after interaction with aq. H_2O_2 could be similar to those of Ti(IV) in titanium silicates due to their isoelectronic properties.

ESR spectroscopy:

The reactivity of Zr-Sil-2 and Zr-impreg. Sil-2 samples towards aq. H_2O_2 showed a remarkable difference in g values for superoxide, O_2^- species consistent with the different coordinations prevailing at each Zr (IV) site. The ESR spectrum of Zr-Sil-2 is characterized by anisotropic g values with $g_1 = 2.031$, $g_2 = 2.0099$ and $g_3 = 2.0045$ (Figure 3.15). These g values are attributed to O_2^- ions stabilized on Zr(IV) sites whereas in Zr-Sil-1, a similar spectra was obtained with g values at $g_1 = 2.0307$, $g_2 = 2.0092$ and $g_3 = 2.0029$. However, an additional weak signal at g = 2.006 due to different crystal field of
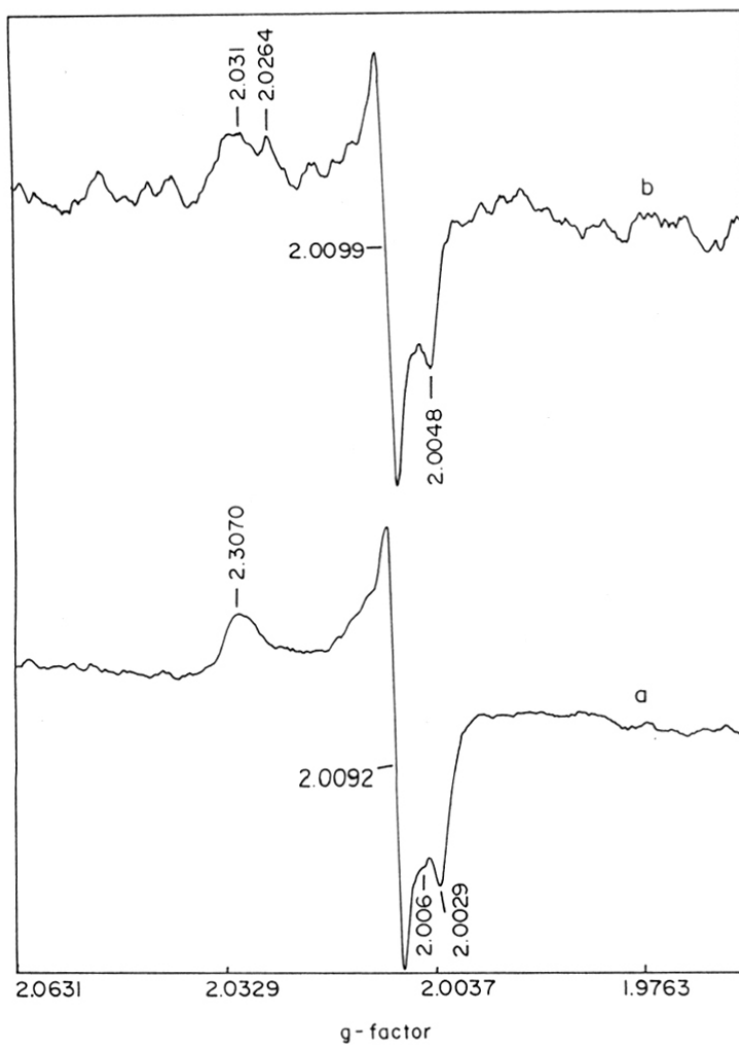
Figure 3.15: ESR spectra recorded on treatment with water + H_2O_2 at room temperature: Zr-Sil-1 (Si/Zr = 158) **(curve a)** and Zr-Sil-2 (Si/Zr = 102) **(b)**, respectively.

Zr(IV) ions in this sample, was observed. The spectra of Zr-Sil-2 sample was compared to that of Zr-impreg. Sil-2 which showed a very weak signal at g = 1.973. It indicates the weak interactions of surface zirconium with H_2O_2. In addition to this, the lower catalytic activity in the hydroxylation of phenol proves that the intermediate species have a very short lifetime to react with phenol.

As water is already present in the hydrogen peroxide, it also may have an important role in this interaction, being a protic solvent. When we performed similar experiments using other solvents of different polarity such as methanol and acetonitrile, we observed that intermediate species formed in these solvents are quite weak to record at room temperature.

In order to distinguish between framework and nonframework Zr species, a similar experimental procedure was applied for the interactions of tertiary butylhydroperoxide (TBHP), a bulkier oxidant with Zr-Sil-2 sample. In this case, the O_2^- formation on the Zr-silicates was no longer observed due to non-availabilty of extraframework Zr species to interact with TBHP. It conforms the presence of Zr(IV) in the framework sites in Zr-silicate samples. It is also evident that diffusion of bulkier TBHP in the channels of Zr-silicate samples becomes difficult due to their medium-pore structure. It is also clarified from these studies that this intermediate formation occurs in the presence of Zr^{4+} ions. These Zr(IV) species in the silicalite framework provides active centers for the catalytic reactions.

UV-visible spectroscopy:

Figure 3.16 represents the diffuse reflectance spectra of Zr-Sil-2 (curve a), treated with water (curve b) and then with H_2O_2 are compared qualitatively. Zr-Sil-2 samples showed a usual strong charge transfer (CT) transition between tetrahedrally coordinated Zr(4d) and O(pπ) orbitals at 212 nm. Addition of water causes a shift of this CT band to the higher wavelength at 214 nm. In addition to this, the spectra showed new transitions at 303 and 358 nm. These new bands indicate a direct insertion of water ligands into the first coordination sphere of Zr(IV) site that changes tetrahedral coordination of Zr(IV) to the higher coordination, mostly hexacoordinated species. All these changes are completely reversible, as shown in Scheme (II).
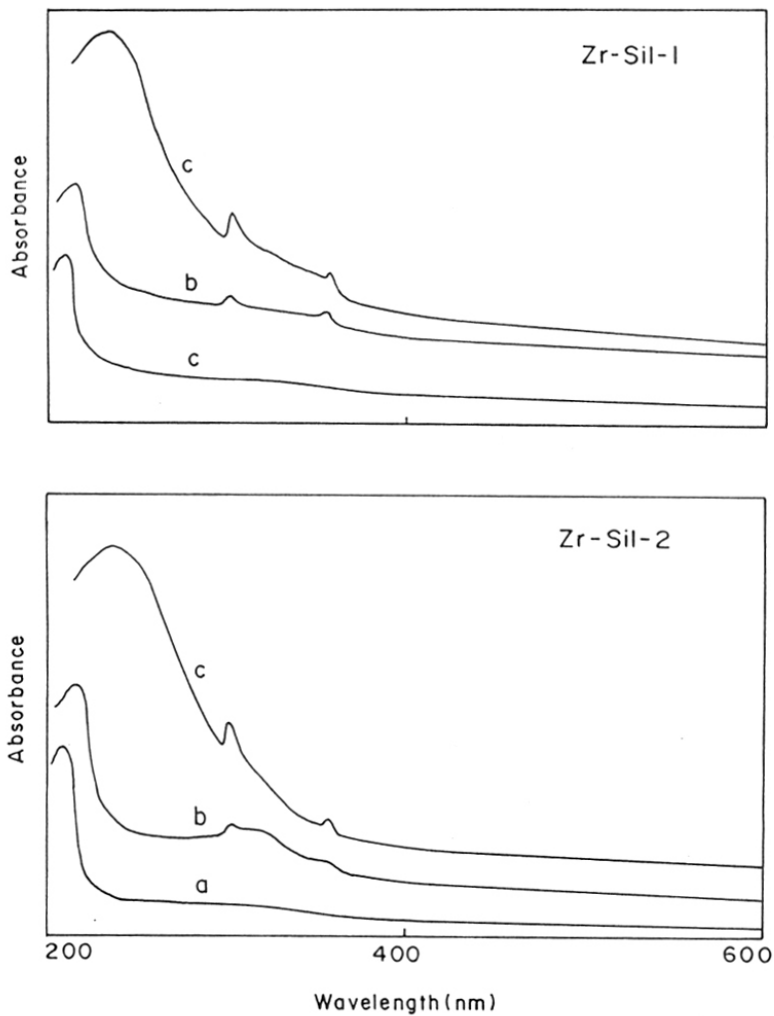
Figure 3.16: DR UV-visible spectra recorded without any treatment **(curve a)**, treated with water **(b)** and with water + aq. H_2O_2 **(c)**, repectively.

114
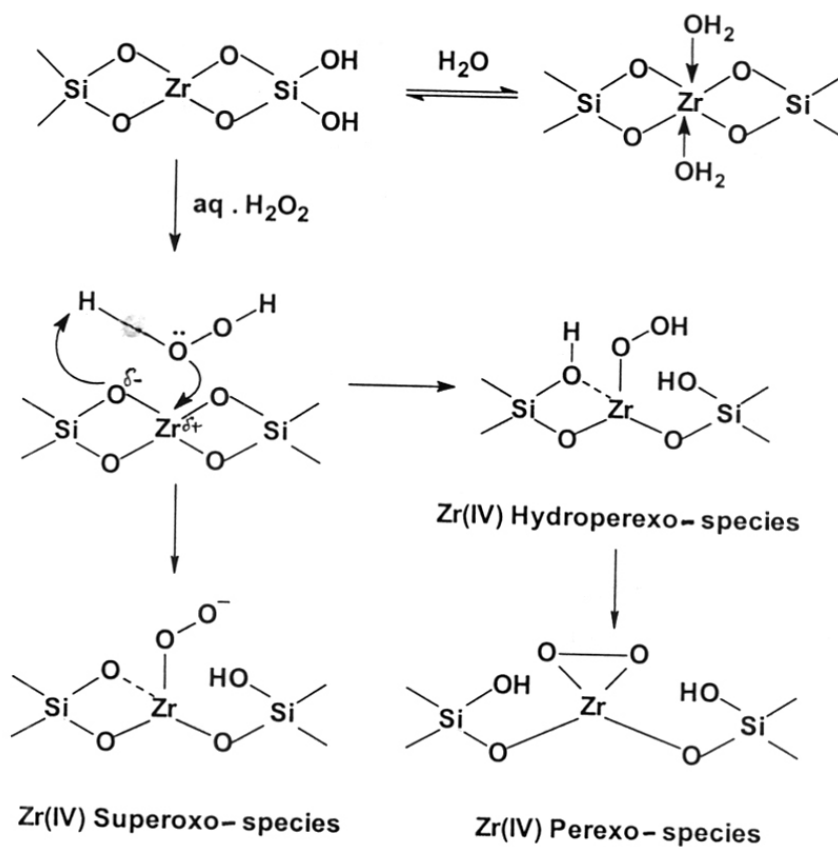
Scheme (II)

Further addition of H_2O_2 gives rise to a spectrum which is characterized by the continuous broad absorption in the range of 250 – 400 nm, centered at 280 nm alongwith the original CT band at 214 nm. This continuous absorption is associated with a charge transfer from a peroxo- species, as shown below. This band disappeared on thermal treatment at 573 K for 1 h and only CT band was observed.

Thus, it is presumed that Zr^{4+} ions in the silicalite matrix are capable for the capture of O_2^- ions, formed in the presence of aq. H_2O_2. All the spectra of Zr-Sil-2 were compared to those of Zr-Sil-1 samples. The spectra of Zr-Sil-1 sample also showed a similar nature of intermediates to those of Zr-Sil-2 sample on contact with water and H_2O_2.

(vii) Nature of active sites

It is evident from the structural investigations by EXAFS and other techniques that Zr-Sil-1 samples contain an appreciable amount of isolated Zr^{4+} active centers, which are uniformly distributed within the crystals. Each Zr atom is surrounded by silicon and is isolated from other zirconium atoms by long -Si-O-Si-O- linkages. This isolation of the Zr^{4+} centers is presumed to be a prerequisite for the high H_2O_2 selectivity of Zr-Sil-2 samples. A probable structure has been proposed for these isolated zirconium sites, incorporated in the silica matrix, as shown in Scheme I A (2) and B (1) and (2).

3.3.3.2 Catalytic decomposition of isopropanol

(i) Introduction

Acid-base properties of a catalyst are usually characterized by measuring their activity as well as selectivity in a test reaction. Isopropanol decomposition is the most widely used reaction to characterize the acid-base properties of metal oxides[27]. These reactions can be performed in the presence of weak Lewis acid sites with a good catalytic activity. From a mechanistic point of view, the dehydration of ispropanol is catalyzed by an acid site whereas the dehydrogenation is catalyzed by both acid and basic sites through a concerted mechanism[28]. The catalytic dehydration of isopropanol by La-Y zeolites at the various temperatures has been recently reported[29]. As the amphoteric character of ZrO_2 allows it to be active in both dehydration and dehydrogenation[30], our aim is to study the effect of incorporation of zirconium in the MEL framework, on the selectivity to propene and acetone. Therefore, the catalytic decomposition of isopropanol to propene and acetone has been investigated in the temperature range of 473 K to 573 K over microporous, crystalline Zr-silicate molecular sieves with MEL structure, containing 1.0 Zr atom per unit cell ($SiO_2/ZrO_2 = 102$). The activity of this catalyst in the reaction is compared with those of Zr-impreg. Sil-2 and Zr-Sil-1 catalysts.

(ii) Results and discussion

Table 3.6(A) summarizes the conversion and product selectivities obtained for Zr-Sil-2 catalyst at different temperatures. The conversion of isopropanol and henceforth,

overall turn over frequency (TOF) of decomposition reactions i.e. mole of isopropanol converted per mole of Zr atom per second increases with temperature.

With a rise in the reaction temperature, dehydrogenation reaction to form acetone occurred either before or simultaneously to the onset of the dehydration reaction to form propene. The catalyst showed selective formation of acetone at the earliest temperature range of 473 – 498 K. Above 498 K, the selectivity shifts in favour of propene formation. The effect of temperature on the selectivities to propene and acetone is shown in Figure 3.17(A). It shows that at lower temperatures (398 - 448 K), a higher selectivity to propene is observed. There is a remarkable increase in the acetone selectivity at about 473 K. At higher temperatures (> 573 K) the reaction was selective in favour of the dehydration reaction. The change in the selectivity pattern is due to the adsorption of isopropyl alcohol molecule on the different active sites around the zirconium active sites. The decomposition reactions are likely to involve heterolytic processes involving pairs of acid and basic sites in the form of $Si-O^{\delta-}....Zr^{\delta+}$ linkages of silicalite framework.

Zr-Sil-1 sample (0.6 Zr/uc) also showed a similar activity at the identical reaction conditions. However, it showed predominately propene formation. As this sample has a lower concentration of framework Zr than Zr-Sil-2 (1.0 Zr/uc), it may have a lower number of acid-base pairs. A very low selectivity to acetone is observed for Zr-impreg. Sil-2 and pure Sil-2 samples at the same reaction temperature, as shown in Table 3.6(B). In the impregnated sample, randomly distributed Zr atoms on the silicalite surface may cause an aggregation of Zr sites[15]. In such cases, the concentration of Zr sites increases where the coordinatively unsaturated structure of Zr^{4+} sites becomes an important factor. This enhanced Lewis acidity causes the formation of propene predominately. It clearly demonstrates the high intrinsic activity of the zirconium linked to –O-Si species to form Si-O-Zr linkages in the zeolite lattice when compared to the extralattice zirconium in an impreg. Sil-2 sample (Figure 3.17 B).

(iii) Mechanism

The *mechanism* of the reaction is somewhat obscure due to presence of two moieties –Zr-OH or Zr^{4+} Lewis acid sites. Adsorbed isopropanol molecules could be held through hydrogen bonding to the surface hydroxyl group or through coordination to a Zr^{4+} ion. It has been generally accepted that the alcohols over oxide surface leads to a mixture of adsorbed alcohol molecules and alkoxide species[31]. Recently, Hussian *et al.*[32,33] have proved by infrared studies that the formation of alkoxide (ethoxide/ isopropoxide)

117

Table 3.6(A): Effect of temperature on the formation of propene and acetone[a]

Temperature (K)	Isopropanol Conversion (mol%)	Selectivity (mol.%)				TOF[c] ($\times 10^{-3}$) (s^{-1})
		Propene	Acetone	water	Others[b]	
423	14.2	74.0	11.1	14.9	0.0	3.53
473	31.3	42.5	48.9	7.03	1.57	7.84
498	36.0	12.3	76.1	10.8	0.8	9.01
523	54.6	11.3	69.2	17.6	1.9	13.7
573	99.9	39.4	52.8	6.0	1.8	25.0

[a]Reaction conditions: WHSV = 1.85 h^{-1}, TOS = 3h

[b]Other products = diisopropyl ether

[c]Turn over frequencey = mole of isopropanol converted per mole of Zr atom per second.

Table 3.6(B) Catalytic decomposition of isopropanol[a]

Catalyst	Isopropanol Conversion (mol%)	Selectivity (mol%)				TOF ($\times 10^{-3}$) (s^{-1})
		Propene	Acetone	water	others	
Zr-Sil-1	35.1	62.1	30.8	7.10	0.0	13.5
Zr-Sil-2	31.3	42.5	48.9	7.03	1.57	7.84
Zr-impreg. Sil-2	30.0	76.7	8.10	3.50	11.7	7.20
Sil-2	23.5	75.7	6.0	18.3	0.0	-

[a]Reaction conditions: Temperature = 473 K, WHSV = 1.85 h^{-1}, TOS = 3 h
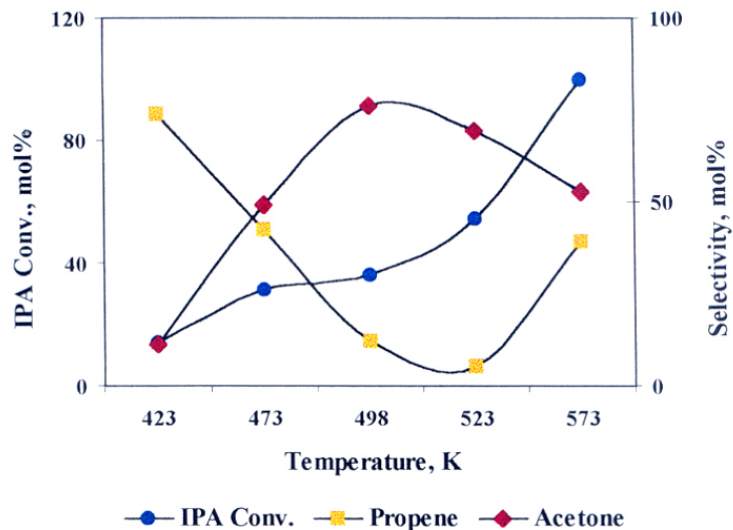
Figure 3.17(A): Effect of temperature on the conversion of ispropanol and product selectivities in the decomposition of isopropanol.
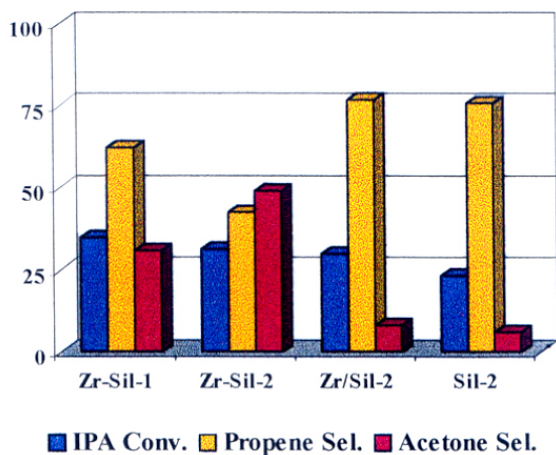
Figure 3.17(B): A comparsion of conversion of isopropanol and product selectivities over Zr-containing silicates with Zr-free Sil-2 in the decomposition of isopropanol at 473 K.

intermediates occurs over Zr^{4+} Lewis acid sites in ZrO_2.

Some of the proposed mechanisms for the decomposition reaction of ispropanol account for both the dehydration and dehydrogenation[34].

• The E_1 *mechanism* is a two-step process in which the rate-determining step is the formation of carbenium ion by abstraction of –OH group of isopropanol molecule that rapidly loses a β proton.

• The E_2 *mechanism* is a single-step process in which both –OH group the proton depart simultaneously, the proton being abstracted by a base.

• A third possibility is E_1cB *mechanism*- a two-step process wherein the proton leaves first and then followed by the –OH group.

The E_1 mechanism operates generally in the presence of acids whereas E_2 and E_1cB mechanisms take place over an acid-base pair. These mechanisms are summarized in Scheme III.

B : = base, A = acid
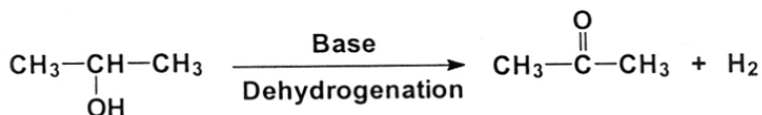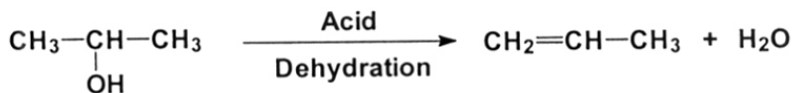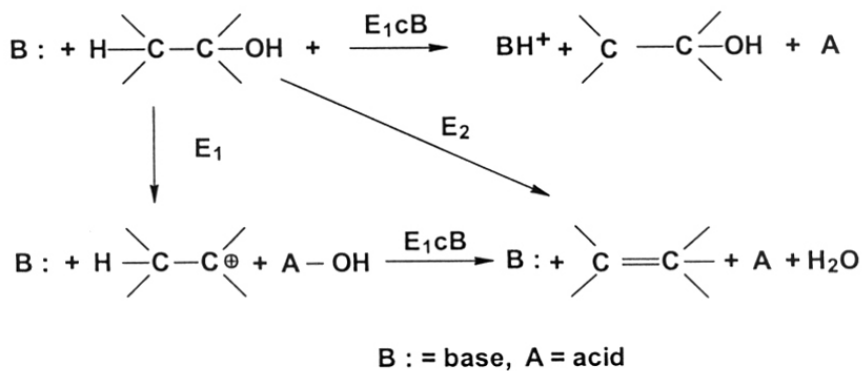
Scheme III

The solids like zirconia, having similar acid-base properties, the dehydration and dehydrogenation may take place via a concerted E_2 mechanism and E_1cB mechanism, respectively[30].

In the case of Zr-Sil-2 catalyst, the active sites involve Zr(IV) as a tetrahedral species, sharing edges with two neighbouring SiO_4 tetrahedra from the silicalite lattice. It is well known that Zr is itself acts as a Lewis acid due to its coordinatively unsaturated nature. Thus it bears a $\delta+$ charge so that $-O^{\delta-}$-Si may be viewed as a Lewis acid-base pair. In agreement to this, we propose that the simultaneous interaction of an acid-base pair with the –OH group and the proton of isporopanol molecule would cause both groups to be released and dehydration product, propene to be formed. In dehydrogenation, the basic site abstracts a proton from the isopropanol molecule. It forms an adsorbed isopropoxide species. The release of a hydride from the isopropoxide carbon atom leads to the formation of acetone. The adsorption of isopropanol on Zr-Sil-2 is shown below:
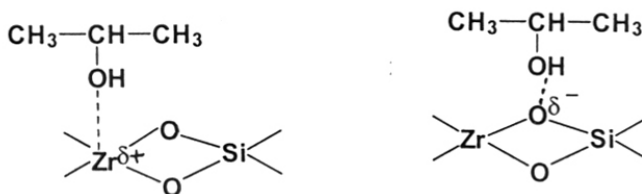
3.3.3.3 Oxidative dehydrogenation of ethanol

(i) Introduction

Selective oxidation of ethanol to acetaldehyde has deserved recently an increasing technological interest as an intermediate in the manufacture of acetic acid and its derivatives[35]. Although silver-based catalysts are commercially used, a number of metal oxide catalysts have been tested in order to find a promising substitute for the commercial catalyst[36]. Many reports of oxidative dehydogenation of ethanol over Ti-, V- containing silicate molecular sieves are available in the literature[37,38]. Dehydrated silica (at 1000 K)[39] and Silicalite-1[40] are also reported to catalyze this reaction to small amounts of acetaldehyde. Isomorphous substitution of zirconium in the framework creates isolated active centers in an ordered matrix, responsible for such unusual activity. This has been projected in the present study by the difference in the activity of incorporated and

impregnated (supported) zirconium in molecular sieves.

(ii) Results and Discussion

During the reaction, acetaldehyde, ethylene and diethyl ether were obtained as major products. In Figure 3.18(A), a variation in the ethanol conversions and product selectivities with temperature at WHSV (weight hourly space velocity) of 2.67 h^{-1} is given. It shows that ethanol conversion increases with increase in temperature, as expected. Zr-Sil-2 sample exhibits a higher selectivity to acetaldehyde in favour of dehydrogenation reaction. At higher temperatures, the selectivity for the secondary dehydration product, ethylene is enhanced with a loss in the selectivity of acetaldehyde and primary dehydration product, diethyl ether.

The influence of temperature at *different space velocities* (WHSV), on the conversion of ethanol over Zr-Sil-2 is presented in Table 3.7(A). With increase in the space velocities from 1.34 to 2.67 h^{-1}, ethanol conversion decreases due to a lower contact time of the catalyst with ethanol. At a lower WHSV of 0.57 h^{-1}, the conversion of ethanol is low due to a higher contact time. It accelerates the formation of ethylene and diethyl ether rapidly and in turn the deactivation of the catalyst, particularly at higher temperatures (>648 K). A selectivity pattern indicates that acetaldehyde is a major product at higher space velocities. However, the selectivity to the dehydrogenation product decreases with temperature at a higher space velocity. There is an enhancement in the formation of other products such as methanol, dimethyl ether with temperature.

Figure 3.18(B) shows the effect of space velocities (WHSV) on the product selectivities at two different conversions of ethanol, 15 mol% and 50 mol%. The selectivity pattern for a lower conversion of ethanol shows that the diethyl ether is predominant at a lower space velocity whereas acetaldehyde is the major product at the higher space velocity. For a higher conversion, ethylene is a major product at a lower space velocity. It also reflects in the lower values of turn over frequencies (mole of ethanol converted per mole of Zr atom per second) than those obtained at a higher space velocity.

Furthermore, the catalytic activity of Zr-Sil-2 was compared to those of Zr-Sil-1, Zr-impreg. Sil-2 and Sil-2 samples (Table 3.7B). Zr-Sil-1 sample showed a higher dehydration activity than those of Zr-Sil-2. These results are in agreement with those obtained for the decomposition of isopropanol. The selectivity pattern of Zr-impreg. Sil-2 is marginally similar to that of Sil-2. However, Sil-2 showed a higher diethyl ether
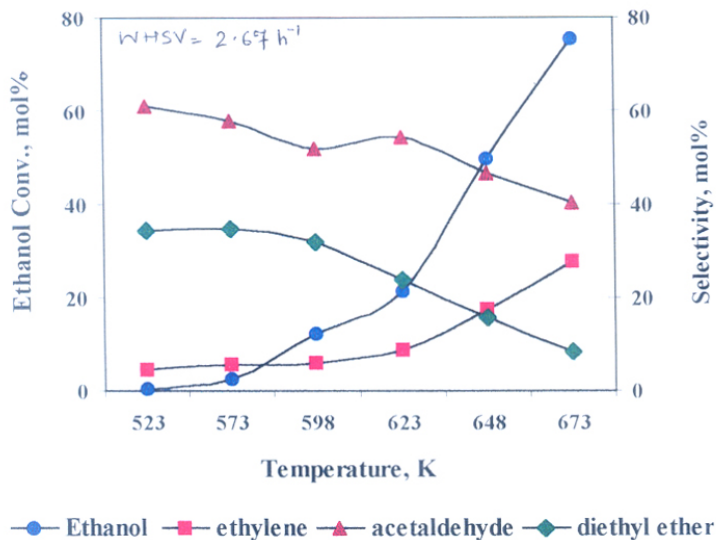
Figure 3.18(A): Effect of temperature on the conversions of ethanol and product selectivities in the oxidative dehydrogenation of ethanol.
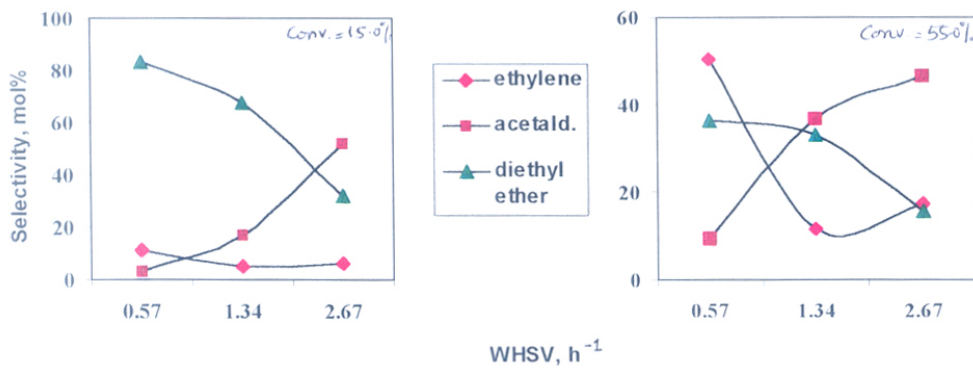
Figure 3.18(B): Effect of space velocities on the product selectivities at 598 K in the oxidative dehydrogenation of ethanol.

Table 3.7(A): Effect of space velocities on the product distribution[a]

WHSV h^{-1}	Temperature (K)	Ethanol Conv. (mol%)	Selectivity (mol %)				TOF[c] ($\times 10^{-3}$) (s^{-1})
			C$_2$H$_4$	CH$_3$CHO	Et$_2$O	Others[b]	
	523	1.5	2.1	9.1	81.5	2.6	0.15
	573	8.6	6.9	5.9	84.2	1.4	0.88
0.57	598	15.1	11.3	3.4	83.2	0.8	1.54
	623	22.5	14.2	2.4	81.1	0.6	2.29
	648	36.0	27.0	2.6	66.6	0.8	3.67
	673	44.4	50.6	9.3	36.4	0.0	4.52
	523	2.2	12.4	7.1	74.6	6.0	0.52
	573	8.2	4.6	14.1	77.3	4.0	1.95
1.34	598	14.7	5.2	16.6	67.7	10.5	3.49
	623	33.3	7.8	17.2	53.1	21.9	7.91
	648	52.2	11.6	36.8	33.0	18.6	12.4
	673	76.8	21.7	43.1	20.2	14.7	18.2
	523	0.4	4.6	60.9	34.4	0.0	0.02
	573	2.6	5.5	57.9	34.6	8.0	1.23
2.67	598	12.3	6.0	52.0	31.8	10.2	5.83
	623	21.3	8.9	54.5	23.9	12.6	10.0
	648	50.0	17.4	46.6	15.8	20.2	23.7
	673	75.3	27.7	40.2	8.4	35.4	35.7

[a]Reaction conditions: TOS = 5 h.

[b]Other products = methanol, dimethyl ether

[c]Turn over frequency (TOF) = mole of ethanol converted per mole of Zr atom per second.

Table 3.7(B): Oxidative dehydrogenation of ethanol

Catalyst	Ethanol Conv. (mol.%)	Selectivity (mol.%)				TOF ($\times 10^{-3}$) (s^{-1})
		C_2H_4	CH_3CHO	Et_2O	Others	
Zr-Sil-1	23.0	19.6	34.3	40.4	5.7	16.7
Zr-Sil-2	21.3	8.9	54.5	23.9	12.6	10.0
Zr-impreg. Sil-2	20.4	24.0	19.0	44.2	12.8	9.6
Sil-2	18.0	25.0	23.0	50.6	1.4	-

[a]Reaction conditions: Temperature = 623 K, TOS = 5 h.

formation. From these different product selectivities over zirconium silicates-incorporated and impregnated, it is evident that the products are formed through the decomposition of ethoxide intermediate adsorbed on energetically different active sites.

(iii) Mechanism

The mechanism of this reaction over supported metal oxide surfaces has been studied extensively (Scheme IV). The important steps involved in the reaction are (a) adsorption and activation of ethanol on the active metals site and (b) decomposition of the ethoxide species to form different products. However, the selective formation of any specific product is essentially controlled by the nature of the active sites present on the

$$CH_3-CH_2-OH \xrightarrow[\text{Oxi-Dehydrogenation}]{} CH_3-\overset{\overset{\displaystyle O}{\|}}{C}-H \ + \ H_2$$

$$CH_3-CH_2-OH \begin{cases} \xrightarrow{+CH_3CH_2OH} CH_3-CH_2-O-CH_2-CH_3 \ + \ H_2O \\ \xrightarrow{\text{β-H abstraction}} CH_2=CH_2 \end{cases}$$

Dehydration
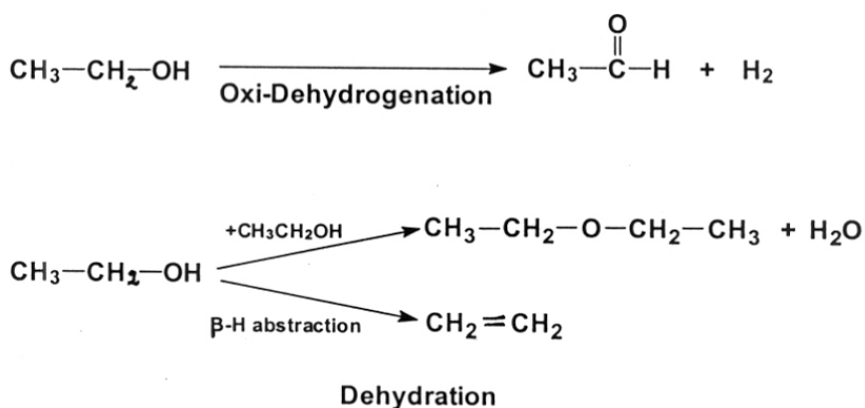
Scheme IV

surface (M=O, M-O-M and M-O-M and M-O-M˙, where M is the active metal ion and M˙ is the support). Thus the reaction can proceed via peroxometal ($M\!\!<^O_O$) or oxometal (M = O) pathways depending on the catalyst used. The metals which are strong oxidizing agents in their highest oxidation state (e.g. Cr^{VI}, V^{V}, Ce^{IV}, Ru^{VII}) react via oxometal species while weakly oxidizing metal ions (e.g. Ti^{IV}, Mo^{VI} and Zr^{IV}) involve peroxometal species in the key oxidative dehydrogenation step[41]. In oxidative dehydrgenation, the rate determining step is the elimination of the proton in which the basicity of the catalyst also plays an important role.

The dual functionality, namely the nature of the Zr(IV) ions with their redox property and the Lewis acidity controls the overall selectivity of the products.

3.4 CONCLUSIONS

Al-free zirconium silicate molecular sieves with MEL structure (Si/Zr >100) have been synthesized using two different zirconium sources viz., zirconium chloride (ZrCl$_4$) and zirconium (IV) acetylacetonate (Zr(acac)$_4$). They have been compared using XRD, SEM, FTIR, UV-Visible, surface area measurements and catalytic activity in the hydroxylation of phenol using aqueous H$_2$O$_2$. Although the increase in unit cell volume is only marginally different in both the samples, the catalytic activity is nearly twofold in the case of samples prepared using Zr(acac)$_4$. This may be due to the smaller particle size and larger surface area of the sample. A higher catechol formation in Zr-Sil-2(B) samples may be due to the external acid sites.

An increase in unit cell volume (from 5341 to 5375 Å^3) corresponding to the theoretical expansion due to the larger size of Zr^{4+} ions, the formation of Si-O-Zr linkages (FTIR spectra) and the characteristic charge transfer transition in the Td configuration (DR UV-visible spectra) indicate that up to 1.0 Zr atom per unit cell is substituted isomorphously in the framework positions of Zr-silicate in the MEL structure. This is further supported by the catalytic activity data in the hydroxylation of phenol and the catechol/hydroquinone ratio of about 0.94 in the products. The pyridine adsorption studies showed the presence of strong Lewis acid sites and weak Brönsted acid sites on the surface of Zr-silicate samples. These acid sites may be favourable for a high selectivity to propene at > 573 K in the reaction, in the decomposition of isopropanol. The active sites involve Zr(IV) as a tetrahedral species, sharing edges with two neighbouring SiO$_4$ tetrahedra from the silicalite lattice. Zr itself acts as a Lewis acid due to its coordinatively unsaturated nature. Thus it bears a δ+ charge so that –O$^{δ-}$-Si may be viewed as a Lewis acid-base pair in the form of Si-O-Zr linkages. Due to these acid-base characterisics, Zr-Silicalite-2 samples showed activity in the decomposition of isopropanol and oxidative dehydrogenation of ethanol.

3.4 REFERENCES

1. G., Bellussi, A. Carati, M. G. Clerici, A. Esposito, R. Millini and F. Buonomo, Belg. Patent 1,001,038 (1989).

2. J. S. Reddy, R. Kumar and P. Ratnasamy, Appl. Catal., L1 (1990) 58.

3. T. Sen, V. Ramaswamy, S. Ganapathy, P. R. Rajmohanan and S. Sivasanker, J. Phys. Chem. 100 (1996) 3809.

4. N. K. Mal, V. Ramaswamy, S. Ganapathy and A. V. Ramaswamy, Appl. Catal. A General 125 (1995) 233.

5. B. Rakshe, V. Ramaswamy, R. Vetrivel and A. V. Ramaswamy, Catal. Lett. 45 (1996) 41.

6. T. Yamaguchi, Catal. Today, 20 (1994) 199.

7. J. B. Miller, E. I. Ko, J. Catal. 153 (1995) 194.

8. M. Toba, F. Mizukami, S. Niwa, T. Sano, K. Maeda, A. Annila, V. Komppa, J. Mol. Catal. 94 (1994) 85.

9. A. T. Bell and A. Pines, *NMR techniques in Catalysis* (Marcel Dekker, Inc., New York, USA) p. 41.

10. G. T. Kokotailo, P. Chu, S. L. Lawton and W. M. Meier, Nature 275 (1995) 119.

11. G.R. Wang, X.Q. Wang, X.S. Wang and S.X. Yu, Stud. Surf. Sci. Catal., 83 (1994) 67.

12. S. Bordiga, F. Boscherini, S. Coluccia, F. Genoni, C. Lamberti, G. Leofanti, L. Marchese, G. Petrini, G. Vlaic and A. Zecchina, Catal. Lett. 26 (1994) 195.

13. C. Lamberti, S. Bordiga, D. Arduino, A. Zecchina, F. Geobaldo, G. Spano, F. Genoni, G. Petrini, A. Carati, F. Villain and G. Vlaic, J. Phys. Chem. B, 102 (1998) 6382.

14. K. Okumura and Y. Iwasawa, J. Catal. 164 (1996) 440.

15. J. Mieche-Brendle, L. Khouchaf, J. Baron, R. Le Dred and M. H. Tuilier, Micropor. Mater. 11 (1997) 171.

16. A. Bittar, A. Adnot, A. Sayari and S. Kaliaguine, Reserach on Chemical Intermediates 18 (1992) 49.

17. A. Zecchina, G. Spoto, S. Bordiga, A. Ferrero, G. Petrini, G. Leofanti and M. Padovan, Stud. Surf. Sci. Catal. 69 (1991) 251.

18. L. M. Kustov, S. A. Zubkov, V. B. Kazansky and L A. Bondar, Stud. Surf. Sci. Catal. 69 (1991) 303.

19. A. M. Prakash and L. Kevan, J. Catal. 178 (1998) 586.

20. C. Morterra, E. Giamello, L. Orio and M. Volante, J. Phys. Chem. 94 (1990) 311.

21. A.V. Ramaswamy and S. Sivasanker, Catal. Lett. 22 (1993) 239.

22. J.P. Gilson, E.G. Derouane, J. Catal. 88 (1984) 538.

23. F. Geobaldo, S. Bordiga, A. Zecchina and E. Giamello, Catal. Lett. 16 (1992) 109.

24. G. Tozzola, M. A. Mantegazza, G. Ranghino, G. Petrini, S. Bordigo, G. Ricchiardi, C. Lamberti, R. Zulian and A. Zecchina, J. Catal. 179 (1998) 64.

25. J. F. Bengoa, N. G. Gallegos, S. G. Marchetti, A. M. Alvarez, M. V. Cagnoli and A. A. Yeramián, Micropor. and Mesopor. Mater. 24 (1998) 163.

26. E. Giamello, M. Volante, B. Fubini, F. Geobaldo and C. Morterra, Mat. Chem. and Phys. 29 (1991) 379.

27. A. Gervasini and A. Auroux, J. Catal.131 (1991) 190.

28. M. Ai, Bull. Chem. Soc. Jpn 50 (1977) 355.

29. R. Rudham and A. I. Spiers, J. Chem. Soc., Faraday Trans. 93, 7 (1997) 1445.

30. M. A. Aramendía, V. Borau, C. Jiménez, J. M. Marinas, A. Porras and F. J. Urbano, J. Chem. Soc., Faraday Trans. 93, 7 (1997) 1431.

31. J. Graham, R. Rudham and C. H. Rochester, J. Chem. Soc., Faraday Trans. 80 (1984) 894.

32. G. A. M. Hussein, N. Sheppard, M. I. Zaki and R. B. Fahim, J. Chem. Soc., Faraday Trans. 85, 7 (1989) 1723.

33. G. A. M. Hussein, N. Sheppard, M. I. Zaki and R. B. Fahim, J. Chem. Soc., Faraday Trans. 87 (1991) 2661.

34. K. Tanabe, M. Misono, Y. Ono, H. Hattori, Stud. Surf. Sci. Catal. 51 (1989) 261.

35. B. O. Palsson, S. Fathi-Afshar, D. F. Rudd and E. N. Lightfoot, Science 213 (1981) 513.

36. J. E. Lgosdon, *Kirk-Othmer Encyclopedia of Chemical Technology*, 4th Ed., Vol. 9 (Wiley, New York, 1994) p. 812.

37. R. A. Sheldon, Bull. Soc. Chim. Belg. 94 (1985) 651.

38. P. R. Hari Prasad Rao, A. Thangaraj and A. V. Ramaswamy, J. Chem. Soc., Chem. Commun. 16 (1991) 1139.

39. S. Kannan, T. Sen and S. Sivasanker, J. Catal. 170 (1997) 304.

40. Y. Matsumura, K. Hashimoto and S. Yoshida, J. Catal. 117 (1989) 135.

41. Y. Matsumura, K. Hashimoto and S. Yoshida, J. Catal. 122 (1990) 352.

CHAPTER 4

Crystalline, microporous Zr-aluminosilicate molecular sieves with BEA structure (Zr-Al-β)
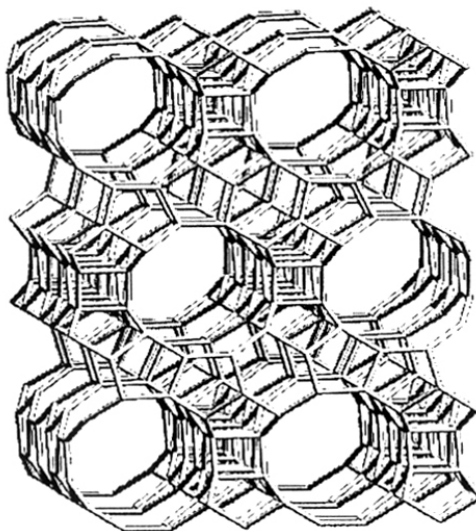
This chapter deals with synthesis and characterization of large pore, crystalline and microporous Zr- aluminosilicate molecular sieves with BEA structure (Zr-Al-β). The effect of zirconium incorporation on acid properties and hence on the catalytic activity in the m-xylene isomerization is investigated.

4.1 INTRODUCTION

The synthesis of medium-pore zirconium silicate molecular sieves with MFI and MEL structures is already discussed in Chapter 2 and 3, respectively. It is presumed that about 0.6 - 1.0 Zr atom per unit cell is located in the MFI and MEL framework which showed good activity in the hydroxylation of phenol using aqueous H_2O_2 and selectivity for the formation of catechol and hydroquinone[1,2]. These mildly acidic catalysts also showed a remarkable activity in the vapour phase decomposition of isopropanol and selectivity to propene and acetone at > 473 K[3]. However, their mild acid sites and relatively small pore openings of the structures limit the applications of such materials. It should be possible to overcome these limitations and improve the performance of Zr-containing molecular sieves by the synthesis of large pore structures such as zeolite beta (β). The possibility of synthesizing similar structures with other heteroatoms has attracted considerable attention recently. For example, Ti-, V- and Sn- modified β zeolites have been shown to be useful as catalysts in the selective oxidation of a number of organic substrates[4-7]. The synthesis methods of Ti- and Sn-containing β zeolites were modified using dealuminated zeolite-β by many researchers[7,8] to prepare Al-free Ti-β and Sn-β zeolites. These catalysts showed an enhanced activity and selectivity in the oxidation reactions with respect to the Al-Ti- and Al-Sn-β samples, respectively.

Zeolite β is of considerable interest due to its large micropore structure as well as high surface acidity and has found application in several reactions such as cracking, isomerization, alkylation and disproportionation[9-12]. Our aim is to incorporate Zr^{4+} ions in the framework of zeolite β and to investigate the effect of zirconium in the aluminosilicates on the acid properties and hence on the catalytic activity.

In this chapter, the synthesis of Zr-containing large pore aluminosilicates with BEA structure is discussed and their properties and catalytic activity with those of Zr-free Al-β and Zr-impregnated Al-β samples of similar Al contents are compared. The structural variations in these samples are characterized using different spectral techniques such as X-ray diffraction, diffuse reflectance UV-visible and FTIR spectroscopy. The intrinsic activity of zirconium is investigated in the isomerization of m-xylene at different contact times in the temperature range of 453 - 523 K. Additional Lewis as well as Brönsted acidities of Zr-Al-β

samples, as demonstrated by pyridine adsorption studies, are correlated with a marginal increase in the activity and selectivity to isomerization products (p- and o-xylenes), particularly at temperatures below 500 K.

4.2 EXPERIMENTAL METHODS

4.2.1 Hydrothermal synthesis

The Zr-Al-β zeolite samples were synthesized under hydrothermal conditions using gels with the following molar composition: SiO_2: x Na_2O: y ZrO_2: z Al_2O_3: 0.55 NEt_4OH: 30 H_2O, where x = 0.02 - 0.04; y = 0.01 - 0.02; z = 0.04 and NEt_4OH = tetraethylammonium hydroxide. In a typical preparation, 23.14 g of NEt_4OH (35% aqueous solution, Aldrich) was added slowly to 6 g of fumed silica (Sigma, S-5005, 99.8 %) in 27 g of deionized water. After stirring for 1 h, 0.48 g of $ZrCl_4$ (Merck, 98%) in 5 g of water was added dropwise to the mixture, under stirring. Then, 2.52 g of $Al_2(SO_4)_3$.16 H_2O (Loba Chemie) dissolved in 5 g of water was added. Finally, 0.4 g of NaOH (Loba Chemie, 99%) in the remaining volume of water was added. After stirring for 1 h, the milky gel (pH = 13.0) was transferred into a stainless steel autoclave and heated at 413 K for 10 days under static conditions. After completion of crystallization, the solid product was filtered, washed with deionized water, dried at 373 K and calcined in air at 873 K for 10 h. Two such Zr-Al-β samples (A and B, respectively) were prepared with different Zr contents and similar Al contents (SiO_2/ZrO_2 = 100 and 50; SiO_2/Al_2O_3 = 25). The Na- form of the synthesized samples was ion exchanged three times with 1 M NH_4NO_3 solution at 363 K and recalcined at 873 K for 10 h to obtain the H-form of Zr-Al-β samples.

The synthesis of Zr-Al-β in the absence of sodium and with lower concentration of aluminium (SiO_2/Al_2O_3 >50) was attempted, but the gel did not crystallize even after 30 days.

4.2.2 Post-synthesis methods

4.2.2.1 Zr-impregnated Al-β

For comparison, Zr-free Al-β (SiO_2/Al_2O_3 = 25) and a Zr-impreg. Al-β (SiO_2/ZrO_2 = 50 and SiO_2/Al_2O_3 = 25) were also prepared.

The Zr-free Al-β zeolite samples were synthesized using gels with the following molar composition: SiO_2: x Na_2O: y Al_2O_3: 0.55 NEt_4OH: 30 H_2O, where x = 0.02 - 0.04; y = 0.04 and NEt_4OH = tetraethylammonium hydroxide. In a typical preparation, 23.14 g of

NEt$_4$OH (35% aq. solution) was added slowly to 6 g of fumed in 27 g of deionized water. Then, 2.52 g of Al$_2$(SO$_4$)$_3$.16 H$_2$O (dissolved in 5 g of water) was added. Finally, 0.4 g of NaOH (Loba Chemie, 99%) in the remaining volume of water was added. After stirring for 1 h, the milky gel (pH = 12.8) was transferred into a stainless steel autoclave and heated at 413 K for 8 days under static conditions. After completion of crystallization, the solid product was filtered, washed with deionized water until free of chloride ions, dried at 373 K and calcined in air at 873 K for 10 h. The Na-form of the synthesized samples was ion exchanged three times with 1 M NH$_4$NO$_3$ solution at 363 K and recalcined at 873 K for 10 h to obtain the H-form of Al-β samples.

For the preparation of *Zr-impregnated Al-β (Zr-impreg. Al-β)*, 2 g of this Al-β sample was mixed with 0.17 g of ZrCl$_4$ in ~ 5 g of deionized water and made into a fine slurry with stirring for 30 min. The resultant mixture was dried at 383 K. Finally, the dried powder again mixed using mortar to obtain a homogeneous mixture. Then it was calcined in air 773 K for 8 h to get 3.2 wt.% Zr loading on Al-β.

4.2.2.2 Zr-impregnation on dealuminated-β

The Al-β sample (1 g) was dealuminated by dispersing it in 100 mL of 11 N HNO$_3$ and then, heated to 353 K with stirring the mixture for 5 h. After cooling to room temperature, the solid material was recovered by filtration, washed thoroughly with deionized water, dried at 383 K and then calcined. Zr-impregnation (SiO$_2$/ZrO$_2$ = 50) was carried out on this dealuminated beta sample (SiO$_2$/Al$_2$O$_3$ > 1000) by a similar method which was applied for the preparation of Zr-impreg. Al-β sample (Section 4.2.2). This sample is extensively characterized using solid state MAS NMR spectroscopy (section 4.3.7).

4.2.3 Characterization

The calcined samples are characterized by X-ray diffraction, scanning electron microscopy, diffuse reflectance UV-visible spectroscopy, FTIR and NMR spectroscopy. The elemental analysis was performed using ICP emission spectroscopy and X-ray fluorescence spectroscopic (XRF) methods. The micropore areas and micropore volumes were determined from the N$_2$ adsorption isotherms at liquid nitrogen temperature.

4.2.3.1 Powder X-ray diffraction

Powder XRD patterns of the calcined Zr-Al-β samples were obtained on a Rigaku diffractometer (model D-MAX III VC), using Ni filtered CuKα radiation and graphite crystal

monochromator. The patterns were recorded in 2θ range of 5° - 50° at a scan rate of $1°\text{min}^{-1}$ with a continuous rotation of the samples during the scanning. Silicon was used as an internal standard. The phase purity of all the samples was checked by comparing the X-ray data available in the literature for BEA topology[13]. The degree of crystallinity of the calcined samples was determined with reference to a highly crystalline Zr-free Al-β sample (prepared under similar conditions). The unit cell parameters were calculated from the corrected d values and refined by using least squares fitting.

4.2.3.2 Scanning electron microscopy

The morphology and particle size was determined using a Leica Stereoscan 440 scanning electron microscope. The samples were finely dispersed in a solvent, ethyl alcohol on the surface of a metallic sample holder. Then these samples were sputtered with a thin layer of silver paint to prevent surface charging and to protect any thermal damage due to the electron beam.

4.2.3.3 Thermal analysis

The calcination process was monitored by thermogravimetry (TG) and differential thermal analysis (DTA) using a Setaram TG/DTA – 92 instrument. About 28 mg of this as-synthesized sample was placed in a platinum crucible and α-alumina was used as a reference. The measurements were performed with a heating rate of 10 K. min^{-1} in the range of 298 – 1273 K.

4.2.3.4 Chemical analysis

In a typical analysis, around 100 mg of sample weighed exactly in a Pt crucible and heated until a constant weight to obtain the dry sample. The anhydrous sample was treated with hydrofluoric acid (HF, 40% aqueous) and evaporated to remove silicon. The loss in the weight of the sample on ignition was determined to calculate the content of silica. The residue was dissolved in 2-3 drops of concentrated sulphuric acid + 10 mL of HF and then transferred to a Teflon container. This solution mixture was heated at 383 K for 6 h. After cooling, the solution was diluted to 100 mL of solution and then analyzed in *inductively coupled plasma* (ICP) spectrometer, model Jobin Yuon-38 VHR.

The Si/Zr molar ratios of the calcined samples were also determined by *X-ray fluorescence* spectrometer (XRF) in Rigaku, model 3070, using CuKβ radiation.

4.2.3.5 Diffuse reflectance UV-visible spectroscopy

Diffuse reflectance (DR) UV-visible spectra of fine powder samples were recorded on a Shimadzu spectrophotometer (model UV-VIS 2101 PC). $BaSO_4$ was used as an external standard to correct the baseline in the spectra.

4.2.3.6 Adsorption methods

The micropore areas and micropore volumes were calculated from the N_2 adsorption isotherms at liquid N_2 temperature (Coulter 100CX Omnisorb). The monolayer volumes were taken at $p/p_o = 0.05$, where all micropores are filled up. The mesopore areas were obtained from the t-plots of N_2 adsorption data at higher partial pressures. The microporous volume and mesopore surface area were calculated using t-plot method.

4.2.3.7 Solid state NMR spectroscopy

^{29}Si and ^{27}Al MAS NMR spectra of the samples at room temperature were obtained on a Bruker MSL-300 MHz spectrometer at a resonance frequency of 59.6 MHz and 78.2 MHz, respectively. Magic angle spinning was carried out in zirconia rotors. The chemical shifts (in ppm) were recorded with respect to tetramethylsilane (TMS) for ^{29}Si and aluminium hydroxide $(Al(OH_2)_6^{3+})$ for ^{27}Al MAS NMR spectra.

4.2.3.8 Fourier transform Infra-red spectroscopy

The framework IR spectra were recorded in the region of $400 - 1300$ cm^{-1} using a 60 SXB Nicolet FTIR spectrophotometer. The samples were prepared by KBr pellet (1:300 mg) technique.

For the determination of acid sites, FTIR spectra of Zr-Al-β(B), Zr impreg. Al-β and Al-β samples were recorded between 4000 and 1300 cm^{-1} (hydroxyl and pyridine) regions. The samples were pressed into self- supported wafers with a radius (R) of 0.5 cm and a weight (W) of 7 mg and placed in the IR cell. The wafers were pretreated at 673 K for 3 h, *in vacuo* (1.33×10^{-4} Pa) and then equilibrated with pyridine (1.33×10^3 Pa) after cooling to 373 K. All spectra (500 scans) were run at a resolution of 4 cm^{-1}, after subsequent desorption of the wafers for 1 h at different temperatures of 373, 473, 573 and 673 K.

4.2.4 Catalytic properties: Isomerization of m-xylene

The isomerization of m-xylene was performed over Zr-Al-β molecular sieves with different Si/Zr atomic ratios in the temperature range of 453 to 523 K. These reactions were

carried out in a fixed-bed down-flow glass reactor (internal diameter = 13 mm) at atmospheric pressure. Prior to a typical catalytic run, the H-form of the zeolite catalyst in the form of pellets (8 × 10-mesh size) was heated to 723 K in air for 2 h. The reactor was then cooled down to the reaction temperature under a flow of nitrogen. The contact times of the samples, expressed as W/F, with 'W' the weight of the catalyst and 'F', the molar flow of m-xylene feed (Aldrich, 99.8%) at the reactor inlet were kept in the range of 1.06 to 4.25 h. The steady state conversions were calculated after 90 min. The analyses of the products were performed in a gas chromatograph (Shimadzu GC-14B) equipped with a flame ionization detector and a 2 m long stainless steel column packed with 5 % bentone and 5% diisodecylphthalate. The mass balances (99.5wt%) were done on the basis of wt. of products i.e. the fractions collected after the reaction with respect to m-xylene fed. The feed used was 99.9% pure. The calibration was done with external standards of different concentrations prior to all GC analyses and corresponding response factors were used for the processing of the GC results.

4.2.4.1 Silynation of the Catalyst

For *silynation*, the catalyst (0.9 g) was exposed to a vaporized feed consisting of 45 wt.% toluene, 48.5 wt.% methanol and 6.5 wt.% tetraethylorthosilicate at 473 K in a fixed bed down-flow reactor. The coke formed during the deposition was burned off by heating the catalyst at 823 K in a flow of dry air. The m-xylene isomerization was subsequently carried out over the silynated catalyst.

4.3 RESULTS AND DISCUSSION

4.3.1 Characterization

4.3.1.1 Powder X-ray diffraction

The powder X-ray diffraction profiles of calcined samples are similar to Al-β (Figure 4.1). The crystallinity was evaluated by a comparison of the area of the most intense diffraction peak in the 2θ range of 20°- 24° to that of parent zeolite (Al-β) sample taken as 100% crystalline, after background subtraction (Table 4.1). It was observed that FWHM (full width of half-maximum intensity)[14] for the first broad peak (2θ = 7.7°) increases with an increase in the concentration of zirconium in BEA framework. This is a consequence of the decrease in the crystallite size, which is in agreement with an increase in the micropore
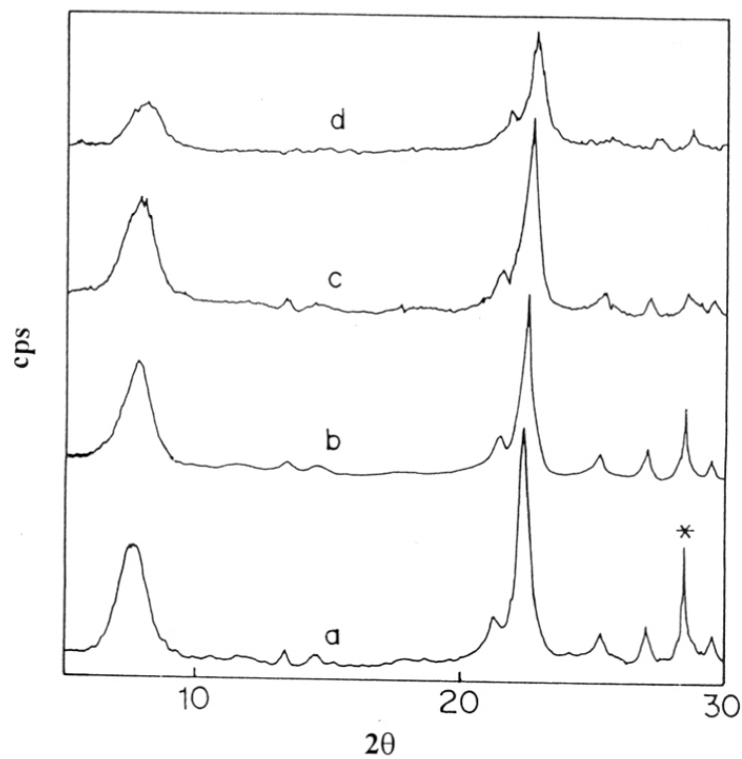
Figure 4.1: X-ray diffraction profiles of calcined Al-β, Zr-impreg. Al-β, Zr-Al-β(A), and Zr-Al-β(B) samples **(curves a to d)**, respectively (* = reference Si peak).

Table 4.1 Physico-chemical characteristics of Zr-Al-β samples

Sample	SiO$_2$/Al$_2$O$_3$		SiO$_2$/ZrO$_2$		XRD parameters							Micropore area, m^{2}g^{-1}	Mesopore area[c], m^{2}g^{-1}
	gel	product	gel	product	crystallinity, %	FWHM	Crystallite size[a], Å	α^{b} = I$_b$ / I$_n$	a (Å)	b(Å)	UCV, Å^3		
Al-β	25	26	-	-	100	1.41	57.1	0.55	12.4938	26.3405	4112	352	13.0
Zr-Al-β (A)	25	27	100	115	88	1.48	54.1	0.57	12.4670	26.4404	4110	501	28.8
Zr-Al-β (B)	25	27	50	63	75	1.59	50.5	0.47	12.4241	26.4519	4083	530	33.0
Zr-impreg. Al-β	25	26	-	52	97	1.42	56.4	0.58	12.4935	26.3400	4111	490	3.2

[a] calculated using Debye-Scherrer equation, D (Å) = kλ/√ b cos θ (14).

[b] I$_b$: Intensity of broad peak at 2θ = 7.7° and I$_n$: Intensity of sharp peak at 2θ = 22.5°.

[c] From the t-plot.

surface area of Zr-Al-β samples.

The combination of sharp and broad features of the X-ray pattern of BEA structure due to the stacking disorder of the atomic planes complicates the interpretation of diffraction data by conventional methods. This interplanar fault probability (the probability of a change in the handedness of the stacking sequence), $\alpha = (I_b / I_n) = 0.1 - 0.58$ approximates polymorph A type structure (tetragonal crystal system), where, I_b = Intensity of first broad peak at $2\theta = 7.7°$ and I_n = Intensity of sharp peak at $2\theta = 22.5°$[15]. All samples including Zr-free Al-β also showed $I_b / I_n = \approx 0.50 - 0.57$ which are found to be in favour of *polymorph A* structure. Therefore, unit cell parameters of the samples were determined by least squares fitting to the corrected 'd' values with respect to silicon as an internal standard, based on a tetragonal system. There is a linear reduction along 'a' axis and an increase along 'c' axis. This results in a marginal change in unit cell volume with an increase of Zr content in the samples. These anisotropic changes in the unit cell parameters may be an indication of the different orientation of crystallites along a particular crystallographic axis, due to Zr-defects. As shown in Table 4.1, all XRD parameters of Zr-impreg. Al-β sample were found to be similar to those of Al-β sample. This shows clearly that extraframework Zr could not modify the properties of β zeolite in comparison to Zr-Al-β samples.

4.3.1.2 Scanning electron microscopy

Scanning electron micrographs (Figure 4.2) confirmed the absence of any amorphous material around the crystals. The samples showed uniformly dispersed cuboid crystals with particle size of $0.5 - 1.0$ μm.

4.3.1.3 Thermal analysis

As-synthesized Zr-Al-β samples were monitored in the range of 373 - 1173 K by TG/DTA analysis. *Thermogravimetric (TG) analysis* showed a sharp weight loss in the range of $623 - 761$ K, which is due to the decomposition of NEt_4OH template, occluded within the channels of the zeolite structure. The total weight loss due to removal of this template is about 10.0 wt.% for all samples.

Figure 4.3 shows two exothermic peaks, one is at 589 K due to a removal of the inner strained bulky TEA^+ ion, which neutralizes the defect Si-O⁻ group in the BEA framework. The second exothermic peak (strong) at 698 K may be attributed to the removal of more symmetrical TEA^+ ions from the channels of the molecular sieve.
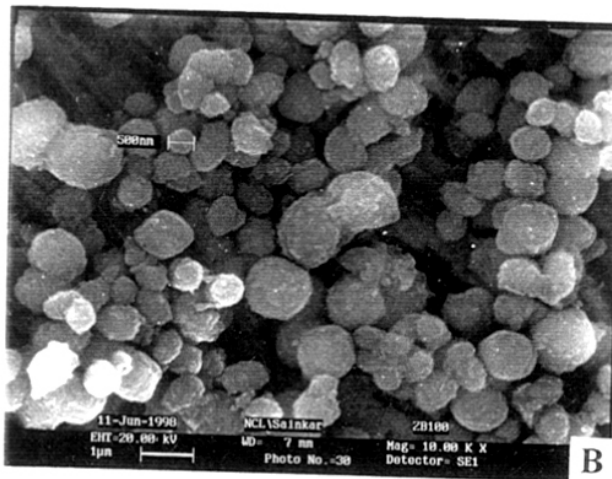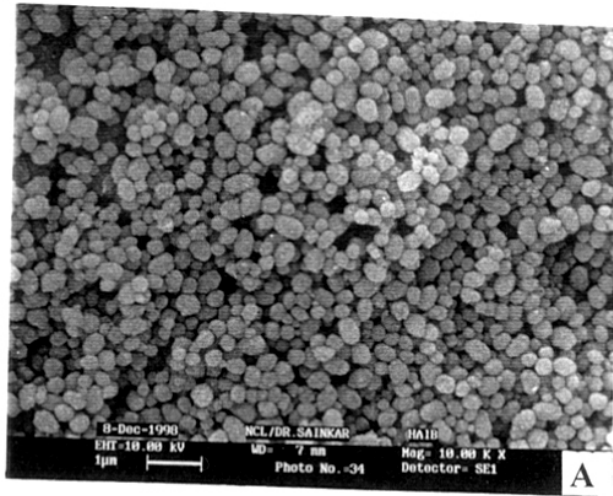
Figure 4.2: Scanning electron micrograph of (**A**) Al-β and (**B**) Zr-Al-β(A) samples, respectively.
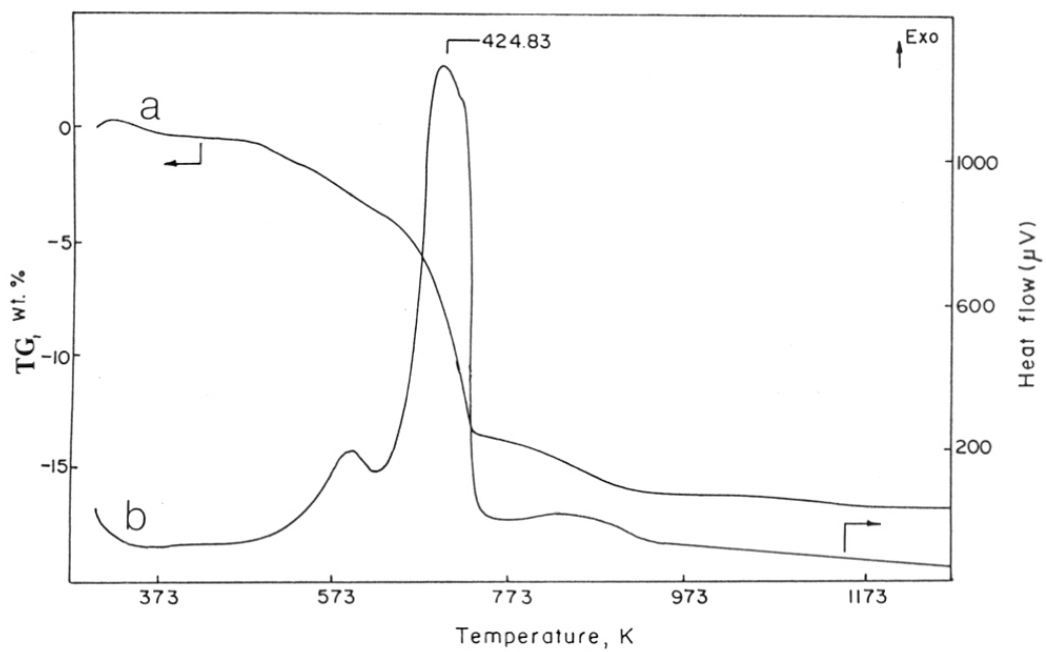
Figure 4.3: Thermogram (TG) **(curve a)** and DTA curve **(b)** of Zr-Al-β(A) sample, respectively.

4.3.1.4 Diffuse reflectance UV-visible spectroscopy

The diffuse reflectance UV spectra of Al-β, Zr-impreg. Al-β, Zr-Al-β(A), Zr-Al-β(B) ZrO$_2$ samples (curves a to e, respectively) are shown in Figure 4.4. An absorption at about 206 nm is attributed to the ligand-to-metal charge transfer involving isolated Zr(IV) atoms in tetrahedral coordination (curve c and d)[16]. There is a remarkable increase in the intensity of 206 nm band with Zr content in the BEA structure. These electronic transitions are clearly distinguishable from those in Zr-impreg. Al-β (curve b) and ZrO$_2$ (monoclinic symmetry) (curve e) which show absorptions at about 210 and 240 nm, respectively. A similar observation is reported by Blasco et al. for Ti-containing Al-β zeolite samples[17]. However, no band at 240 nm corresponding to zirconia was detected in our samples (curve c and d).

4.3.1.5 Adsorption methods

The N$_2$ adsorption isotherms are characteristic of microporous materials. The micropore volumes are in the range of 0.18-0.20 mL g^{-1}. The micropore surface areas are in the range of 530 m^{2}g^{-1} in comparison to a value of 452 m^{2}g^{-1} obtained for Al-β sample. A small contribution of mesopore area is observed in the sample of Zr-Al-β(B) which has a higher Zr content (6.2 %). (Figure 4.5)

4.3.1.6 Solid state NMR spectroscopy

The chemical shifts observed in ^{29}Si MAS NMR are always sensitive to the nature as well as the number of heteroatoms as nearest neighbours of SiO$_4$ in the tetrahedral framework of zeolites.

^{29}Si MAS NMR spectra of all samples exhibit predominately an intense and broad signal at around −109 ppm, as shown in Figure 4.6(A). It corresponds to Td framework Si atoms in Si(OSi)$_4$ environment, located in different crystallographic sites[18]. Zr-Al-β sample showed an additional peak centered at -101 ppm (curve d). This downfield resonance is assigned to the superposition of signals of Si atoms in Si(OSi)$_3$(OAl) or Si(OH)(OSi)$_3$ environment[19]. However, the spectra of dealuminated Zr-β (Si/Al > 1000) also showed this type of species (curve c). Therefore, this signal is likely to be due to the distorted Si species in Si(OSi)$_3$ (OZr) environment. A broadening of this resonance line was observed with Zr content. These results indicated that Zr^{4+} ions are probably linked to the defect silanol groups in tetrahedral coordinations. Earlier ^{29}Si MAS NMR studies on the homogeneous zirconia-silica materials by Terry et al.[20] have shown similar resonance at − 99 ppm in the spectra due
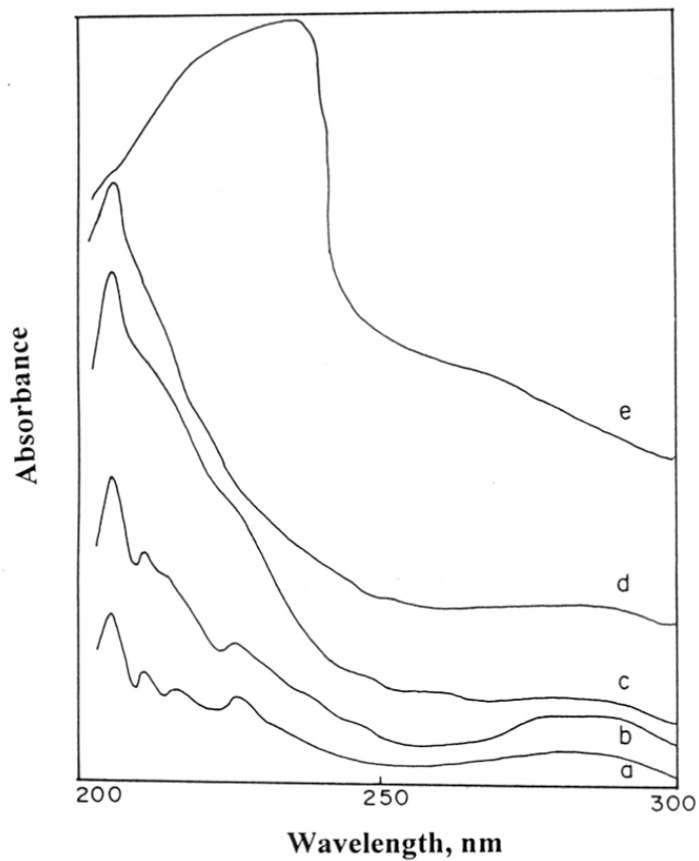
Figure 4.4: Diffuse reflectance UV spectra of Al-β, Zr-impreg. Al-β, Zr- Al-β(A), Zr-Al-β(B) and ZrO$_2$ samples **(curves a to e)**, respectively.
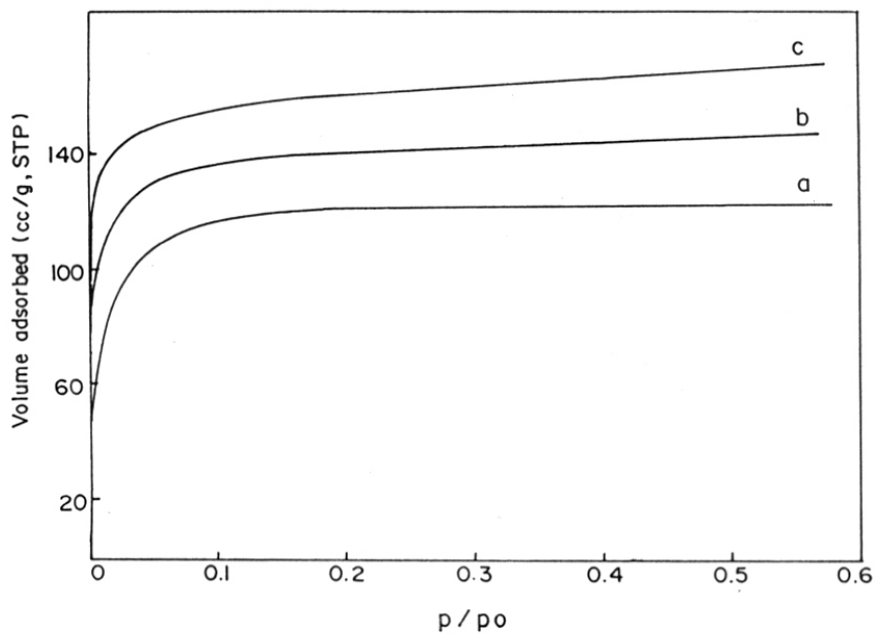
Figure 4.5: Nitrogen adsorption isotherms of Al-β **(curve a)**, Zr-impreg. Al-β and Zr-Al-β(A) **(curves b to c)**, respectively.
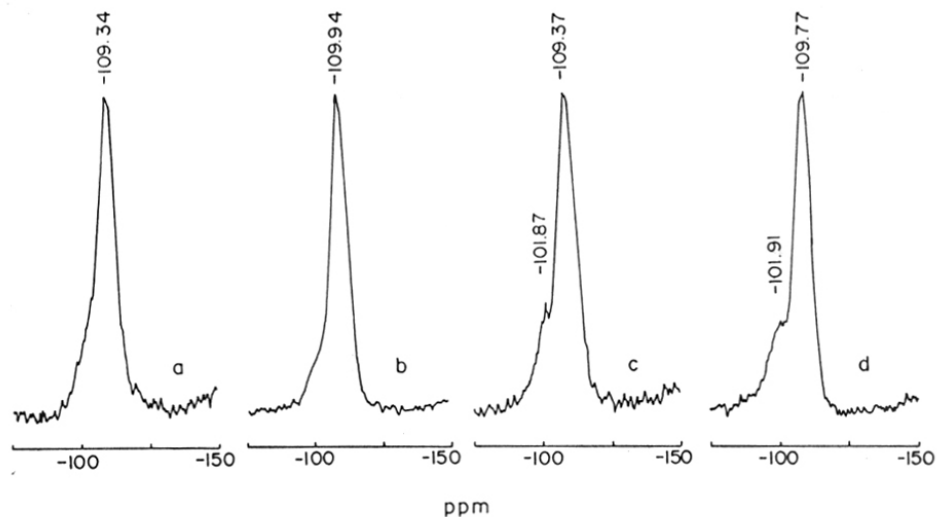
Figure 4.6(A): ^{29}Si MAS NMR spectra of Al-β **(curve a)**, Zr-impreg. Al-β, Zr-impreg. dealuminated Al-β and Zr-Al-β(A) **(curves b to d)**, respectively.
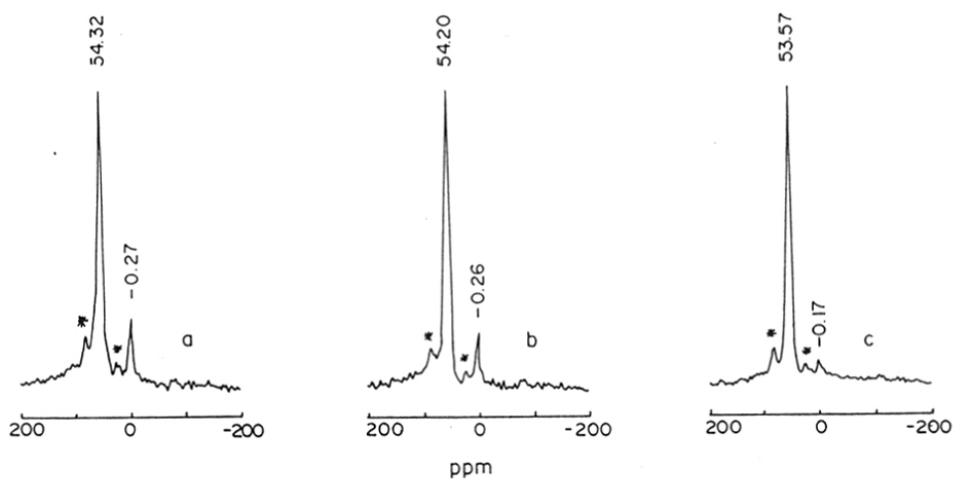
Figure 4.6(B): ^{27}Al MAS NMR spectra of Al-β **(curve a)**, Zr-impreg. Al-β and Zr-Al-β(A) **(curves b to c)**, respectively. (Spinning side bands (*).

to Si $(OSi)_{4-n}(OZr)_n$ sites ($n = 1,2$; designated as Q^3 and Q^2 sites, respectively).

27Al MAS NMR spectra of the samples exhibit predominately an intense peak due to tetrahedral (Td) framework aluminium atoms. In addition to this, a signal at -0.2 ppm was observed which indicates the presence of octahedral (Oh) aluminium. The relative intensity of these additional peaks due to a higher coordination of Al atoms remarkably decreases in Zr-Al-β samples (curve c). H-Al-β exhibits the broadest NMR lines and therefore, contains a distribution of Al in both Td and Oh coordination, due to a considerable number of defect sites $(Si-O^-)$[21]. It could be due to removal of TEAOH, which leads to the transformation of some of the Td framework Al to the Oh Al species.

4.3.1.7 Fourier transform infra-red spectroscopy

(i) The framework region

The FTIR spectra in the region of *framework vibrations* were recorded to ascertain the high degree of crystallinity of Al-β, Zr-Al-β(A), Zr-impreg. Al-β and Zr-Al-β(B) samples (Figure 4.7, curves a to d, respectively), using the KBr pellet technique. All the spectra showed sharp features at 1232, 1098, 850, 580, 565 and 468 cm^{-1}, which are typical of zeolite beta structure[15,22]. The band at 1232 cm^{-1}, due to asymmetric stretching vibrations of Si-O-T (T= Al, Zr) in Zr-free Al-β and Zr-impreg. Al-β (curves a and c) is shifted to lower wavenumbers of 1222 cm^{-1} in Zr-Al-β (B) sample (curve d) with increasing Zr content in the BEA framework. A characteristic band (shoulder) at ~ 963 cm^{-1} is also observed in the Zr-Al-β as well as Al-β samples, which may be due to internal $Si-O^-$ defect sites[23].

(ii) Determination of acid sites

Infrared spectra of Al-β, Zr-impreg. Al-β and Zr-Al-β(B) samples in the *hydroxyl region* are shown in Figure 4.8 (curves a to c, respectively). The spectrum of Zr-Al-β (curve c) showed relatively higher integrated intensities than the spectra of Al-β (curve a) and Zr-impreg. Al-β (curve b) samples in the region of 4000 - 3000 cm^{-1}. All spectra exhibited the classical absorptions at 3607 $(Si-OH^+-Al)$ and 3731 cm^{-1} which are due to framework bridging acidic OH and terminal silanols, respectively. A weak band at 3780 – 3775 cm^{-1} is attributed to extra-framework hydroxyl groups. The band at 3660 cm^{-1} due to alumina like species is not observed. The broad band at 3700-3000 cm^{-1} is generally assigned to H-bonded SiOH groups which may be located in the hydroxyl nests or framework defect sites[24].

The *nature of acid sites* in the samples of Zr-Al-β(B), Zr-impreg. Al-β and Al-β
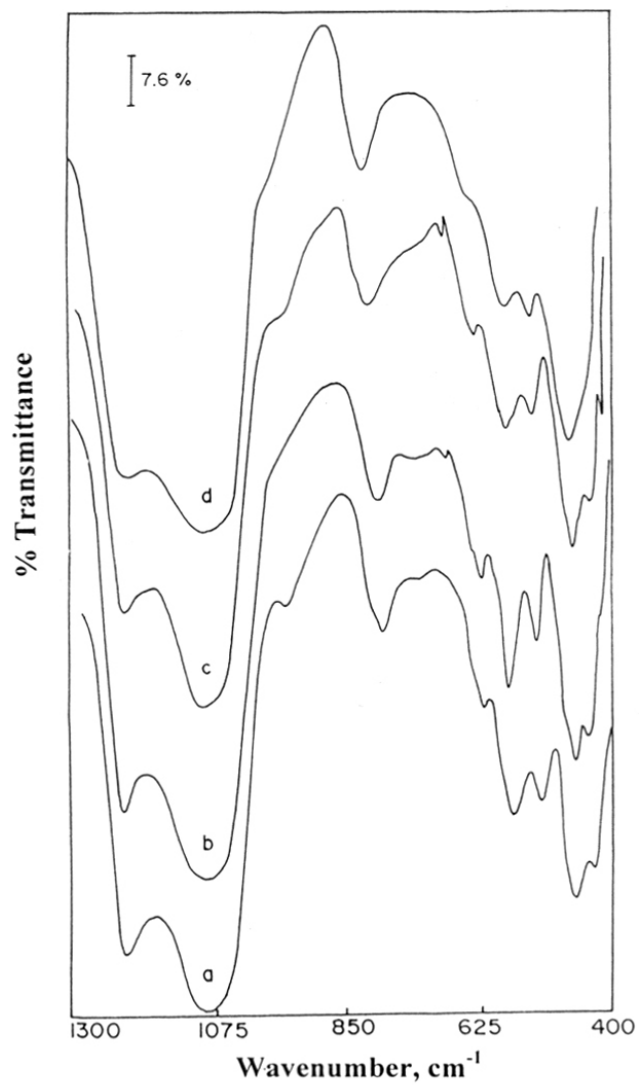
Figure 4.7: Infrared spectra of Al-β, Zr-Al-β(A); Zr-impreg. Al-β and Zr-Al-β(B) samples (curves a to d), respectively.
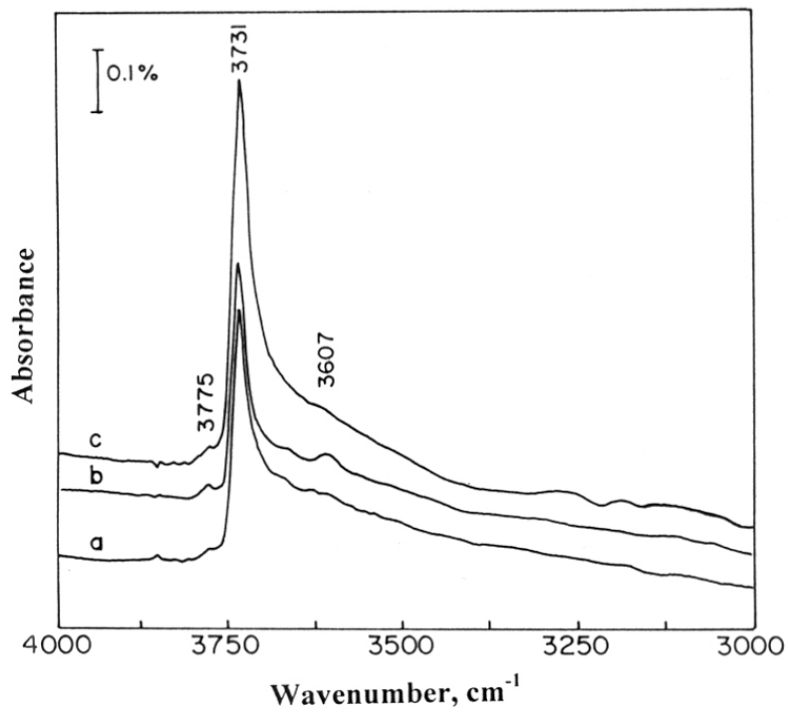
Figure 4.8: Infrared spectra of Al-β, Zr-impreg. Al-β and Zr-Al-β(B) samples in the hydroxyl region, after evacuation at 673 K (curves a to c), respectively.

samples (Figure 4.9 A to C, respectively) was characterized by adsorption of pyridine at 373 K (curve a) and stepwise desorption at increasing temperatures of 473, 573 and 673 K (curves b to d, respectively). In the range of $1750 - 1300$ cm^{-1} of the spectra of all samples, chemisorbed pyridine was revealed by the usual set of bands: the band at 1540 cm^{-1}, indicative of pyridinium ion (pyH$^+$); and the bands at 1445 and 1618 cm^{-1}, related to Lewis-bonded pyridine. The superposition of signals of both protonic acid sites (N$^+$-H) as well as on Lewis acid adsorbed species at 1490 cm^{-1} is also observed[25]. The coordinately bonded pyridine (1445 cm^{-1}) and some pyridinium ions (1540 cm^{-1}) are retained even after evacuation of the samples at 673 K. Also, the higher intensities of the bands at 1620 cm^{-1} and 1445 cm^{-1} indicate that the surface acidity of the samples is predominately of the Lewis type.

For the determination of the fractions of *Brönsted and Lewis acid sites* on the surface, the integrated intensities of PyH$^+$ and PyL bands (1540 and 1445 cm^{-1}, respectively) were estimated, after background subtraction. A plot of these values at different desorption temperatures is shown in Figure 4.10. The integrated intensities of Brönsted and Lewis acid sites of these samples after evacuation at different desorption temperatures show that Zr-Al-β sample appears significantly more acidic than either Zr- free Al-β or the Zr-impreg. Al-β samples.

The concentrations of Brönsted and Lewis acid sites were calculated from the integrated intensities of PyH$^+$ and PyL bands and the molar extinction coefficients of these bands (1.67 and 2.22 cm. μmol^{-1}, respectively)[26]. A comparison of these values with the concentration of total acid sites (in forms of Al and Zr atoms in millimoles per gram of the sample) is presented in Table 4.2. It indicates that incorporation of Zr^{4+} ions in Al-β structure generates additional acidity due to the strong polarization of possible Si-O$^{\delta-}$...Zr$^{\delta+}$ linkages. Thus, it verifies that there are two types of linkages viz., Si - O...Zr and Si – O...Al, which due to their different polar nature play an important role in the acid site distribution of Zr-Al-β samples.

In Chapter 3, the IR spectra of pyridine adsorbed on the samples of Zr-silicates with MEL structure have also been interpreted as an indication that the tetrahedral Zr in the silicalite lattice bears a $\delta+$ charge so that O$^{\delta-}$...Zr$^{\delta+}$ bond may be viewed as a Lewis acid-base pair.
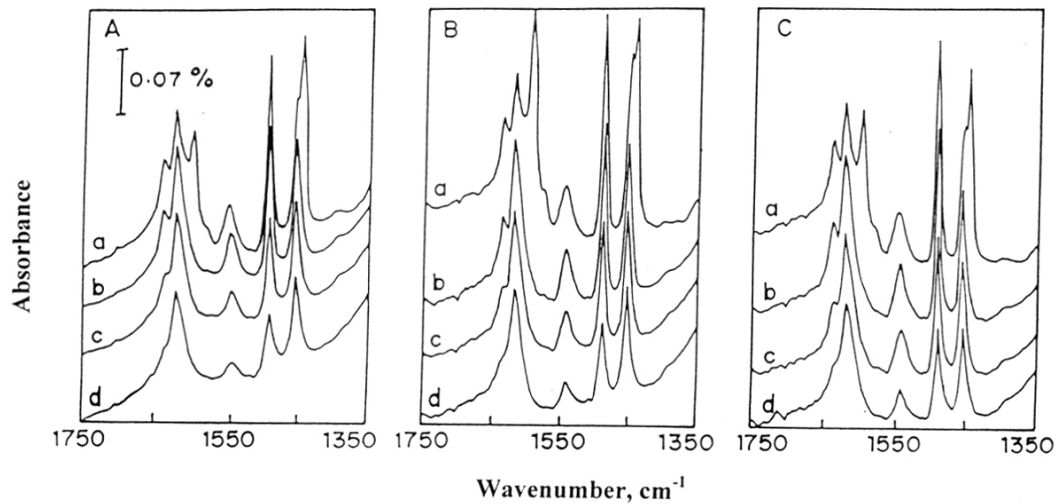
Figure 4.9: Infrared spectra of pyridine adsorbed on the **(A)** Zr-Al-β(B); **(B)** Zr-impreg. Al-β and **(C)** Al-β samples after evacuation at the different temperatures of 373, 473, 573 and 673 K (curves a to d), respectively.
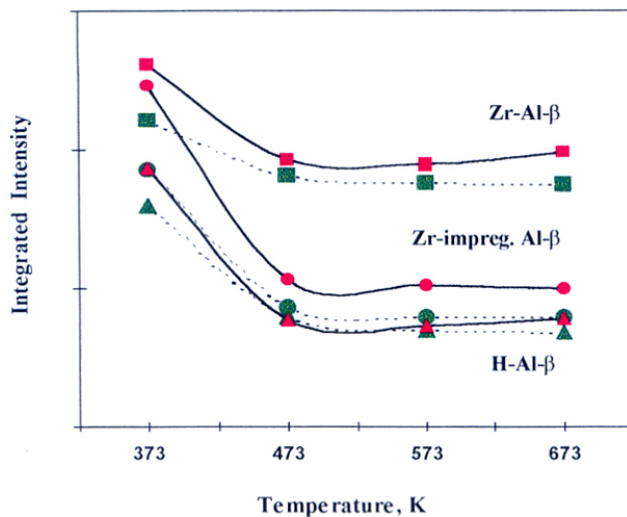
Figure 4.10: A plot of integrated intensities of the bands 1540 cm^{-1} (Brönsted bound pyridine) and 1445 cm^{-1} (Lewis bound pyridine). as shown by dotted (green bullets) and solid line (pink bullets), respectively vs. desorption temperatures of Al-β (▲) and Zr-impregnated Al-β (●) and Zr-Al-β(B) (■) samples.

Table 4.2: Effect of different desorption temperatures on the Brönsted and Lewis Acidity

Sample	Desorption Temp. , K	I_{1540}/I_{1445}	Concentration, mmol.g^{-1} of sample			
			B[a]	L[a]	B+L	(Al + Zr)[b]
	373	0.86	1.07	0.94	2.01	2.56
Al-β	473	1.02	0.53	0.39	0.92	(only Al)
	573	0.96	0.47	0.36	0.83	
	673	0.87	0.46	0.39	0.85	
	373	0.80	1.24	1.16	2.40	3.00
Zr-impreg. Al-β	473	0.82	0.58	0.53	1.11	
	573	0.78	0.53	0.51	1.04	
	673	0.79	0.54	0.50	1.04	
	373	0.90	1.48	1.23	2.71	2.90
Zr-Al-β(B)	473	0.94	1.21	0.96	2.17	
	573	0.93	1.18	0.95	2.13	
	673	0.89	1.18	0.99	2.17	

[a]Concentration of pyridine adsorbed on Brönsted (B) and Lewis (L) acid sites per gram of sample, respectively, using Beer's law: $(C = \varepsilon \times IA \times \pi R^2/W)$.

[b]Concentration of Al and Zr atoms (calculated from molar output Si/Al and Si/Zr ratios) per gram of the sample.

4.3.2 Catalytic properties: Isomerization of m-xylene

The isomerization of m-xylene to p- and o- isomers is an important petrochemical process[27]. This reaction is widely used in the laboratory to characterize the zeolites with ten- and twelve-membered rings, such as ZSM-5 and mordenite on the basis of their different shapes and dimensions of the intracrystalline cavities[28-30]. The isomerization of m-xylene to p- and o- xylenes occurs by intramolecular 1,2 methylshift (unimolecular mechanism). Whereas disproportionation of m-xylene into toluene and trimethylbenzenes occurs by intermolecular 1,2 methyl shift (bimolecular mechanism), as shown in Scheme I (A). The isomerization to disproportionation selectivity is determined by the strong isolated acid sites which are present in the cavities that allow the formation of at least one of the possible bimolecular transition state complexes for disproportionation, in the group of twelve-membered ring zeolites[31] (Scheme I B). Here, we have estimated the values of selectivities towards isomerization (I) and disproportion (D) products with a comparison of the acidity of Zr-Al-β(B), Zr-impreg. Al-β and Al-β samples.

4.3.2.1 Effect of temperature

Table 4.3 summarizes the effect of different temperatures in the range of 453 - 523 K on the product distribution of Al-β, Zr-impreg. Al-β and Zr-Al-β(B) catalysts, at a contact time of 1.06 h. The catalytic activity of Zr-Al-β(B) sample is marginally higher than that of Al-β and it increases further with temperature. It was observed that the formation of isomerization products i.e., p- and o- xylenes is favoured at lower temperatures. At higher temperatures, however, the selectivity for the disproportionation products, i.e., toluene and trimethylbenzenes is enhanced with a loss in the selectivity for isomerization products. As the temperature increases (> 523 K), the conversion of m-xylene increases rapidly and reaches equilibrium values.

4.3.2.2 Isomerization/Disproportionation selectivity

The p-/o- xylene ratio in the products is about 1.0-1.4, suggesting that there is no diffusion controlled product shape selectivity, as the pores are large enough to allow rapid diffusion of the xylene isomers. In contrast to ten-membered ring zeolites, the p/o-selectivity in twelve-membered ring zeolites is not influenced by diffusion but by the transition-state shape selectivity[32]. Martens et al. have reported the values of p/o- selectivity to be of 1.0 – 1.4 for various 12- membered ring zeolites with mono-, bi- and tri-dimensional

o-xylene   p-xylene

Isomerization

Toluene   1,2,3 -TMB   1,2,4 -TMB   1,3,5 -TMB
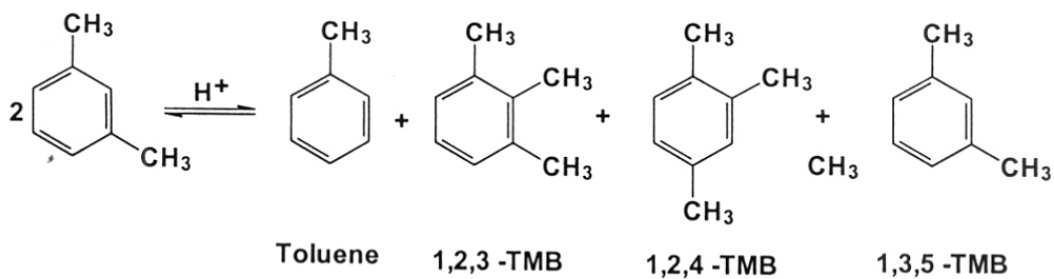
Disproportionation

A. Reactions during the isomerization of m-xylene
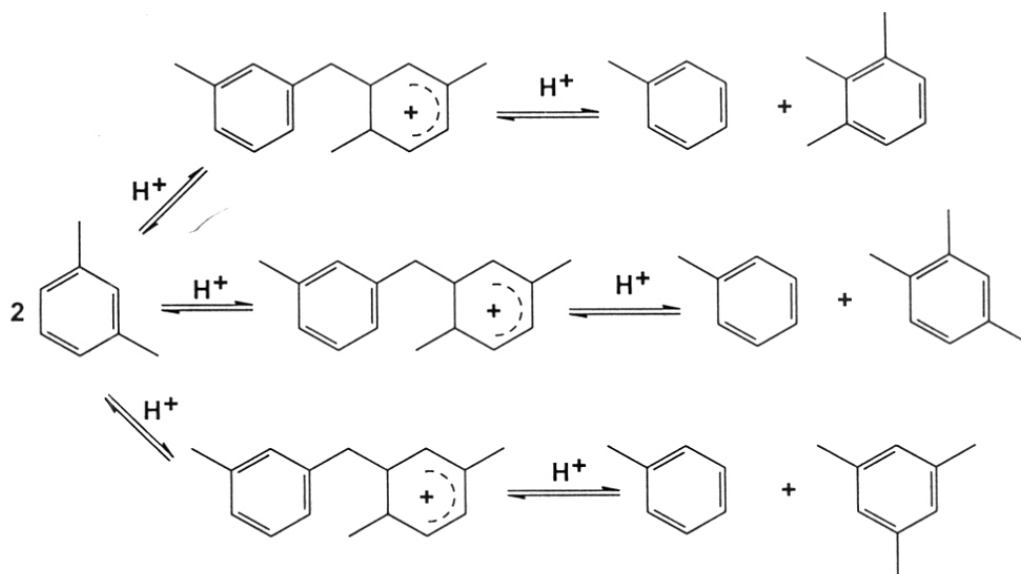
B. Possible transition states during the disproportionation of m-xylene

Scheme (I)

Table 4.3: Effect of temperature on the product distribution in the isomerization of m-xylene[a]

Catalyst	Temp .(K)	m-xylene Conv. (mol%)	p-xylene	o-xylene	I[b] (total)	toluene	Trimethylbenzenes			D[c] (total)	I/D
							1,3,5-	1,2,4-	1,2,3-		
	453	5.0	41.5	40.5	82.0	10.1	1.8	6.0	0.1	18.0	4.6
	473	6.3	39.7	39.7	79.4	10.3	3.2	6.7	0.4	20.6	3.9
Al- β	498	15.0	43.3	38.0	81.3	8.9	3.3	6.0	0.5	18.7	4.3
	523	33.6	40.3	35.0	75.3	10.4	3.0	10.3	1.0	24.7	3.0
	453	1.0	56.0	23.2	79.2	20.8	0.0	0.0	0.0	20.8	3.8
Zr-impreg.	473	4.2	43.0	33.9	76.9	12.9	1.2	9.0	0.0	23.1	3.3
Al-β	498	8.2	38.4	35.4	73.8	13.2	2.6	10.1	0.4	26.2	2.8
	523	30.5	35.8	32.6	68.4	14.2	4.6	11.5	1.1	31.5	2.2
	453	5.7	53.0	41.7	94.7	3.5	0.0	0.0	0.0	5.3	17.9
Zr-Al-β	473	8.5	51.7	43.6	95.3	4.7	0.0	0.0	0.0	4.7	20.3
(sample B)	498	20.0	52.5	38.0	91.5	5.0	0.0	3.5	0.0	8.5	10.8
	523	34.1	41.9	34.3	76.2	12.3	3.2	8.2	0.1	23.8	3.2

[a]Contact time : 1.06 h; [b]Selectivity for isomerization products; [c]Selectivity for all disproportionation products.

Table 4.4: Effect of different contact times on the conversion and selectivities of isomerization and disproportionation products at various temperatures

Catalyst	Temp., K	Contact time, h											
		1.06			1.42			2.12			4.25		
		m-xylene Conv. (mol%)	Selectivity		m-xylene Conv. (mol%)	Selectivity		m-xylene Conv.(mol%)	Selectivity		m-xylene Conv. (mol%)	Selectivity	
			I[a]	D[b]		I	D		I	D		I	D
Zr-Al-β (B)	453	5.7	94.7	5.3	7.4	82.4	17.6	11.1	68.5	31.5	13.8	65.2	34.8
	473	8.5	95.3	4.7	15.3	79.7	20.3	18.8	64.4	35.6	31.9	60.8	39.2
	498	20.0	91.5	8.5	30.2	76.8	23.2	36.0	66.4	33.6	47.0	57.4	42.6
	523	34.1	76.2	23.8	40.8	71.3	28.7	49.4	57.7	42.3	56.6	55.2	46.8
Al-β	453	5.0	82.0	18.0	6.5	77.0	23.0	9.0	61.1	38.9	10.1	65.8	34.2
	473	6.3	79.4	20.6	12.0	74.2	25.8	15.5	60.6	39.4	28.5	54.0	45.8
	498	15.0	81.3	18.7	25.3	59.3	40.7	30.5	65.6	34.4	43.0	55.8	44.2
	523	33.6	75.3	24.7	39.4	58.9	41.1	44.6	55.2	44.8	50.1	45.2	54.8

[a] I (Isomerization products) = Σ mol % selectivities of p- and o- xylenes.

[b] D (Disproportionation products) = Σ mol% selectivities of toluene and trimethylbenzenes.

pore systems with or without lobes and/or intersections[33]. The value of p/o- selectivity in our sample of zeolite β was found in the range of 1.0 - 1.2 in agreement with the presence of 12-membered rings. However, in Zr-Al-β catalyst, the formation of p-xylene is favoured (p/o-selectivity = 1.2 –1.4). It could be due to steric hindrance exerted by the framework in the formation of o-isomers. One possibility is that the protonation of m-xylene at the least accessible C_2 atom, leading to o-xylene formation is sterically hindered. Preferred protonation at C_4 and C_6 could explain the higher p- selectivity of Zr-Al-β catalyst. Another possibility is that the size and shape of the pores hinders the formation and rearrangements of some of the intermediate species. At this moment, it is not possible to distinguish between these different mechanisms, especially because the positioning of the catalytic intermediates in the channels is unknown.

Similar trend was observed for the distribution of products in both the catalysts, except the formation of trimethylbenzenes over Zr-Al-β catalyst which occurs only at >498 K, resulting in a significant decrease in the isomerization to disproportionation (I/D) ratios (17.9 and 3.2 at 5.7 and 34.1 mol% conversions). The 1,3,5- to 1,2,4- trimethylbenzenes ratio in the product is 0.3-0.4, which is similar to the values reported already, at a conversion level of about 10% at 623 K for beta zeolite[32,33].

In order to eliminate or poison the non-selective acid sites, impregnation of Al-β with ZrO_2 at the external surface is attempted, referred to as *Zr-impregnated Al-β* (discussed in the section 4.2.2). It allowed an overall decrease in the activity (15.0 to 8.2 mol% at 498 K) as well as isomerization selectivity (75.3 to 68.4 mol% at around 30.0 mol% conversion) of Al-β sample, as shown in Table 4.3. However, Zr-Al-β catalyst showed a higher activity (20.0 mol% at 498 K) and isomerization selectivity (76.2 mol% at around 30.0 mol% conversion). These results clearly demonstrate the higher intrinsic activity of (framework) Zr in Zr-Al-β in comparison to the extraframework Zr in Zr-impreg. Al-β sample.

4.3.2.3 Effect of different contact times

The effect of different contact times (1.06 - 4.25 h) of the catalysts on the conversion and selectivities of isomerization and disproportionation at various temperatures was studied and the data are given in Table 4.4. The conversion of m-xylene over Zr-Al-β catalyst increases with an increase in contact time and temperature, while the selectivity of isomerization products is maximum at the lower contact time and at 453 K. At lower

temperature and lower contact time, the conversions of m-xylene are not so high and consequently, the differences in the isomerization and disproportionation selectivities are more significant. The conversion increases rapidly with increase in temperature and approaches to equilibrium values.

The rate constants were determined from the plot of mol % conversions of m-xylene vs. contact time at different temperatures in the range of 453 – 523 K. From the slope of Arrhenius plot (log r vs. 1/T K^{-1}) using linear regression method, the apparent activation energy values (E_a) were evaluated[34] as follows:

$$Slope = - E_a \div 2.303 \, R, \text{ where } R = 8.314 \text{ joules deg}^{-1} \text{ mole}^{-1}.$$

The apparent activation energy for isomerization of m-xylene over Zr-Al-β catalyst is marginally lower (E_a = 36.8 kJ/mole) than observed over Zr-free Al-β sample (E_a = 38.9 kJ/mole).

4.3.2.4 Effect of silynation

The disproportionation reaction is a bimolecular reaction, occurs via 1,1-diphenylmethane intermediates that are bulkier than the reagent and product molecules. The acid sites located at the channel opening or preferably at the external surface of the zeolite crystals may play an important role in the formation of these intermediates[35]. In order to passivate these external acid sites, we attempted to modify the samples with a deposition of a silica layer by means of chemical vapor deposition technique using tetraethylorthosilicate (TEOS)[36,37]. In the silynated samples, silica covers the external surface, leaving the intrinsic active sites within the channels unperturbed[38]. The effect of silynation on the conversion and selectivities in the isomerization of m-xylene is illustrated in Table 4.5. Silynation of the samples, in general, decreases the conversion of m-xylene at all temperatures. However, the silynated Zr-Al-β (B) (SiO_2 loading = 1.5 wt.%) sample showed a significant increase in the conversions of m-xylene (29.0 mol%) as compared to the silynated Al-β catalyst (10.5 mol% at 473 K) at similar SiO_2 loading. After silynation, there is an increase in the isomerization selectivity in both the samples, as observed in the case of H-ZSM-5 catalyst. The selectivity for isomerization of the silynated Zr-Al-β sample is more pronounced (ΣI = 77.2 mol%) than that observed before silynation of the samples (ΣI = 60.8 mol%) at around 30.0 mol% conversions. Thus, it is evident that the enhancement in the activity as well as the isomerization selectivity of Zr-Al-β catalyst in the reaction is due to Zr and Al metal atoms.

Table 4.5 Effect of Silynation on the conversion and selectivities in the m-xylene isomerization reaction[a]

Catalyst	Reaction Temp. (K)	453	473	498
Al-β (before Silynation)	m-xylene Conv. (mol%)	10.1	28.5	43.0
	Σ I[b]	65.8	54.0	55.8
	Σ D[c]	34.2	45.8	44.2
Al-β (after Silynation)	m-xylene Conv. (mol%)	4.8	10.5	34.0
	Σ I	83.0	74.4	68.5
	Σ D	17.0	25.6	31.5
Zr-Al-β (B) (before Silynation)	m-xylene Conv. (mol%)	13.8	31.9	47.0
	Σ I	65.2	60.8	57.4
	Σ D	34.8	39.2	42.6
Zr-Al-β (B) (after Silynation)	m-xylene Conv. (mol%)	4.4	29.0	42.0
	Σ I	90	77.2	70.0
	Σ D	10	22.8	30.0

[a] Contact time = 4.25 h;

[b] mol% selectivities of p- and o- xylenes (Isomerization).

[c] mol% selectivities of toluene and trimethylbenzenes (Disproportionation).

158

which are present inside the micropore system.

4.3.2.5 *Effect of acid sites*

Besides pore size distribution, several other explanations have been proposed to explain the differences in isomerization and disproportionation selectivity in twelve-membered ring zeolites. One hypothesis is related to the presence of appropriately positioned Lewis acid center with respect to Brönsted acid sites, may strengthen the acidity of these Brönsted acid sites[39]. It has been suggested that disproportionation requires stronger acid sites than isomerization. Siliceous zeolites contain stronger Brönsted acid sites than high-alumina containing zeolites and show a significant activity for disproportionation. The presence of appropriately positioned Lewis acid center with respect to Brönsted acid sites, which may strengthen the acidity of these Brönsted acid sites. Similarly Zr which itself is a Lewis acid, seems to enhance the overall Lewis acidity of Al-β zeolite. Thus it may alter the acid site distribution of Al-β sample, in such a way that results in a lower selectivity for disproportionation than for isomerization. The higher selectivity for isomerization in Zr-Al-β sample is correlated with the strong Lewis as well as Brönsted acid sites over and above those present in Al-β samples.

4.4 CONCLUSIONS

Two samples of zirconium- containing aluminium beta samples have been prepared and characterized by different techniques. These are compared with Zr-free Al-β and Zr-impreg. Al-β samples for different properties. Significant is the enhancement of acidity of Zr-Al-β by incorporation of Zr^{4+} ions probably in the lattice. It is presumed that Zr^{4+} Lewis acid sites may strengthen the Brönsted acid sites (due to Al^{3+} ions) and hence influence the isomerization of m-xylene. A marginal increase in m-xylene conversion and selectivity advantages for the isomerization products are noted with Zr-Al-β samples. Silynation studies further confirm the enhancement of activity and isomerization selectivity of Zr-Al-β catalysts.

4.5 REFERENCES

1. B. Rakshe, V. Ramaswamy and A. V. Ramaswamy, J. Catal. 163 (1996) 503.

2. B. Rakshe, V. Ramaswamy, S. G. Hegde, R. Vetrivel, and A. V. Ramaswamy, Catal. Lett. 45 (1997) 4.

3. B. Rakshe, V. Ramaswamy and A. V. Ramaswamy, Paper presented in "*1st Conf. of the Indo-Pacific Catalysis Association (IPCAT 1)*", Cape Town, South Africa, 26-28 Jan, 1998.

4. A. Corma, M. A. Camblor, P. Esteve, A. Martínez and J. Pérez-Pariente, J. Catal. 145 (1994) 151.

5. M. A. Camblor, A. Corma, A. Martínez and J. Pérez-Pariente, J. Chem. Soc., Chem. Commun. (1992) 589.

6. T. Sen, M. Chatterjee and S. Sivasanker, J. Chem. Soc., Chem. Commun. (1995) 207.

7. N. K. Mal and A. V. Ramaswamy, Chem. Commun. (1997) 425.

8. M. A. Camblor, M. Costantini, A. Corma, L. Gilbert, P. Esteve, A. Martínez and S. Valencia, Chem. Commun. (1996) 1339.

9. L. Bonetto, M. A. Camblor, A. Corma, and J. Pérez-Pariente, Appl. Catal. 82 (1992) 37.

10. R. B. Lapierre, R. D. Partridge, N. Y. Chen and S. S. F. Wong, US Patent, 4 501 926 (1983).

11. K. S. N. Reddy, B. S. Rao and V. P. Shiralkar, Appl. Catal. 95 (1993) 53.

12. T.C. Tsai, C. L. Ay and I. Wang, Appl. Catal. 77 (1991) 199.

13. M. M. J. Treacy, J. B. Higgins and R. von Ballmoos, *Collection of simulated XRD powder patterns for zeolites*, 3rd revised Ed. (Elsevier, 1996) p. 393.

14. D. L. Bish and J. E. Post, *Modern Powder Diffraction* (Reviews in Mineralogy), Vol.20 (The Mineralogical Society of America, Washington, D. C., 1989) p. 204.

15. J. M. Newsam, M. M. Treacy, W. T. Koetsier and C. B. De Gruyter, Proc. Royal Soc. London A 420 (1988) 375.

16. A. Tuel, S. Gontier and R. Teissier, Chem. Commun. (1996) 651.

17. T. Blasco, M. A. Camblor, A. Corma and J. Pérez-Pariente, J. Amer. Chem. Soc. 115 (1993) 11806.

18. C. A. Fyfe, H. Strobl, G. T. Kokotailo, C. T. Pasztor, G. E. Barlow and S. Bradley, Zeolites 8 (1993) 132.

19. J. Pérez-Pariente, J. Santz, V. Fornés, J. A. Martens, P. A. Jacobs and A. Corma, J. Catal. 124 (1990) 217.

20. K. W. Terry, C. G. Lugmair and T. D. Tiller, J. Am. Chem. Soc. 119 (1997) 9745.

21. E. Bourgeat-Lami, P. Massiani, F. Di Renzo, P. Espiau and F. Fajula, Appl. Catal., 72 (1991) 139.

22. J. Pérez-Pariente, J. A Martens and P. A. Jacobs, Appl.Catal. 31 (1987) 35.

23. M. A. Camblor, A. Corma, A. Mifsud and J. Pérez-Pariente, Stud. Surf. Sci. Catal. 105 (1997) 341.

24. C. Jia, P. Massiani and D. Barthomeuf, J. Chem. Soc., Faraday Trans. 89 (1993) 3663.

25. T. M. Miller and V. H. Grassian, Catal. Lett. 46 (1997) 213.

26. C. A. Emeis, J. Catal. 141 (1993) 347.

27. F. W. Dwyer, P. J. Lewis, and F. M. Schneider, Chem. Eng. 83 (1976) 98.

28. J. Dewing, J. Mol. Catal. 27 (1984) 25.

29. P. B. Weisz, Pure and Appl. Chem. 52 (1980) 2091.

30. S. M. Csicsery, Zeolites 4 (1984) 202.

31. J. Pérez-Pariente, E. Sastre, V. Fornés, J. A. Martens, P. A. Jacobs and A. Corma, Appl. Catal. 69 (1991) 125

32. R. Kumar and K. R. Reddy, Microporous Mater. 3 (1994) 195.

33. J. A. Martens, J. Pérez-Pariente, E. Sastre, A. Corma and P. A. Jacobs, Appl. Catal. 45 (1988) 85.

34. S. H. Maron and C. F. Prutton, *Principles of Physical Chemistry*, 4th Ed. (1969) p. 572.

35. E. Benazzi, S. De Tavernier, P. Beccat, J. F. Joly, C. Nedez, A. Choplin and J. M. Basset, Chemtech 24 (1994) 13.

36. T. Hibino, M. Niwa and Y. Murakami, J. Catal. 128 (1991) 551.

37. R. W. Weber, J. C. Q. Fletcher, K. P. Möller and C. T. O'Conner, Microporous Mater. 7 (1996) 151.

38. P. J. Kunkeler, D. Moeskops and H. van Bekkum, Microporous Mater. 11 (1997) 313.

39. M. L. Poutsma, *Zeolite Chemistry and Catalysis* ACS Monograph No. 171, J. A. Rabo, Ed. (Amer. Chem. Soc., Washington, DC. 1976) p. 437.

CHAPTER 5

Summary

The results obtained in the present investigations on Zr-containing crystalline, microporous molecular sieves with MFI, MEL and BEA topologies and the conclusions drawn from these studies are summarized in this chapter.

The isomorphous substitution of Si^{4+} by other tetravalent metal ions such as Ti^{4+}, Sn^{4+}, etc. in the medium pore as well as large pore, microporous molecular sieves with MFI, MEL and BEA structures has led to the invention of novel metallo-silicate molecular sieves which show significant improvements in product selectivities in the oxidation as well as acid catalyzed reactions, respectively. However, it is very difficult to prove unequivocally the isomorphous substitution of any transition metal in the zeolite framework of different structures. Recently, for metallosilicates other than the titanium silicates (TS-1, TS-2), research studies are oriented in this direction to understand the location and environment of such metal ions in the silicalite/aluminosilicate structures.

Since zirconium is a versatile element, it can be included in any classification of materials considered to have interesting and potential catalytic properties. A demand for the catalysts having improved stability, activity and selectivity has encouraged research into the possible use of zirconium as a functional element in heterogeneous catalysis. The substitution of silicon by zirconium in the framework of ZSM-5 (MFI) by hydrothermal synthesis has been attempted but not really substantiated by experimental evidence. Our attempts to incorporate Zr(IV) in the microporous silcalite as well as aluminosilicate molecular sieves, which may lead to an improvement in their catalytic properties, are discussed extensively in the chapters 2 to 4.

In the *introduction* of thesis (*Chapter 1*), a fundamental zeolite chemistry and isomorphous substitution of tetravalent metal ions in the zeolite lattice, particularly of MFI, MEL and BEA structures are discussed. It highlighted the principles of different physicochemical techniques applied in the said research work. This chapter also scanned the literature on Zr-containing zeolites/molecular sieves. Finally, the objectives of the thesis work are discussed.

In *Chapter 2 and 3*, the hydrothermal synthesis, spectral characterization and catalytic properties of Zr-containing, medium pore molecular sieves referred to as Zr-Silicalite-1 (MFI topology) and Zr-Silicalite-2 (MEL topology) are studied, respectively. The course of hydrolysis of silicate species during the gel preparation of the samples synthesized in alkaline medium was monitored by ^{29}Si liquid NMR studies. The IR study of adsorbed pyridine has shown that strong Lewis and weak Brönsted acid sites exist on these samples at 473 K. The

phsico-chemical as well as catalytic properties of these samples were compared with Zr-impregnated silicalite samples, prepared by post-synthesis method. Zr-impreg. silicalite, amorphous Zr-silica and Zr-free silicalite samples under identical conditions were found to have negligible activity in the hydroxylation of phenol. Apparently, only those zirconium ions present in the silicalite framework are active in the reaction. The salient features are as follows:

The hydrothermal synthesis of Zr-Silcalite-1 samples (SiO_2/ZrO_2 = molar ratios 300-50) both in alkaline and HF/CH_3NH_2 is discussed in *Chapter 2*. The dependence of the physico-chemical, structural and catalytic properties of samples prepared through these two routes is discussed. Incorporation of Zr^{4+} in the place of Si^{4+} in MFI framework causes an increase in unit cell volume (21 $Å^3$). There seems to be an upper limit on the extent of incorporation of Zr^{4+} in the framework limiting it to 0.6 Zr/unit cell (SiO_2/ZrO_2 = 158). The absence of amorphous matter is confirmed by XRD and SEM studies. The framework IR spectra showed the presence of Si-O-Zr linkages (asymmetric stretching vibrations at 965 cm^{-1}) predominantly. A linear decrease in the position of T-O-T vibrations at 1100 cm^{-1} is observed with Zr content, due to the higher mass of Zr atom with respect to Si and polarized character of Zr-O bond, the Si-O bond stretching character is perturbed by the presence of framework Zr species.

Furthermore, a characteristic absorption at 212 nm in the UV-visible spectrum and the two peaks with binding energy values about 184.0 and 186eV for $3d_{5/2}$ and $3d_{3/2}$, respectively in the XPS spectrum support the presence of Zr in tetrahedral coordination. The IR spectra in the hydroxyl stretching region showed the presence of Si-OH and Zr-OH groups on the surface. The IR spectra of the adsorbed pyridine showed the presence of strong Lewis and weak Brönsted acid sites. The pyridinium ion at the Brönsted acid sites are weakly bound in correspondence with the Si-OH and Zr-OH type weak Brönsted acid sites.

The catalytic activity in the hydroxylation of phenol is quite high (TON = 112) for the samples prepared in alkaline medium than those prepared in HF/CH_3NH_2 medium (TON = 8.3). In these samples, the ratios of catechol to hydroquinone selectivities are 1.0 and 2.0, respectively. The relative stability of cluster models representing various possible lattice structures and the ordering of molecular orbitals derived from Extended Hückel Molecular Orbital calculations are discussed to understand the nature of active sites in the zirconium

silicates.

The product selectivity obtained in the reaction indicates the presence of Zr^{4+} in the channels, rather than on the surface. The ordering and shift in the molecular orbitals are not significantly different for monoclinic zirconia and orthorhombic zirconium silicate structures, as derived from the cluster calculations. However the binding energy of pyridine is significantly higher when it is coordinated to zirconium in comparison to the pyridinium ion formation with surface hydroxyl groups. The substitution energy calculations showed a possible location of framework Zr at the T2 and T12 crystallographically distinct sites of MFI structure.

Zr-Silicalite-2 molecular sieves with MEL structure (SiO_2/ZrO_2 = 300 - 65) have been synthesized using two different zirconium sources viz., $ZrCl_4$ and $Zr(acac)_4$, referred to as Zr-Sil-2 (A) and (B) samples, respectively (*Chapter 3*). They have been compared using ^{29}Si liquid NMR, XRD, SEM, FTIR, UV-Visible, surface area measurements and catalytic activity in the hydroxylation of phenol using aqueous H_2O_2. The increase in unit cell volume is only marginally different in both the samples. The catalytic activity is nearly twofold in the case of samples prepared using $Zr(acac)_4$. This may be due to the smaller particle size and larger surface area of the sample. However, a higher catechol formation in Zr-Sil-2(B) samples may be due to the surface species. On the basis of ^{29}Si liquid NMR studies and catalytic properties, the samples synthesized using $ZrCl_4$ for further characterization were found to be better.

An increase in unit cell volume (34 $Å^3$) corresponding to the theoretical expansion due to the larger size of Zr^{4+} ions, the formation of Si-O-Zr linkages (FTIR spectra) and the characteristic charge transfer transition in the Td configuration (DR UV-visible spectra) indicate that up to 1.0 Zr atom per unit cell (SiO_2/ZrO_2 = 100) is substituted isomorphously in the framework positions of Zr-silicate in the MEL structure. Zr-edge EXAFS spectral analysis supported the tetrahedral coordinations of Zr (N-cor = 3.9) in the MEL structure. It is noticeable that the bond distances at 1.94 Å in the first shell and 3.35 Å in the second shell are due to the Si-O-Zr linkages in edge sharing structures. The ESR signals at g = 2.04 and 1.97, in Zr-Sil-2 as well as Zr-impregnated Sil-2 samples, respectively, on photoreduction of Zr (IV) at room temperature are observed. These signals are assigned to Zr^{3+} ions formed on the interaction of Zr^{4+} ions with H_2 molecules as a consequence of the reductive process. It is apparent that the crystal field associated with Zr(IV) active site present in these samples is

different from each other.

This is further supported by the catalytic activity (TON =71.4) in the hydroxylation of phenol and the catechol to hydroquinone ratio of about 0.94 in the products. During this reaction, the effect of different solvents such as water, methanol acetone and acetonitrile were studied. The key events could be the interaction of H_2O_2 and a protic solvent, water with Zr active site and the transfer of a peroxide oxygen species to the phenol to be oxidized. The reactive intermediates formed on contact with $H_2O + H_2O_2$ are compared to those of Zr-Silicalite-1 sample using ESR and diffuse reflectance UV-visible spectral techniques, at room temperature. These peroxo- and hydroperoxo- species formed due to presence of Zr(IV) active sites are similar to those reported in the literature for titanium silicates.

The effect of possible acid-base properties due to zirconium incorporated in the silicalite lattice is investigated in the decomposition of isopropanol and oxidative dehydrogenation of ethanol at different temperature. The active sites involve Zr(IV) as a tetrahedral species, sharing edges with two neighbouring SiO_4 tetrahedra from the silicalite lattice. Zr itself acts as a Lewis acid due to its coordinatively unsaturated nature. Thus it bears a $\delta+$ charge so that $-O^{\delta-}$-Si may be viewed as a Lewis acid-base pair in the form of Si-O-Zr linkages. Due to these acid-base characteristics, Zr-Silicalite-2 as well as Zr-Silicalite-1 samples showed activity in the decomposition of isopropanol and oxidative dehydrogenation of ethanol. Zr-Sil-2 catalyst showed selective formation of acetone at the earliest temperature range of 473 – 498 K. Above 498 K, the selectivity shifts in favour of propene formation. The change in the selectivity pattern is due to the adsorption of isopropyl alcohol molecule on the different active sites around the zirconium active sites. In oxidative dehydrogenation reaction, the sample exhibits a higher selectivity to acetaldehyde in favour of dehydrogenation reaction. At higher temperatures, the selectivity for the secondary dehydration product, ethylene is enhanced with a loss in the selectivity of acetaldehyde and primary dehydration product, diethyl ether. These dehydration and/or dehydrogenation reactions are likely to involve heterolytic processes involving pairs of acid and basic sites in the form of Si-$O^{\delta-}$....$Zr^{\delta+}$ linkages of silicalite framework. However, the product selectivity pattern is different (higher dehydration product formation) in the case of Zr-Sil-1 samples than those of Zr-Sil-2 due to difference in the active site distribution.

Even though these medium-pore Zr-silicates showed a remarkable activity in the dehydration and/or dehydrogenation reactions, their mild acid sites and relatively small pore openings of the structures limit the applications of such materials. It should be possible to overcome these limitations and improve the performance of Zr-containing molecular sieves by the synthesis of large pore structures.

In *Chapter 4*, our attempts to incorporate Zr^{4+} ions in the framework of zeolite β and to investigate the effect of zirconium in the aluminosilicates on the acid properties and hence on the catalytic activity are described.

In this chapter, the hydrothermal synthesis of a large pore, Zr-containing alumino-silicate with BEA structure, Zr-Al-β (SiO_2/ZrO_2 = 100 and 50; SiO_2/Al_2O_3 = 25) is discussed. The structural variations in these samples are characterized using different spectral techniques such as X-ray diffraction, DR-UV-visible and FTIR spectroscopy to show that Zr^{4+} ions are isolated and are probably linked to the framework of the aluminosilicate of BEA structure. The FTIR studies of adsorbed pyridine, evacuated at different temperatures show an increase in Lewis as well as Brönsted acidity of Zr-Al-β samples in comparison to Zr-free Al-β and Zr-impregnated Al-β, having similar Al contents. The enhancement is probably the result of incorporation of Zr^{4+} ions into the β structure as $Si-O^{\delta-}...Zr^{\delta+}$ linkages. The intrinsic activity of zirconium is investigated in the isomerization of m-xylene at different contact times in the temperature range of 453 - 523 K. Additional Lewis as well as Brönsted acidities of Zr-Al-β samples, as demonstrated by pyridine adsorption studies, are correlated with a marginal increase in the activity and selectivity to isomerization products (p- and o-xylenes), particularly at temperatures below 500 K.

Significant is the enhancement of acidity of Zr-Al-β by incorporation of Zr^{4+} ions probably in the lattice. It is presumed that Zr^{4+} Lewis acid sites may strengthen the Brönsted acid sites (due to Al^{3+} ions) and hence influence the isomerization of m-xylene. A marginal increase in m-xylene conversion and selectivity advantages for the isomerization products are noted with Zr-Al-β samples. The apparent activation energy for isomerization of m-xylene over Zr-Al-β catalyst is marginally lower (E_a = 36.8 kJ/mole) than observed over Al-β sample (E_a = 38.9 kJ/mole). Silynation studies further confirm the enhancement of activity and isomerization selectivity of Zr-Al-β catalysts.

In conclusion, The characterization and catalytic studies of these molecular sieves clarify that substantial substitution of Si atoms by Zr to form Si-O-Zr bonds, could be occurring. Even though there is a large difference between the ionic radii of Si^{4+} (0.26 Å) and Zr^{4+} (0.59 Å), due to the flexibility of the zeolite framework structures, such a large cation is likely to have occupied framework position (tetrahedral site) in zeolite lattice to a limit of about 1.0 Zr atom per unit cell in the Silicalite 1, Silicalite-2 and beta structures.

List of Publications:

1. Synthesis, characterization of Sn-containing ZSM-48 type molecular sieves using different templates.
   N.K. Mal, V. Ramaswamy, **Bhavana Rakshe** and A.V. Ramaswamy
   Paper presented in 11th IZC Seoul, Korea, (12-17th August, 1996);
   Stud. Surf. Sci.Catal. **105**, 357 (1997).

2. Synthesis and characterization of crystalline, microporous zirconium silicates with MEL structure.
   Bhavana Rakshe, V. Ramaswamy and A.V. Ramaswamy
   J. Catal. **163**, 503 (1996).

3. Synthesis and characterization of crystalline, microporous zirconium silicates with MFI structure.
   Bhavana Rakshe, V. Ramaswamy, S.G. Hegde, R. Vetrivel and A.V. Ramaswamy
   Catalysis Letters **45**, 41 (1997).

4. Synthesis and characterization of zirconium silicate molecular sieves of MEL type using two different zirconium sources.
   Bhavana Rakshe, V. Ramaswamy
   Paper presented in 13th National Symposium on Catalysis (2-4th April, 1997);
   Stud. Surf. Sci. Catal. **113**, 219 (1998).

5. A large pore zirconium-containing alumino-silicate with BEA structure.
   Bhavana Rakshe, V. Ramaswamy and A.V. Ramaswamy
   Paper presented in 12th IZC, Baltimore, (5-10th July, 1998), *Materials Research Society* (in Press).

6. Acidity and m-xylene isomerization activity of large pore, zirconium-containing alumino-silicate with BEA structure.
   Bhavana Rakshe, V. Ramaswamy and A.V. Ramaswamy
   J. Catal., communicated (May 1998).

Presentations at Symposia/Conferences:

1. Characterization of crystalline, microporous zirconium silicates with MFI structure by Infrared spectroscopy.

   Bhavana Rakshe, A.A. Belhekar, S.G. Hegde and V. Ramaswamy

   National Workshop on Catalysis, Bhavnagar, 20-22th December, 1995.

2. Synthesis, characterization and catalytic properties of alumino-, titano- and tin-silicates with MFI structure.

   N.K. Mal, **Bhavana Rakshe**, V. Ramaswamy and A.V. Ramaswamy

   National Workshop on Catalysis, Bhavnagar, 20-22th December, 1995.

3. Catalytic decomposition of Propan-2-ol over crystalline, microporous Zr-silicates with MEL structure.

   Bhavana Rakshe, V. Ramaswamy and A.V. Ramaswamy.

   Paper presented (Snapshot poster) in 1st Conference of the Indo-Pacific Catalysis Association (IPCAT 1), Cape Town, South Africa, 26-28th January, 1998 (in Press).

4. A large pore zirconium-containing alumino-silicate with BEA structure.

   Bhavana Rakshe, V. Ramaswamy and A.V. Ramaswamy

   Paper presented in 12th IZC, Baltimore, (5-10th July, 1998), *Materials Research Society* (in Press).

5. A large pore zirconium-containing alumino-silicate with BEA structure: Synthesis, Characterization and catalytic properties.

   Bhavana Rakshe and A.V. Ramaswamy

   Paper presented in Golden Jubilee symposium, University of Pune, India (5th December, 1998).

6. ^{29}Si liquid NMR Studies of the gels used for the preparation of Zr-Silicalite-2 molecular sieves

   Bhavana Rakshe, Veda Ramaswamy and A.V. Ramaswamy.

   14th National Symposium on Catalysis (16-18th December, 1998).

Patents:

1. A process for the preparation of zirconium-containing crystalline, microporous molecular sieves of MEL type.

   Bhavana Rakshe, V. Ramaswamy and A.V. Ramaswamy

   Indian Patent (NF-75/96) filed on 29th March, 1996.

2. A process for the preparation of zirconium-containing large pore, crystalline alumino-silicate with BEA structure.

   Bhavana Rakshe, V. Ramaswamy and A.V. Ramaswamy

   Indian Patent, filed on 1st March, 1998.